Surveys for Primeval Galaxies

Thesis by

David Thompson

In Partial Fulfillment of the Requirements

for the Degree of

Doctor of Philosophy

California Institute of Technology

Pasadena, California

1995

(Submitted October 24, 1994)

Acknowledgements

I was but 12 years old back in 1976, but I can still vividly remember getting up every morning to catch another glimpse of comet West as it rose above the horizon before dawn. What a spectacular sight! This marks the beginning of my interest in astronomy, though it has taken nearly 20 years to turn this longtime hobby into a profession. Fortunately, not *all* of it was spent in graduate school!

Of all of the people I have had the privilege and pleasure of working with, the one to whom I owe the lion's share of thank you's is my advisor, George Djorgovski. His broad interest in so many areas of astronomy has been a constant source of inspiration and amazement to me, and his...interesting...sense of humor entertaining. Our conversations about various aspects of modern astronomy on many a night at the 200-inch telescope have helped to spark my imagination and build my enthusiasm for this fascinating field. For helping to turn this former Chemist into an Astronomer, George, thanks.

Many thanks also to Julia Smith, with whom I have shared an office as well as an advisor for several years. To my other officemate, Lin, as well as the rest of the students and postdocs, thanks for making Caltech an enjoyable place to work. It has been a pleasure, a privilege, and an honor to pursue this career at Caltech, and to make use of the telescopes at Palomar Observatory.

Josh, Michal, and Tyler, the trip we took to Costa Rica was great, and the solar eclipse was absolutely breathtaking! Like comet West, the image of the Sun's corona is something I will never forget. Gracias!

Many wonderful memories of my time here in Pasadena involve my "extended family," especially Patty, John, and Sonja. My gratitude and thanks to them for their friendship over these past six years. I will miss the hikes, the dinners, the parties, the trips to the beach, the impromptu jam sessions, and their general enthusiasm. Never again will I touch another drop of tequila, though!

Thanks to my fiancée Viviane, for her love, support and patience while finishing this thesis, and for doing the impossible and turning this longtime night owl into a morning person. Finally, I would like to thank my parents, brothers, and sister for their love and encouragement throughout the years. It was a long road getting to this point, and I could not have done it without them.

Abstract

We present the results from two complementary surveys for young and forming ellipticals or spheroids at high redshift, one based on a narrowband imaging technique using a Fabry-Perot interferometer, and the other a serendipitous long-slit spectroscopic survey.

The Fabry-Perot survey is sensitive to Lyα emission in four discrete redshift ranges: $z = 2.80 - 2.98$, $3.27 - 3.45$, $4.42 - 460$, and $4.75 - 4.89$. The total area of the survey was 0.63 deg^2, surveyed to a 1σ limiting line flux of $\sim 8.5 \times 10^{-17}$ erg cm^{-2} s^{-1} . An area of 0.05 deg^2 was surveyed to a fainter flux limit of $\sim 1.5 \times 10^{-17}$ erg cm^{-2} s^{-1} . A total comoving volume of 110,000 Mpc^3 was surveyed to a 1σ limiting restframe emission line luminosity of $\sim 2.0 \times 10^{43}$ erg s^{-1} (a Friedman cosmology with $H_0 = 75$ km s^{-1} Mpc^{-1} and $\Omega_0 = 0.2$ is assumed throughout this thesis).

The long-slit survey is sensitive to Lyα in the range of $3.1 \leq z \leq 5.2$, with lesser areas surveyed across the entire optical passband. A total of 421 independent spectroscopic frames were searched, covering an area of 0.0042 deg^2 (14.97 arcmin^2). 65 emission-line candidates were identified, including 30 galaxies with $z \lesssim 1$ and 2 quasars. An additional 20 objects were assigned tentative redshifts, all with $z \lesssim 1.2$, and have properties consistent with the galaxies seen in the deep field redshift surveys. The remaining objects are candidate Lyα galaxies at high redshift, with isolated, unidentified emission lines and little or no continuum. They require further spectroscopy to check on their nature. A total comoving volume

of 102,600 Mpc^3 was surveyed to a 1σ limiting restframe emission line luminosity of $\sim 2.45 \times 10^{43}$ erg s^{-1}.

In neither case was an obvious population of primeval galaxies revealed, despite the combined surveys covering a volume of space sufficient to include ~ 200 galaxies with $L \geq L_*$ (using the local space density of massive galaxies, and assuming no density evolution). These galaxies could have been detected if they were unobscured by dust and were actively forming stars at a rate of 100 $M_\odot$ yr^{-1}. A number of candidates remain to be followed up with spectroscopic observations, and may yet prove to be the elusive PGs. The lack of detection of a population of Lyα-luminous objects could be due to dust quenching of the Lyα line, a higher redshift of formation than surveyed, short lifetime in the Lyα-bright phase, or even masking of the star-formation emission-line signature by an active nucleus.

A study on the feasibility of conducting primeval galaxy surveys in the near infrared, based on emission-lines of [O II], [O III], and the Balmer lines, and the results of a preliminary survey based on these techniques, are also presented. It is shown that the new large-format infrared arrays will reach the necessary sensitivities over large enough areas to make such surveys practical.

Contents

List of Figures

List of Tables

Chapter 1

Introduction

The discovery of a population of high-redshift primeval galaxies (PG) would provide important constraints on the formation of galaxies, as well as their star formation and chemical evolution histories. As luminous matter is currently the only marker we have to trace structure, populations of objects at high redshift would also constrain models of the formation and evolution of large-scale structure. Primordial density fluctuations, recently detected (statistically) by the *COBE* satellite (Smoot et al. 1992) as fluctuations on the near-isotropic microwave background, limit the initial conditions under which PGs can begin to collapse. The non-detection of an obvious population of primeval galaxies, despite numerous attempts over the past several years to discover them, is thus still one of the major unanswered problems in observational cosmology today.

In this thesis, we adopt the definition that PGs are high-redshift elliptical galaxies or massive spheroids undergoing their first major bursts of star formation. This is generally thought to be the most luminous period in the formation of a galaxy. Disk formation and evolution has probably already been detected in the damped Lyα systems (Wolfe 1993a), seen in absorption against background QSOs, though this is thought to be a separate phenomenon from the formation of spheroids and ellipticals. We exclude objects containing or associated with an active nucleus (AGN) as well. Although it is possible that all massive galaxies

undergo an AGN phase during their formation (Haehnelt & Rees 1993), this issue is difficult to resolve (Terlevich 1992).

Several lines of evidence suggest that this is a reasonable picture for the formation of the first galaxies. Age sensitive colors such as $(B-R)$ or $(U-B)$, spectroscopic indicators, and models of stellar populations generally indicate that ellipticals and spheroids are $\gtrsim$ 10 Gyr old. Lack of evidence for any appreciable evolution since $z \sim 1$ in the massive galaxies, as implied by the results of the deep field spectroscopic surveys (Koo, & Kron 1992), suggest that these stellar populations are relatively old, settled systems by this redshift. The existence of quasars with high metallicities at $z > 4$ (Hamann, & Ferland 1993) indicates that significant quantities of metals have already been formed and returned to the interstellar medium by at least one generation of massive stars. At the other end of the timeline, massive star formation in significant numbers of spheroidal systems is unlikely to have occurred at $z \sim 1$ anyway, as they would presumably be bright and would have been discovered by now.

Theoretical arguments pertaining to the formation epoch of galaxies provide only a limited amount of help in answering the timing question. An upper limit on $z_{gf} \lesssim 30$ can be set by requiring PGs to be able to cool via inverse Compton scattering off the microwave background photons. One then runs into the problem of collapsing the protogalaxies by a factor of $\sim$ 10 (cf. Peebles 1989) in so short a period of time (the universe is at most a few hundred million years old at $z \sim 30$) when starting with the remarkably low-amplitude fluctuations implied by the *COBE* results (Smoot et al. 1992). Hierarchical build-up of structure in the CDM models, on the other hand, prefer to have galactic-sized units forming relatively late and over an extended period of time, with appreciable formation continuing to $z \sim 1$. The formation of PGs is thus an empirical problem which needs to be solved by observations.

The relevant parameter space probed by surveys for primeval galaxies has 3 axes: area on the sky, wavelength (or redshift), and limiting flux. Although it is possible to probe this parameter space with broadband imaging techniques, e.g., looking for the Lyman discontinuity ar $\lambda_{\rm rest} = 912$Å (Giavalisco, Steidel, & Szalay 1994), the resulting candidates are extremely faint ($R \sim 25^m$). Assigning redshifts based on continuum spectral energy distributions is fraught with difficulties and notoriously uncertain, thus we are driven to look for emission-line signatures in the spectrum of PGs. Strong emission lines are expected to result from active star-formation, and are seen in local star-forming regions. Indeed, strong Lyα emission has been detected from a number of high-redshift galaxies (Spinrad 1987, Djorgovski 1988, and references therein).

There are two general, complementary approaches to surveying this parameter space which make use of emission lines: narrowband imaging and spectroscopy. These techniques make efficient use of the fact that the apparent brightness of emission-line objects is significantly greater in the emission-line than in the continuum (see section 2.1.3). Surveys based on the narrowband imaging technique look at large areas on the sky, but cover only a small interval of wavelength ($\Delta\lambda$ or Δz). Surveys based on long-slit spectroscopic data, on the other hand, probe very small areas on the sky (typical slit widths are of order 2 arcseconds by 2 arcminutes) but sample a large $\Delta\lambda$ (Figure 1.1). It is also worthwhile to consider limits expressed in terms of restframe coordinates, where area and redshift coverage translate into comoving volume, and the flux limits and redshift transform into the limiting emission-line luminosities. The use of comoving volumes allows for a fairer and more intuitive comparison between different surveys, and line luminosity limits are directly relatable to limits on the star formation rate.

There is also the problem of recognizing a bona fide primeval galaxy. There are a number of radio galaxies and Lyα companions of quasars known out to $z \sim 4.2$, and quasars out to $z \sim 4.9$ (Schneider, Schmidt, & Gunn 1991). Some

of them have been found using techniques similar to the ones used in this thesis. These objects include the galaxy companion of PKS 1614+051, at $z = 3.215$ (Djorgovski et al. 1985), or the pair of diffuse Lyα emission objects at $z = 3.273$ near MG 2016+112 (Schneider et al. 1986), and the companion to the quasar Q1548+0917 (Steidel, Sargent, & Dickinson 1991). Several objects associated with powerful radio sources have been found at $z \simeq 1.8 - 3.8$ (McCarthy et al. 1987, 1990; Chambers et al. 1988). While many of these objects have a number of characteristics expected for PGs, they have generally all been interpreted to be associated with an active nucleus, e.g., strong radio emission, proximity to an AGN, or the presence of relatively strong C IV emission (difficult to produce with a purely stellar population). It is also difficult to tell if these are truly PGs producing their first generation of stars, or the product of mergers, as many of the ultraluminous IRAS starbursts appear to be. It thus becomes necessary to search for PGs at the highest redshifts possible, to minimize the time available for merging events or the formation of an active nucleus.

Currently, astronomical instrumentation on 4m – 5m telescopes is capable of detecting emission-line fluxes of a few $\times 10^{-17}$ erg cm^{-2} s^{-1} with reasonable integration times. The Lyα line luminosities derived from the stellar population synthesis models by Charlot & Fall (1993), with a $L_{Ly\alpha} \sim 10^{43.9}$ erg s^{-1} for a star formation rate of 100 $M_\odot$ yr^{-1}, agree well with the original prediction by Partridge & Peebles (1967) that several percent of the total bolometric luminosity of a PG might escape in the Lyα line. Simple case B recombination scaling arguments and the empirical relation between the star formation rate (SFR) and Hα line intensity (Kennicutt 1983) yield similar numbers for Lyα , $\sim 10^{43.4}$ erg s^{-1} for the same 100 $M_\odot$ yr^{-1} SFR. The consistency of these estimates, despite the disparate approaches, lends confidence to the results. For a range of reasonable cosmologies ($H_0 = 75$ km s^{-1} Mpc^{-1} and $\Omega_0 = 0.2$ are specifically adopted throughout this thesis, "reasonable cosmologies" span the range of $50 \leq H_0 \leq 100$ and $0.0 \leq \Omega_0 \leq$

1.0), and for cosmologically interesting redshifts, the expected *observable* Lyα line flux would be $\sim 10^{-16\pm1}$ erg cm^{-2} s^{-1} , well within the limits imposed by the available instrumentation. The majority of PG surveys to date have concentrated on the range $1.9 \leq z_{gf} \leq 5$, where Lyα is redshifted into the optical passband, primarily because the available detectors have the necessary sensitivity and are able to search a wide area on the sky.

We make our own estimates of the Lyα line parameters using the models of Bruzual (1983, and more recent updates), integrating the ionizing radiation from the stellar population and making the assumption that each photon ultimately produces a Lyα photon. Models are used which have an exponentially-declining star formation rate ($\mu = 0.95$, and an e-folding time of 1/3 Gyr) and a baryonic mass of 10^{11} M$_\odot$. Both Scalo and Salpeter initial mass functions are plotted for two different redshifts of formation, 5 and 10 (Figure 1.2). These models should bracket the range of reasonable expectations for the Lyα emission line from unobscured PGs. Emission-line fluxes derived in this manner agree with the other methods of estimating this quantity.

The subject of primeval galaxies and surveys to look for them has been reviewed or discussed by Koo (1986), Cowie (1988), Djorgovski (1992), Djorgovski & Thompson (1992) and Pritchet (1994). Surveys which target Lyα emission from possible PGs, using a number of different techniques, include those of Pritchet & Hartwick (1987,1990), Cowie & Hu (in Cowie 1988), Lowenthal et al. (1990), De Propris et al. (1993), Smith, Thompson & Djorgovski (1993), Giavalisco, Steidel & Szalay (1994), Parkes, Collins & Joseph (1994), Thompson, Djorgovski, & Trauger (1995, see chapter 2), and Thompson, & Djorgovski (1995, see chapter 3). Other works based primarily on narrowband data, but generally targeting specific objects, e.g., damped Lyα absorbers (Wolfe et al. 1992, others), can also be interpreted as PG surveys, as they would pick up any emission-line objects within their survey volume.

This thesis is composed of several papers, published or submitted, which are related to the general topic of surveys for primeval galaxies. Since they need to stand by themselves in the journals, the reader will find a certain amount of information repeated in the introductions to each chapter. In chapter 2, I present the results from a narrowband imaging survey for Lyα emission at high redshifts, using an imaging Fabry-Perot interferometer built for this project. Chapter 3 covers a serendipitous long-slit spectroscopic survey for Lyα . Chapter 4 discusses the feasibility of conducting narrowband surveys in the infrared, using the new large-format IR arrays currently being developed, and presents the results from a preliminary survey at Palomar. Chapter 5 is concerned with the conclusions that can be drawn in considering the combined results of these projects.

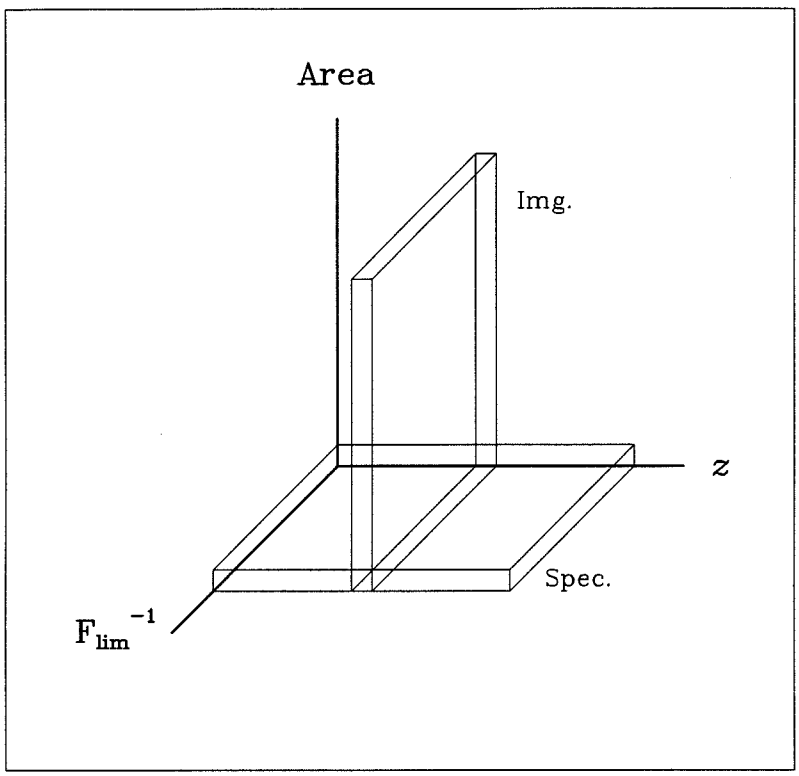

Figure 1.1 PG Survey Parameter Space

Imaging surveys sample large areas but only small redshift intervals, while spectroscopic surveys sample a long redshift baseline but only a small area on the sky. Both techniques are capable of reaching similar flux limits.

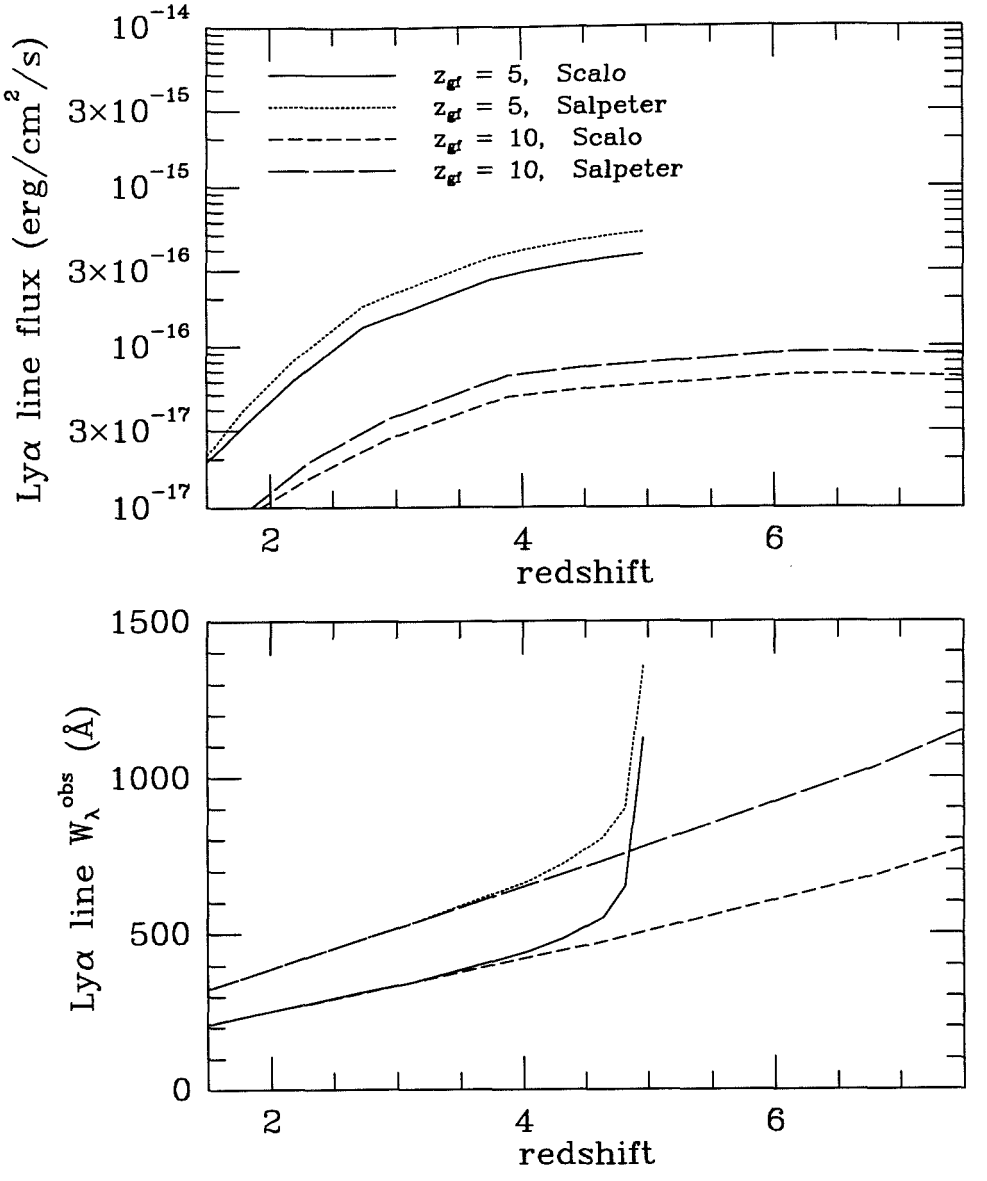

Figure 1.2 Lyα Emission Line Parameters

Estimated observed properties of Lyα emission powered by star formation, using Bruzual $\mu = 0.95$ population synthesis models with baryonic mass of 10^{11} $M_\odot$. Both Scalo and Salpeter IMFs are plotted for two different redshifts of formation (5 and 10, $H_0 = 75$ km s^{-1} Mpc^{-1} and $\Omega_0 = 0.2$ are used). These models should bracket the range of reasonable expectations for the Lyα emission line from PGs. The top panel shows that the expected fluxes from Lyα fall in the range currently observable by modern instrumentation, while the bottom panel shows the observed equivalent width expected for the Lyα line.

Chapter 2

The Fabry-Perot Survey*

ABSTRACT

We present the results of a narrowband imaging survey for Lyα emission from young and forming ellipticals or spheroids at high redshifts. A total of 11 independent datacubes, each consisting of 6–11 images at slightly different central wavelengths, were obtained using a Fabry-Perot imaging interferometer on fields of $\sim$5 arcmin square. Each datacube spans $\Delta z \sim 0.2$ while the total survey spans a redshift range of 2.78–4.89 for Lyα line emission. We reach a 1σ limiting line flux (in an aperture of twice the seeing FWHM) of $\sim 1.5 \times 10^{-17}$ erg cm^{-2} s^{-1} over 0.05 deg^2, with a total of 0.63 deg^2 surveyed to a limiting line flux of $\sim 8.5 \times 10^{-17}$ erg cm^{-2} s^{-1} . The survey reaches a 1σ average limiting restframe Lyα emission line luminosity of $\sim 1.5 \times 10^{42}$ erg s^{-1} over a volume surveyed of 3,000 comoving Mpc^3, with a total volume of 110,000 comoving Mpc^3 surveyed to an emission line luminosity of $\sim 2.0 \times 10^{43}$ erg s^{-1} (for $H_0 = 75$ km s^{-1} Mpc^{-1} and $\Omega_0 = 0.2$). No obvious population of Lyα luminous primeval galaxies has been detected so far, although a number of candidates remain which need to be checked by follow-up spectroscopy. Possible explanations for the lack of detection of a population of primeval galaxies at optical wavelengths in this and similar surveys include the possibility that they were obscured by dust or that the bulk of galaxy formation occurred at redshifts $z_{gf} \geq 5$. The instrument used for this survey is also briefly described.

---

* Adapted from a paper entitled "A Narrowband Imaging Survey for Primeval Galaxies," by D. Thompson, S. Djorgovski, and J. Trauger, submitted to the Astronomical Journal.

2.1 Introduction

The discovery of primeval galaxies (PG) has been a major focus of research in modern observational cosmology over the past decade. The detection and study of PGs would provide constraints on galaxy formation, the star formation and chemical evolution histories of galaxies and stellar populations, and also on the formation and evolution of large-scale structure and the primordial density fluctuations. Recent reviews of this subject can be found in Djorgovski (1992), Djorgovski & Thompson (1992) and Pritchet (1994).

For this work we have adopted the observationally-biased definition that PGs are high-redshift elliptical galaxies or massive spheroids undergoing their first major burst of star formation. This is generally thought to be the most luminous period in the formation of a galaxy. We specifically *exclude* objects containing or associated with an active nucleus. This does not preclude the possibility that all massive galaxies have an active galactic nucleus (AGN) stage in their formation (Haehnelt & Rees 1993), but it is currently difficult to resolve the issue of whether such an object obtains most of its energy from the AGN or through star formation (Terlevich 1992).

A number of sources with strong Lyα emission are currently known at high redshift. These include: radio galaxies (RG) such as 3C326.1 (McCarthy et al. 1987), B2 0902 +34 (Eisenhardt & Dickinson 1992), and 4C41.17 (Chambers, Miley & van Breugel 1990); companions to RGs or QSOs such as the PKS 1614+051 companion (Djorgovski et al. 1985) and C1548+0917 (Steidel, Sargent, & Dickinson 1991); the gravitationally lensed system MG 2016+112 (Schneider et al. 1986); systems discovered near damped Lyα absorbers such as PHL 957 (Lowenthal et al. 1991) and QSO 0000−269 (Macchetto et al. 1993); and luminous infrared sources such as FSC 10214+4724 (Rowan-Robinson et al. 1991). While many of these objects have a number of characteristics expected for PGs, they have generally all been interpreted to be associated with an active nucleus, e.g.,

strong radio emission, proximity to an AGN, or the presence of relatively strong C IV emission (difficult to produce with a purely stellar population). The formation and evolution of disks in spiral galaxies has probably already been detected in the damped Lyα systems (Wolfe 1993a), seen in absorption against background QSOs, though this is thought to be a separate phenomenon from the formation of spheroids and ellipticals.

Constraints on the epoch of galaxy formation can be placed by some of the extant observations and theories. Massive star formation in spheroidal systems is unlikely to have taken place at redshifts $z \leq 1$, because the resulting PGs would be relatively bright and thus would presumably have been detected in the spectroscopic surveys reaching to $B < 24^m$ (Broadhurst et al. 1988, Colless et al. 1990, Colless et al. 1993). Age-sensitive colors such as $(U-B)$, spectroscopic indicators, and models of stellar populations suggest that the ages of elliptical and spheroid populations are $\sim 14 \pm 6$ Gyr, with a corresponding redshift of formation of $z \geq 3-5$ for a range of reasonable cosmologies (Bower et al. 1990; Bower, Lucey & Ellis 1992). An upper limit on z_{gf} can be set by requiring PGs to be able to cool via inverse Compton scattering off the microwave background photons, which is inefficient at $z \gtrsim 30$.

The majority of PG surveys to date have concentrated on the range $1.9 \leq z_{gf} \leq 5$, where Lyα is redshifted into the optical passband, because the available detectors have been able to reach the necessary flux limits over a wide enough area to make such surveys possible.

2.1.1 Energetics of Galaxy Formation

There are some basic arguments on the energetics of galaxy formation which suggest how bright PGs may be. There are three main sources of energy production during the formation of a galaxy: the release of gravitational potential energy as

the mass collapses, conversion of hydrogen into helium and metals in the nuclei of stars, and the presence of a possible active nucleus.

It is generally believed that PGs collapsed by about a factor of 10 (c.f. Peebles 1989). This process must have involved the dissipation of binding energy. From the virial theorem, we can get an estimate for the binding energy of a galaxy. Assuming a baryonic mass (M_{bar}) for an average galaxy to be 10^{11} $M_\odot$, and an average 3-dimensional velocity dispersion or rotational speed (σ_0) of 250 km s^{-1} , the binding energy is:

$$|E_{bind}| \sim \frac{1}{2} \cdot M_{bar} \cdot \sigma_0^2 \approx 6.3 \times 10^{58} \mathrm{erg} \left(\frac{M}{10^{11}\ \mathrm{M}_\odot} \right) \left(\frac{\sigma_0}{250\ \mathrm{km\ s^{-1}}} \right)^2$$

This assumes that any dark matter is non-baryonic and unable to cool radiatively. Obviously, the total energy produced via this mechanism would be much higher if dark matter was baryonic. Dissipation of the binding energy of protostars is of a comparable order of magnitude (Djorgovski 1992).

AGN are a rare phenomenon and excluded by our definition of PGs, but they can easily outshine the combined light from all of the stars in a galaxy. Assuming a typical AGN luminosity to be $L_{AGN} \sim 10^{12}$ $L_\odot$, active over a lifetime $\tau_{AGN} \sim 10^8$ yr, we estimate the energy production of AGN over its lifetime to be:

$$|E_{AGN}| \sim L_{AGN} \cdot \tau_{AGN} \approx 1.2 \times 10^{61} \mathrm{erg} \left(\frac{L_{AGN}}{10^{12} \mathrm{L}_\odot} \right) \left(\frac{\tau_{AGN}}{10^8 \mathrm{yr}} \right)$$

Again, while it is possible that *all* PGs harbor AGN during some part of their formation stage, it is difficult to determine how much light from a galaxy is contributed by the non-thermal AGN and how much is contributed by any purely stellar population present. The equivalence of AGN and PGs was first suggested by Meier (1976), and further developed by Terlevich (1992, and references therein).

The main source of energy released in the formation of a PG comes from nuclear burning of hydrogen in stars. We assume that PGs form from gas with primordial abundances, and convert some fraction of their hydrogen (ΔX) into helium and metals ($\Delta Y + \Delta Z$). Using Pagel's (1993) estimate of $\Delta Y/\Delta Z \sim 4$, based on local, low-metallicity galaxies, we obtain $\Delta X = \Delta Y + \Delta Z = 5\Delta Z$. The bulk of the nuclear fusion energy is released in the formation of helium from hydrogen. The energy produced in the subsequent burning of helium into heavier elements is only a small fraction ($\sim 5\%$) of that generated by the production of helium, and can be neglected here. The efficiency of hydrogen burning is:

$$\epsilon = (4\mathrm{m_H} - \mathrm{m_{He}})/4\mathrm{m_H} = 0.007 \tag{1}$$

Assuming a total mass of stars to be $M_\star = 10^{11}\mathrm{M}_\odot$, and scaling to a metals production equivalent to half-solar metallicity yields:

$$E_{nuc} \sim \epsilon \cdot \Delta X \cdot M_\star \cdot c^2 \approx 6.3 \times 10^{61}\mathrm{erg} \left(\frac{M_\star}{10^{11}\mathrm{M}_\odot}\right) \left(\frac{\Delta Z}{0.01}\right) \tag{2}$$

To convert these energies into luminosities, we must also assume a timescale over which the energy is released. This can range from a free-fall or (local) starburst gas consumption time scale of $10^7 - 10^8$ yr, or a merger or cluster-crossing timescale of 10^9 yr, to gradual formation over a Hubble time, 10^{10} yr. Dividing a timescale for PG formation (t_{PG}) into the energy derived above yields:

$$L_{PG} \approx 2.0 \times 10^{45}\mathrm{erg\ s^{-1}} \left(\frac{M_\star}{10^{11}\mathrm{M}_\odot}\right) \left(\frac{\Delta Z}{0.01}\right) \left(\frac{10^9\mathrm{yr}}{t_{PG}}\right) \tag{3}$$

The luminosities thus derived range from $\geq 10^{12}$ $\mathrm{L}_\odot$, comparable to quasars or ultraluminous *IRAS* starbursts, to $\sim 10^{10}$ $\mathrm{L}_\odot$, similar to that of present-day normal galactic disks. The merging timescale leads to a luminosity of $\sim 5 \times 10^{11}$ $\mathrm{L}_\odot$ and an *average* star formation rate (SFR) of 100 $\mathrm{M}_\odot$ yr^{-1}. The peak SFR is

likely to be higher than this at some point during the formation of the PG. We adopt this luminosity and SFR as a reasonable estimate of what to expect from a PG.

2.1.2 Lyα Emission from Protogalaxies

Strong emission lines are expected in the spectra of actively star-forming galaxies, and are seen in nearby starburst galaxies. One of the strongest lines is expected to be the λ1215.7Å Lyα line. With the assumption that PGs were relatively free of obscuration by dust, the models by Partridge & Peebles (1967) suggest that several percent of the bolometric luminosity could be carried in the Lyα line.

One can make a simple estimate of the expected Lyα line flux by assuming a star formation rate ($\mathcal{R}_{SF}$) of 100 $M_\odot$ yr^{-1}, then using the $\mathcal{R}_{SF}$ to Hα conversion of Kennicutt (1983) and case B recombination (Lyα/Hα = 8.74, Brocklehurst 1971) we derive a Lyα line luminosity of:

$$L_{\mathrm{Ly}\alpha} = \mathcal{R}_{SF} \cdot (L_{\mathrm{H}\alpha}/1M_\odot yr^{-1}) \cdot (L_{\mathrm{Ly}\alpha}/\mathrm{H}\alpha)$$

$$\approx 2.45 \times 10^{43} h^{-2} \text{ erg s}^{-1} (\mathcal{R}_{SF}/100 M_\odot \mathrm{yr}^{-1}) \quad (4)$$

Where $h = H_0/100$ km s^{-1} Mpc^{-1}. This estimate of the Lyα line luminosity agrees well (for $h = 0.5$) with the stellar population synthesis models of Charlot & Fall (1993), who find $L_{Ly\alpha} \approx 8 \times 10^{41}$ erg s^{-1} for a 1 $M_\odot$ /yr star formation rate. The Lyα luminosity works out to be $\sim 1\% - 5\%$ of the total luminosity derived in equation 3 above, depending on the cosmology assumed, as predicted by Partridge & Peebles (1967). At $z \sim 4.5$, and for a range of standard cosmologies, the luminosity distance is $\sim 10^{29}$ to 10^{30} cm, which translates to an expected

observable Lyα line flux of $\sim 10^{-16\pm1}$ erg cm^{-2} s^{-1} , well within the limits of CCD imaging on 4m-class telescopes.

There are a number of other mechanisms by which Lyα photons can be produced, with supernova remnants (SNR) and AGN the largest contributors. Other sources of Lyα emission exist, such as Lyα cooling of the first protostars (Silk 1985). Charlot & Fall (1993), following the derivation of Shull & Silk (1979), find that for a reasonable IMF, the Lyα emission from SNR amounts to no more than $\sim 10\%$ of that produced by photoionization from massive stars. It is interesting to note, however, that SNR *could* be responsible for the weak C IV λ1549Å emission seen in some known Lyα objects such as the companions to the damped Lyα absorbers towards the quasars PHL 957 (Lowenthal et al. 1991) and QSO 0000−269 (Macchetto et al. 1993), where other indicators of an active nucleus (e.g., radio emission, polarization, rapid variability) are not present.

By virtue of their harder spectra, AGN can produce more Lyα emission than purely stellar populations. Without the underlying contribution to the continuum from massive stars, the equivalent width of the Lyα emission can easily exceed the maximum equivalent width from photoionization. Charlot & Fall (1993) find that for a reasonable range in the power law index, the equivalent width of Lyα can be in the range of 200Å to 600Å for AGN, while pure photoionization can only produce a maximum equivalent width of 200Å. While most luminous quasars have Lyα equivalent widths $\lesssim 200$ Å, their emission lines have velocity widths several times that expected from stellar populations in PGs.

2.1.3 Narrowband Imaging Technique

The probable presence of a strong emission-line signature in the spectra of PGs suggests an observing technique which takes advantage of this fact: narrowband imaging. The effectiveness of this technique has been demonstrated in the

discovery of Lyα luminous objects at high redshift, such as the companion to PKS 1614+051 (Djorgovski et al. 1985), and the companions to damped Lyα absorbers along the line-of-sight to PHL 957 (Lowenthal et al. 1991) and QSO 0000−269 (Macchetto et al. 1993).

There are several advantages to selecting objects through narrowband imaging. The sky background, *the* most significant limitation to the detection of faint objects in broadband data, is greatly reduced in narrowband images. Emission-line objects also appear relatively brighter in their emission lines than in their continuum. When imaging through a narrowband filter, the resulting increase in contrast can be quite significant. Charlot & Fall (1993) find that for their stellar population synthesis models with a constant SFR, reasonable IMF slopes, and an upper cutoff on the main sequence mass at 80 $M_\odot$, the rest frame equivalent width of the Lyα line would be $\sim$ 100Å. If this were observed through broadband (1000Å) and narrowband (20Å) filters at a redshift of 4.5, such an object would appear 3.1 magnitudes brighter through the narrowband filter than nearby continuum objects (relative to its appearance through the broadband filter)! Conversely, the continuum magnitudes for these PGs would be 3^m fainter than their narrowband magnitudes. The contrast enhancement, assuming equal fluxes from an emission-line object and a continuum object in the broadband filter, is given by the relation:

$$\frac{\mathrm{F}_{em}}{\mathrm{F}_{cont}} = \frac{B}{N}\left(\frac{W_r(1+z)+N}{W_r(1+z)+B}\right)$$

where W_r denotes the restframe equivalent width of the emission line at a redshift of z. N and B are the FWHM of the narrow and broadband filters, and the subscripts *em* and *cont* refer to the emission-line object and the continuum object. This demonstrates the power of the narrowband imaging technique.

Surveys specifically designed to uncover PGs, using narrowband imaging techniques similar to the one presented here, have been conducted by a number of

groups. For example, Pritchet & Hartwick (1987, 1990) have imaged blank fields at several different redshifts ($z = 1.9$, 4.2, 4.6, 5.2, and 5.7), while De Propris et al. (1993) surveyed fields centered between QSO pairs at $z = 2.2 - 3.3$. Parkes, Collins & Joseph (1994) attempt to detect Lyα redshifted into the the near IR J band ($z = 7.2 - 9.3$) on blank fields. A survey targeting known $z \geq 4$ QSOs, looking for quasar-marked protoclusters, is currently underway (Smith, Thompson & Djorgovski 1993).

Other search strategies for high-redshift PGs do exist. Deep Lyman-limit imaging, using a strategically chosen set of broadband filters, has been used by Giavalisco, Steidel & Szalay (1994) to discover a possible cluster of objects at $z = 3.4$, based on statistical arguments and similarity of colors to a spectroscopically-confirmed galaxy at that redshift. While this method does not rely on the presence of strong emission lines in the spectra of galaxies, it requires imaging of the galaxies in their continuum light. As argued before, this can be $\sim 3^m$ fainter than the corresponding narrowband magnitude, and thus would require very long exposure times. Deep spectroscopic surveys for high-redshift Lyα emission have been reported by Lowenthal et al. (1990) and Cowie & Hu (in Cowie 1988), as well as a survey in progress by two of the authors (DT & SD). This technique is complementary to the narrowband imaging surveys in that it probes a long baseline in redshift space, but only covers a small solid angle on the sky. Both techniques are able to reach similar line flux detection limits.

This paper presents a description of our Fabry-Perot (FP) narrowband imaging survey and the analysis techniques used in selecting candidate emission-line objects. Follow-up spectroscopy of the survey candidates will be presented in a later paper.

2.2 The Fabry-Perot Survey

2.2.1 Description of the Experiment

A number of high galactic lattitude blank fields were chosen with selection criteria designed to minimize interference from foreground objects. Large regions on the sky were found on the *IRAS* 100μm maps (Boulanger & Perault 1988) to have low extinction due to dust in our Galaxy, generally with $E_{B-V} \leq 0.05$. We restricted the fields to declinations near 34 degrees so that they would pass overhead at Palomar Observatory, minimizing the effects of atmospheric extinction. These large regions were then inspected on the POSS I survey plates, and a number of $\sim$10 arcmin square fields were chosen which were free of bright foreground galaxies, had no known galaxy clusters, and were generally free of stars brighter than 18th magnitude, both so that the CCD wouldn't saturate in our long exposures, and to minimize any reflections in the system.

Four spectral windows ($z = 2.80-2.98$, $3.27-3.45$, $4.42-460$, and $4.75-4.89$ for Lyα) were chosen to give good coverage in redshift space while avoiding the bright night-sky emission lines (Figure 2.1). The main advantage in choosing these windows is that they provide a relatively dark sky for observations from a light-polluted site like Palomar. Although we have taken data in all four windows, the majority of the data were obtained in the two highest redshift windows. Finding charts for all of the survey fields are presented in Figure 2.2. A summary of the FP observations on survey fields is given in Table 2.1.

2.2.2 Pointed Observations: Proof of Concept

As a test of this experiment's ability to detect line emission objects at high redshift, several pointed observations were made towards previously known line-emission targets. The observations are summarized in Table 2.2. These data were

processed in an identical manner as the survey data, described in detail in section 3. Two 3C radio galaxies were imaged in redshifted [O II] λ3727 emission: 3C265 and 3C368. Both of these $z \sim 1$ galaxies have extremely strong line emission, at least several hundred times the 1σ limiting line flux of the blank field survey. Both galaxies are well detected with exposure times less than that of the survey data. On-line and On-Off difference images of these two galaxies are presented in Figure 2.3.

3C265 ($z = 0.811$) appears to be an interacting pair or group of galaxies with one nucleus dominating the [O II] emission. We derive an integrated line flux of 1.1×10^{-14} erg cm^{-2} s^{-1} from our FP data, though this is likely to be an underestimate as the off-line images were shifted by less than a FWHM and thus contain a significant amount of [O II] emission. This is consistent with the spectroscopically determined line flux of 2.27×10^{-14} erg cm^{-2} s^{-1} (P. McCarthy, 1988).

3C368 ($z = 1.132$) shows extended [O II] emission strongly aligned with the radio axis (Djorgovski et al. 1987a). Our on-line observations of 3C368 were made at 7945Å, where the FP is poorly calibrated. Assuming a FWHM for the etalon of 30Å and a zero-point calibration similar to other observations taken on the same night, we derive an integrated [O II] emission-line flux of 5×10^{-15} erg cm^{-2} s^{-1} . Djorgovski et al. (1987a) find a line flux of 8.2×10^{-15} erg cm^{-2} s^{-1} . Uncertainties in the wavelength and FWHM calibration of the FP etalon at $\lambda \geq 7300$å can easily account for the difference.

In addition to the two [O II] galaxies, we obtained data on two Lyα emission-line objects at high redshift: PKS 1614+051, at $z = 3.218$, which has a strong Lyα companion; and MG 2016+112 a possible lens system at $z = 3.273$. Images centered on the redshifted Lyα line are presented in Figure 2.4.

The companion to PKS 1614+051 was discovered during a targeted search for companions to known high-redshift radio galaxies and quasars by narrowband

imaging in redshifted Lyα (Djorgovski et al. 1985, 1987b). This object has an integrated emission line flux of 8×10^{-16} erg cm^{-2} s^{-1} , determined from narrowband imaging (Hu et al. 1991), though earlier measurements found considerably higher flux (3×10^{-15} erg cm^{-2} s^{-1} from Djorgovski et al. 1985, 1×10^{-15} erg cm^{-2} s^{-1} from Hu & Cowie 1987, and 1.1×10^{-15} erg cm^{-2} s^{-1} from Steidel, Sargent & Dickinson 1991). We derive a Lyα line flux of 2.6×10^{-16} erg cm^{-2} s^{-1} from our FP data. While our low determination of the Lyα flux could be due to an inexact placement of the bandpass on the emission line, these five sets of data are consistent with the Lyα companion of PKS 1614+051 fading by a factor of 10 over the past decade, a result which should be verified with further observations.

MG 2016+112 is an interesting gravitational lens system, with the 3 main radio components also bright in Lyα (Schneider et al. 1986, 1987). Narrowband imaging by Schneider et al. (1986) also revealed two possible Lyα clouds similar to the PKS 1614 companion, though only one was confirmed spectroscopically. From our FP images, we derive an integrated Lyα line flux of 5×10^{-16} erg cm^{-2} s^{-1} for component A and 3×10^{-16} erg cm^{-2} s^{-1} for component B. These are a factor of 3 less than the fluxes derived from the broad and narrowband magnitudes given for this system in Schneider et al. (1986). The FP data were taken close to dawn, and the wavelength calibration was not verified immediately prior to the observations, so the low flux determined from the FP data could easily be accounted for by a mis-centering of the emission-line in the FP bandpass. Component C and the two additional Lyα clouds noted in that paper are not seen in our FP data, but they are slightly below the limit of our imaging based on their published magnitudes.

We thus conclude that Lyα-luminous, high redshift objects with Lyα fluxes comparable to those expected from PGs can be readily detected by our observing technique.

2.3 Observations and Reductions

2.3.1 The Blank Field Survey

2.3.1.1 Description of the Reduction Process

A total of 12 "datacubes" have been obtained on blank fields for this project, each datacube consisting of 6-11 images, or "slices," with slightly different central wavelengths. There are 11 independent data sets, with a repeat observation on one field and spectral window to help quantify the completeness and contamination issues. The nights were mostly clear or slightly hazy, with non-photometric but steady conditions. All datacubes have been searched and candidates emission-line objects chosen. The follow-up spectroscopy is in progress.

The observations consisted of a nightly bias frame and dome flatfield frames taken at each of the etalon settings used in acquiring the survey data, as well as the datacubes on the target fields and standard stars. In some cases, two passes through the datacube were made on survey fields, both to increase the total exposure time and to aid in the removal of cosmic rays. Exposures on the sky were of sufficient length to ensure that the noise was dominated by photon statistics. The etalon's bandpass was stepped by 10-15% less than the FWHM between successive exposures because of the triangular bandpass of the FP etalon (Appendix A).

The data were initially bias subtracted and flatfielded following standard reduction procedures using the VISTA (Stover 1988) and FIP (Djorgovski, private communication) data reduction software packages. Significant gradients across the chip, at the 10% level, remained after the initial flatfielding, most likely due to differences in the illumination pattern of the chip between the dome flats and the night sky. In addition, these residual gradients varied considerably from frame

to frame, making it necessary to correct for them individually. This was accomplished by binning the images and interpolating over the galaxies and stars visible in each frame, then smoothing to destroy any residual pixel-to-pixel information. The resulting gradient images were then rebinned back to the original scale and used to correct the domeflats and re-flatfield the data. The resulting variations in the sky level were typically less than 1% over the entire chip. Local variations on the scales relevant to this PG search were much smaller.

After flatfielding, the images were cleaned of cosmic rays and hot pixels, shifted into coincidence at the sub-pixel level, sky subtracted, and chopped to include only the overlap region of all images in a given datacube. Images not taken in 2×2 binning mode were also binned and data taken in two passes through a datacube were added together. Candidate selection was performed on these resulting images (see section 3.1.2 below).

To calibrate the data onto the AB_{79} system (Oke & Gunn 1983), we used exposures of the spectrophotometric standard stars BD +17°4708, BD +26°2606, and HD 84937 (Oke & Gunn 1983), Hiltner 102, Feige 15, Feige 25, Hiltner 600, Feige 34, Feige 56, BD +25°3941, and BD +28°4211 (Stone 1977), and Feige 67 (Massey et al. 1988). Typically, at least one exposure of a standard star in each slice of a datacube was available.

Finally, calibrations were corrected for small fluctuations in the stability of the atmosphere by normalizing the average response of the system to several of the bright, unsaturated stars in each datacube to a flat spectrum. These corrections were typically less than ±10%. Zero point fluctuations in the flux calibrations, estimated from multiple exposures of standard stars at any given etalon setting, are also estimated to be ±10%.

2.3.1.2 Selection of Candidates

Three different methods of candidate selection were tried: an automatic search algorithm, based on a flux-threshold requirement within some aperture; blinking, where we inspect images on the workstation monitor while rapidly switching between adjacent pairs of images in a datacube; and continuum subtraction (CS), where each slice of a datacube is inspected on the workstation monitor after having subtracted the average of the remaining images in the datacube. The search algorithm was not sophisticated, and tended to find an unreasonably large number of candidates if the threshold was set too low. Since the brighter candidates were easily recovered with all 3 methods, the algorithm search was not used for the final survey. Of the remaining 2 methods, CS appeared to be slightly more thorough at recovering faint candidates than the blinking method. It proved relatively simple to train the neural-network of the brain to reject obviously false detections such as single-pixel events, bad columns, and reflections, which kept the number of candidates down to a reasonable level.

Continuum images were constructed by averaging all but one of the slices in a datacube, with a slight rescaling as necessary to allow the majority of the brighter objects to be well-subtracted or slightly over-subtracted. We did not find it necessary to convolve the data to the same seeing as the seeing did not vary much over the majority of the data. For those data with seeing variations, it was found that while the brighter star images left residuals on continuum subtraction, the fainter stars and galaxies subtracted out fairly well.

These continuum subtracted images were then inspected on the workstation monitor for objects which show some residual flux. Any and all reasonable objects which show this emission-line signature were noted and added to the list of initial candidates. In general, candidates were not selected if they appeared to be considerably smaller than the seeing FWHM (i.e., cosmic rays or hot pixels which were missed in the cleaning process) or were introduced by the continuum subtraction

process (negative peaks in the continuum image appear as positive peaks in the CS image). Typically, this method found from 50 to 130 candidates per datacube (5-15 objects per slice).

These initial candidates were then numbered, and their pixel-coordinates on the sky noted. The original flatfielded data were then inspected and candidates were removed from the list if they were at or very near the position of a cosmic ray, hot or cold pixels, or bad columns in the appropriate slice of the datacube. Despite the careful removal of such bad pixels before candidate selection, as many as 20 objects were deleted from the list for each datacube. Candidates were also dropped if they were at the position of a reflection of one of the brighter stars in the field. If two images in a given slice (with the same λ_{cent}) were available, then these were also checked for inconsistencies such as a candidate appearing relatively bright in one of the images and not detected in the other, though allowances were made for variations attributable to changes in seeing or sensitivity. 5–20 candidates were deleted from the list for this reason, which suggests that the contamination from random events is not insignificant at the faint levels to which we were trying to work, and that a larger fraction of the fainter candidates in the data for which we have only one pass through the datacube are likely to be false detections.

A flux-calibrated Fabry-Perot spectrum (Figure 2.5) is extracted for each candidate and all objects for which the flux in the emission-line slice falls below the 1σ level are immediately rejected. Datacube images consisting of small subregions of each slice centered on the objects and reassembled into one image are extracted for all of the remaining candidates (Figure 2.6). These images were then inspected as above and dropped from the list of candidates if any inconsistencies between the datacube and spectrum were noted. The 12-30 most interesting or obvious emission-line objects are selected as the "final" list of candidates, which makes up the input list of targets for follow-up spectroscopy.

We note that reference to deep broadband images has not been used to this point in the selection of candidate objects. Experience with the Palomar spectroscopy has shown us that most of the obvious emission-line objects detected in this survey are likely to be nearby galaxies detected through their [O II], [O III], or Balmer emission. This is easily determined from the broadband data as well, as the colors and morphology of the galaxies are consistent with their being at a redshift of a few tenths. True PGs at the high redshifts probed by this survey, with the bulk of their energy derived from star formation, would be expected to have continuum magnitudes well below the depth of our continuum imaging. As shown in the introduction, reasonable assumptions for what a PG might look like would mean that a PG detected at 23^m in our narrowband data would have a continuum magnitude of $\sim 26^m$.

In principle, this could be used to bias the survey towards finding high-redshift objects by omitting all of the brighter candidates from the list. In practice, there are usually only a few of the brighter objects per frame, and it is helpful to have at least one probable emission-line object included in the multi-slit observations to verify that the targets were indeed properly located on the slits. Thus, all selected emission-line objects remain as plausible targets for follow-up spectroscopy.

2.3.1.3 Calibration of Detection Limits

The program which extracts out the Fabry-Perot spectra of the candidate objects also randomly selects 2000 pixels in each slice of the datacube and extracts out and calibrates the flux in 3 different apertures (9, 21, and 37 pixels in area, or 3.5 to 23.7 square arcsec, depending on the pixel scale). Sigma is evaluated from the quartile points (Q25 and Q75, defined as those values in a distribution for which 25% and 75% of the data are below that value, Q50 would be the median) and is defined as 0.7415(Q75−Q25). This robust, nonparametric method of estimating sigmas is equal to sigma for a Gaussian distribution.

Tests on the survey data similar to the methods described in Howell (1989) indicate that the optimal aperture to use in determining the flux from an object (maximizing the SNR, as the eye does in the original candidate selection) is 1.5–2 times the seeing FWHM. Figure 2.7 presents the results of these tests on data spanning a range of seeing (1.3-2.2 arcsec) in which the photometry as a function of aperture on a number of faint objects in a given frame was extracted, normalized, and averaged to yield a single curve per image. Also plotted is a continuous model based on a Gaussian PSF and Poissonian noise from the object and the sky; both dark current and readout noise were assumed negligible.

It should be emphasized that there is a distinction between an aperture used for optimal detection and that used for minimum bias in the extracted flux. Generally, optimal detection is made on a smaller aperture than would be used for photometry, as the candidates are most easily selected from their high SNR cores. These cores are generally less than or equal to the seeing FWHM. Minimum bias is attained by using a larger aperture, including the flux from the wings of the PSF. For a Gaussian PSF, 94% of the flux is contained within an aperture of diameter 2×FWHM. One would lose slightly more flux from extended objects if a fixed aperture was used, so the photometry for obviously extended objects was extracted in larger apertures as necessary. No aperture corrections were made to the data in this survey since we are simply trying to detect PG candidates.

The actual noise limits set for this survey are those calibrated in the aperture which is twice the seeing FWHM. The areas covered have been modified to exclude the corners of the fields with the worst vignetting and a 1% correction for known bad columns, hot pixels, and cosmic rays. In addition, the flux limits for the 1989 data outside of a 3 arcminute diameter circle are increased by a factor of 1.2, determined empirically on the data, to account for the lower signal due to the vignetting.

2.3.1.4 Completeness and Contamination Tests

To measure the completeness in this survey, we constructed a fake datacube which had similar noise characteristics as the real survey data. This datacube was then populated by a random assortment of continuum and emission-line objects and processed through the same candidate selection procedures as the real data. The model images were 400 pixels square with an assumed image scale of 0.8 arcsec/pixel (identical to the 1989 survey data), and 1.6 arcsec seeing (2 pixels FWHM). A total of 8 images were generated. The observations were also assumed to be in the 711nm survey window and have an exposure time of 800 seconds per slice for calibration purposes.

The 1σ noise in a 4 arcsecond aperture calibrated out to be 3.5×10^{-17}erg cm^{-2} s^{-1} , which is comparable to the survey data. All of the modelled sources were stellar, no resolved test objects were included. The noise limits for extended objects scales linearly with aperture (square-root of the number of pixels contained in the aperture), and are expected to be no more than a factor of 2 worse for galaxy-sized objects at high redshift. Figure 2.8 shows the percentage of the test objects recovered as a function of their input flux. The survey should be about 90% complete at approximately the 3σ level. All objects brighter than 5σ are recovered, while very few objects near the 1σ level ($\sim$5%) would be recovered. It is important to note that of the 66 objects deleted from the initial candidate list for various reasons, only 2 were actual test objects! This demonstrates that the eye is a good discriminator between real objects and noise, even at faint levels.

As a test of our flux extraction and calibration procedure, we also compare the recovered flux to the modelled input flux of our test objects (Figure 2.9). The majority of the objects above the 3σ limit have a recovered flux within $\pm$12% of their input fluxes. Note, also, that a fair number of objects are recovered *below* the 3σ level, though these are dominated by the objects scattered by the noise to higher detected fluxes than were modelled.

Contamination of the final candidate object list by spurious detections of random noise fluctuations is much more difficult to quantify. The number of spurious detections, expressed as a percentage of the real objects recovered, depends heavily on the luminosity function assumed. As no luminosity function exists for Lyα luminous galaxies at high redshift, interpreting the data in this manner has no physical meaning. In Figure 2.10 we present the number of excess counts as a function of their flux. As the number of real test objects and spurious detections is somewhat higher than the corresponding numbers in the survey data, the relevant points to note are that no spurious detections occurred above the 5σ level, and that the excess counts peak somewhere between the 2σ and 3σ level.

A repeat observation was obtained on the FP 0031+23 field to help quantify these completeness and contamination issues. While none of the candidates in the 1989 data were recovered in the 1993 data, this is consistent with the noise limits and completeness estimates as there are only ~ 10 candidates which overlap, all with fluxes $\lesssim 3\sigma$.

2.3.2 Spectroscopic Follow-up: Initial Results

Some spectroscopic follow-up on FP candidate emission-line objects has been performed at Palomar Observatory. Combining this with deep broadband imaging seems to indicate that the candidate objects fall into two main groups: a "bright" group, where the emission line detection is almost certainly real, and a "faint" group, which look promising on the basis of the FP data, but which have no strong detection in the broadband data. The majority of the objects in the latter group tend to have line fluxes from the FP data which are only $1-3$ times the 1σ noise limit, and therefore are not high priority for follow-up spectroscopy.

Example long-slit spectra of eight of the objects with confirmed FP emission lines are presented in Figure 2.11. These have so far all turned out to be relatively

low-redshift emission-line galaxies or AGN, detected by the FP through their [O III], or Balmer emission. The broadband imaging is sufficient to reject these objects as high-redshift PGs, as they all look like galaxies on the CCD image and have colors consistent with their being at low redshift.

We are continuing the spectroscopic follow-up of our FP candidates, using the multi-slit capabilities of the LRIS spectrograph on the Keck telescope. We hope to obtain spectra of all candidates with emission-line fluxes $\geq 3\sigma$, with additional faint candidates included as space on the slit masks allow. Results will be presented in a future paper.

2.4 Results and Discussion

2.4.1 Limits on High-z Protogalaxies

While no obvious population of Lyα emission-line objects at high redshift have been confirmed so far, only a small fraction of the total number of candidates have been followed-up spectroscopically. We can set some significant limits on Lyα-luminous objects at high redshift, assuming that none of our candidates are true PGs. Figure 2.12 presents a limiting surface number density vs. line flux plot of the limits attained in this survey, along with those of a number of other recent PG surveys based on the Lyα line. For surveys which imaged the same field through multiple filters (Parkes et al. (1994), this work), each image was treated separately since they probe different volumes of space. A number density vs. flux plot is primarily useful as a first-order comparison of different surveys, but does not contain any redshift information.

The PG parameter space is perhaps more thoroughly described by the 3 coordinates of comoving volume density, limiting restframe line luminosity, and redshift. Transformation from surface density on the sky to comoving volume density naturally takes into account the different filter widths used in narrowband surveys, though the redshift axis still needs to be retained in order to fully describe the parameter space. This is evident if one considers that recent PG surveys have covered a range in redshift spanning 1.9–9.3! Projections of the relevant limits onto the comoving volume density vs. limiting restframe Lyα luminosity plane are presented in Figure 2.13. For comparison, a number of other Lyα-based PG surveys are plotted, with their published limits transformed to an $H_0 = 75$ km s^{-1} Mpc^{-1}, $\Omega_0 = 0.2$ cosmology and with 1σ limits determined within an aperture twice the seeing FWHM, the standard adopted in this work. Also plotted is a model Lyα emission line luminosity function which is an integral of the $z =$

0 Schechter function (i.e., assuming no density evolution), with a normalization appropriate for spheroids today: $\phi^* = 0.004h^3$ and $\alpha = -1.25$ (Baron & White 1987). We also assume a characteristic luminosity of $L^*_{Ly\alpha} = 2.45 \times 10^{43} h^{-2}$ erg s^{-1}, as given by equation 4 and corresponding to an unobscured star formation rate of 100 $M_\odot$ yr^{-1}.

This survey covers a significantly larger comoving volume and to deeper levels than the majority of previous PG surveys based on the Lyα emission line. The survey by Pritchet & Hartwick (1990), which is comparable to this work, is centered at $z = 1.9$ and thus probes a different region of the parameter space. Several surveys reach fainter flux limits than this work (Lowenthal 1991, Møller & Warren 1993, and Wolfe et al. 1992). All three are targeted surveys on damped Lyα absorbers, and thus trade volume surveyed for depth. No obvious population of Lyα luminous primeval galaxies has been detected in any of these PG surveys so far, although a number of candidates from this work still require follow-up spectroscopy.

2.4.2 Dust Obscuration

Perhaps the most obvious explanation for the current lack of success in identifying a population of PGs is that the formation of spheroids and ellipticals was an inherently dusty process. Theoretically, multiple resonant scatterings of Lyα photons in a dusty environment can quench this strong emission line. The evidence for dust extinction in star-forming and high redshift galaxies is somewhat conflicting.

Locally, star-forming dwarf galaxies do not seem to show much Lyα emission, despite being UV-bright and fairly low metallicity (Meier & Terlevich 1981, Deharveng et al. 1985, Hartmann et al. 1988), but some do (Terlevich et al. 1993, Calzetti & Kinney 1992), where case-B recombination levels of Lyα were recovered from the observed Balmer decrement. The real situation is likely to be

more complex than simple extinction by dust. Valls-Gabaud (1993) suggests that shortly after a burst phase terminates and the most massive stars die, Lyα absorption in cooler stars can overwhelm the Lyα emission. Calzetti, Kinney & Storchi-Bergmann (1994) find evidence for emission-line extinction *in addition* to that inferred from adjacent continuum regions! It is unclear, however, if one can extrapolate with any certainty from low-redshift dwarfs to high-redshift massive galaxies.

One spectacular example of a dusty object at high redshift is FSC 10214+4724 (Rowan-Robinson et al. 1991, $z = 2.286$). Despite its huge far-IR luminosity of 3×10^{14} $L_\odot$, and an inferred dust mass of $10^9 - 10^{10}$ $M_\odot$, this object does show weak Lyα emission. The presence of high-ionization lines in the spectrum and strong polarization suggest that FSC 10214+4724 harbors a quasar in its nucleus (Jannuzi et al. 1994, Elston, et al. 1994), and thus would not be considered a PG by our definition. In addition, deep narrowband surveys for Lyα emission from damped Lyα absorbers at high redshift have yielded negative results (Wolfe et al. 1992, Møller & Warren 1993, Lowenthal et al. 1991, Macchetto et al. 1993), generally attributed to dust extinction.

On the other hand, several tens of $z > 2$ Lyα-bright objects are known in the form of radio galaxies. While these objects also do not meet our definition of a PG, the active nucleus lives within a galaxy which does not appear to contain large quantities of dust (P. McCarthy 1993). An important point to consider is that complete radio surveys have not uncovered any examples of dusty RGs similar to FSC 10214, which suggests that dust may not be too prevalent at high redshift.

If PGs were dusty, and similar to the ultraluminous *IRAS* starbursts we know at $z \approx 0$, then the UV light from massive stars would be processed into the restframe IR at $\lambda \sim 100\mu$m (Kormendy & Sanders 1992). If the bulk of galaxy formation took place at high redshifts, then the processed energy would be redshifted into the submillimeter and millimeter regimes and appear as deviations

from a smooth blackbody on the cosmic microwave background (CMB) spectrum. The COBE satellite's FIRAS instrument has set limits on the maximum deviations allowable in the CMB at $\lesssim 0.03\%$, with an r.m.s. scatter of $\approx 0.01\%$ (Mather et al. 1994). Since the CMB radiation has an energy density of 4.25×10^{-13} erg s^{-1}, this sets an upper limit on the energy density fluctuations in the submillimeter background (SMB) of $u_{SMB} \lesssim 5 \times 10^{-17}$erg s^{-1}.

We can estimate the energy contribution to the SMB expected from dusty PGs at a redshift of formation of z_{PG}. Following the derivation for equation 2, and taking $\Omega_\star \rho_{crit}$ to be the baryonic mass in the universe converted into stars, we have:

$$u_{PG} = \epsilon \cdot \Delta X \cdot (\Omega_\star \cdot \rho_{crit}) \cdot c^2 \cdot (1 + z_{PG})^{-1}$$

$$\approx 5.9 \times 10^{-15} \left(\frac{\mathrm{erg}}{\mathrm{cm}^3}\right) h^2 \left(\frac{\Omega_\star}{0.01}\right) \left(\frac{\Delta Z}{0.01}\right) \left(\frac{10}{1 + z_{PG}}\right) \qquad (5)$$

where ϵ is given by equation 1 and ΔX and ΔZ are as in equation 2. The $(1 + z_{PG})^{-1}$ term represents the energy lost in expansion of the universe from z_{PG} to now. Comparing equation 5 to the *COBE* limits, one can see that *at most* a few percent of the energy released in primordial starbursts was reprocessed by dust. This is perhaps the strongest constraint that can be placed on dusty galaxy formation at high redshifts. A similar derivation is given in Blain & Longair (1993), who obtain limits comparable to our estimate here. However, whereas fully obscured PGs may be ruled out by the *COBE* data, even a slight amount of obscuration could greatly attenuate the Lyα emission from PGs.

2.4.3 Other Explanations

Another possible explanation for the lack of detection of a population of PGs is that galaxies do not spend much time in their Lyα-bright phase. The burst models of Charlot & Fall (1993) show strong Lyα emission for only $\sim 4 \times 10^7$ years, after which the most massive stars have evolved off of the main sequence and the majority of the UV radiation is provided by cooler stars with atmospheric Lyα absorption (see also Valls-Gabaud 1993). The Lyα line does recover somewhat, after $\sim$ 1 Gyr, when the central stars of planetary nebulae outlive their envelopes. While the equivalent width of the Lyα line at this stage is rather large ($\geq$ 200Å), the absolute luminosity is 2 to 4 orders of magnitude less than during the initial burst. It should be noted that Charlot & Fall use an extreme case of a burst for their model, with 10^{11} $M_\odot$ of stars being produced with an e-folding time of only 10^7 yr. If this is the case, then PGs spend only $\sim$ 1% of their lifetime in a Lyα-bright phase.

It is also possible that the Lyα-bright stage in the formation of massive bulges and ellipticals occurred at even higher redshifts than are accessible to optical CCD-based surveys. Lyα enters the J band at $z \sim 8$. Again, with the development of large-format IR arrays, such surveys can better probe the relevant parameter space. Such a survey was recently published by Parkes, Collins & Joseph (1994).

Active nuclei may be a natural phase in the formation of all massive galaxies (Haehnelt & Rees 1993, Small & Blandford 1992), with the active phase developing quickly and outshining any photoionization signature from a starburst. Kormendy (1993) summarized the kinematical evidence for the presence of quiescent supermassive black holes in the nuclei of several nearby galaxies. If indeed every young elliptical or bulge undergoes an immediate AGN phase, then perhaps PGs have already been discovered in the form of quasars and radio galaxies (Meier 1976, Djorgovski 1988).

If clustering was important at high redshifts (Wolfe 1993b, Djorgovski, Smith & Thompson 1991), then the blank field surveys would, on average, look between the clustered PGs. This could possibly account for the current lack of PGs in unbiased field surveys. Targeted surveys now in progress may soon cover sufficient volumes to detect clustered PGs (Djorgovski, Thompson & Smith 1993, Smith, Thompson & Djorgovski 1993).

2.4.4 Options for the Future

If PGs were at least slightly dusty, then one option for future PG surveys would be to base them on the oxygen or Balmer emission lines considerably redward of Lyα and thus much less subject to extinction by dust. These lines are shifted into the near infrared for redshifts less than 5.5 (which places [O II] λ3727 at the red edge of the K band window), where the new IR arrays are making such surveys feasible. This has been discussed in more detail by Thompson, Djorgovski & Beckwith (1994), and surveys along these lines are currently under progress by at least two groups (S. Djorgovski & M. Pahre, private communication; S. Beckwith, private communication; see also Mannucci, Beckwith & McCaughrean 1994).

Optical surveys for PGs based on unobscured Lyα emission have now extensively probed the relevant parameter space over the redshift range $1.9 \leq z \leq 5.5$. If interpreted directly, the current limits are in conflict with simple models of galaxy formation. Dust remains the most-likely explanation for the lack of detection of Lyα-luminous PGs, although other explanations remain viable. In any case, the near-IR may be the next great frontier for PG surveys.

2.A Appendix – The Fabry-Perot Camera

A special low-resolution Fabry-Perot imaging camera was constructed for this survey. It was designed to cover the optical region with about 1000 km s^{-1} resolution for Lyα in our survey windows. The camera uses a standard reimaging system with the etalon in the parallel beam, and will not be covered in detail here. There were, however, several quirks we ran into during the course of this project which would be worth mentioning. A scanning Fabry-Perot interferometer was chosen over individual narrowband filters to maintain flexibility and access to the entire visible spectrum. The reader is referred to any standard text on geometric optics for a detailed discussion of the theory behind the operation of Fabry-Perot etalons.

The current reimaging system is comprised of the collimator from the old PFUEI camera (Gunn & Westphal 1981), a 135mm f/2 Xero Nikkor lens, and an off-the-shelf Nikkor 105mm f/1.8 telephoto camera lens (replacing a 58mm UV Nikkor), both with standard broadband antireflection coatings which restrict the useful range of the camera to 4000-7500Å (Nikon technical representative, private communication). To eliminate light loss associated with reflection off of the secondary mirror, the reimaging system is mounted at the prime focus of the Hale 200-inch telescope at Palomar Observatory with the Wynne corrector, giving a final image scale of 15.04 arcsec/mm (0.36 arcsec/24μm pixel).

A Queensgate Ltd. piezoelectrically-driven Fabry-Perot etalon was obtained for this project. It has broadband coatings suitable for use across the range of this survey (4500-7300 Å, see Figure 2.14). The filter's nominal 4μm spacing was designed to give a resolution of about 1000 km s^{-1} in the restframe for Lyα in the higher redshift survey windows (Figure 2.15). Variations of the phase-shift of the light on reflection from the dielectric mirrors of the etalon as a function of wavelength are responsible for the variations in resolution (14 - 48Å), finesse (20

- 30), and free spectral range (500 - 900Å) of the system. Characteristics of the four blocking filters obtained for this project are listed in Table 2.3.

The optical axis of the system passes through the etalon at normal incidence. Reflections are present in the images, caused by an autocollimation reflection of a stellar image between the CCD and the back reflective surface of the etalon. These reflections have been measured at 4.4 magnitudes fainter than the primary image, and directly across the optical axis of the system. Since both their positions and magnitudes are easily determined, it was decided to keep the system calibration simple by retaining normal incidence through the etalon.

Due to the fast optics used at prime focus and the wide field covered by this imager, there is a considerable shift in the central wavelength of the bandpass (λ_{cent}) as one moves off axis, amounting to ~ 30Å at the edge of the field of view. This should have no significant effect on the results of a blank-field survey such as the one reported on in this paper, as only small shifts on the sky were made between images in a datacube. No thermal control of the etalon was implemented on the imager, and shifts in λ_{cent} attributable to temperature and/or humidity changes were noted, but were generally ≤ 5Å. For observations targeting a known emission line, the laboratory calibration of the etalon was verified by observing either a low-pressure sodium dome light or a planetary nebula, scanning the etalon bandpass through the peak of the emission line. The offset $\Delta\lambda_{(\mathrm{sky-lab})}$ thus obtained was then applied to the laboratory calibrations for the duration of the observations of that target.

It should be noted that the transmission function for a standard Fabry-Perot etalon is an Airy function (Figure 2.16), basically triangular near the peak, following a $[1 + \mathrm{Fsin}^2(\delta/2)]^{-1}$ curve (Hecht 1987) where F is related to the reflectivity of the etalon plates (here $\sim$121), and δ is the phase difference between adjacent rays. This is different than the usual rectangular-bandpass filters normally used. The main consequence of this is that an off-center line would be detected as fainter

than an equivalent, centered line. For this reason, the filter is stepped by slightly less than a FWHM between individual images (slices) in the datacubes for this survey. Also, a line which is a full FWHM offcenter still transmits 25%, so a strong line centered in one slice's bandpass would still be detected in the adjacent slices. For a continuum source, the extended triangular wings of the passband effectively pass the same number of photons as a rectangular bandpass filter of the same FWHM.

Three different CCDs have been used with this imager to obtain the survey data. Originally, a JPL TI 800^2 CCD (0.4 arcsec/pixel unbinned, April 1989 to December 1989), and then a JPL *Craf/Cassini* 1024^2 CCD (0.313 arcsec/pixel unbinned, March 1991 only) were used with the 58mm camera lens. Neither of these chips were especially sensitive in the blue, so survey data taken with these CCDs was restricted to the two high-redshift survey windows. The instrument was updated with the 105mm camera lens when a blue-sensitive, thinned, backside-illuminated TEK 1024^2, 24μm pixel CCD (0.361 arcsec/pixel unbinned, November 1992 on) became available at Palomar Observatory. In all cases, the useful field of view of the camera is $\sim$5.5 arcminutes square.

The system has an excellent total throughput (atmosphere through detector), summarized in Table 2.4. The total QE of the system agrees well with calibrations using standard star exposures taken on clear nights. The quantum efficiency of the CCD is where the most improvement remains to be made, though the use of custom optics could also improve the total throughput at a considerable increase in cost.

TABLE 2.1: Blank-Field Observations

Field	RA (1950.0)	Dec	UT Date	λ_{cent} (Å)	See (")	t_{exp} (s)	Bin
0031+23	00 31 30	+23 35 00	1989 Sep 05	7110	1.3	2×8×500	1×1
0031+23	00 31 30	+23 35 00	1993 Sep 24	7110	1.5	2×6×600	1×1
0738+34	07 38 25	+34 41 00	1992 Nov 21	4740	2.2	8×800, 8×700	1×1
1027+33	10 27 30	+33 30 00	1989 Dec 30	6710	2.9	2×11×600	2×2
1254+34	12 54 15	+34 28 00	1989 Apr 29	7110	1.6	8×1000	1×1
1333+30	13 33 05	+30 01 00	1989 May 01	6710	2.4	11×800	2×2
1333+30	13 33 05	+30 01 00	1991 Mar 12	7110	1.4	8×800	1×1
1454+34	14 54 40	+34 09 00	1989 Apr 30	7110	2.6	8×1000	2×2
1606+34	16 06 40	+34 53 00	1989 Apr 29	7110	1.6	8×1000	1×1
1623+34	16 23 25	+34 53 00	1989 May 01	6710	2.1	11×800	2×2
1656+33	16 56 25	+33 58 00	1989 Apr 30	7110	2.2	8×800	2×2
1656+33	16 56 25	+33 58 00	1993 Jun 10	5140*	1.6	6×800, 6×600	1×1

* Observations obtained using a standard Gunn g blocking filter.

TABLE 2.2: Pointed Observations

Field	UT Date	λ_{cent} (Å)	See (")	t_{exp} (s)	Bin
PKS 1614+051	1993 Jun 10	5125[1]	1.8	600 on, 600 off	1×1
MG 2016+112	1993 Jun 10	5192[1]	1.4	800 on, 600 off	1×1
3C265	1989 May 01	6750	1.6	700 on, 3×400 off	2×2
3C368	1989 Sep 05	7945[2]	1.7	3×300 on, 4×300 off	1×1

[1] Observations obtained using a standard Gunn g blocking filter.

[2] Observations obtained using an RG-9 blocking filter.

TABLE 2.3: Blocking Filters

Filt	FWHM (Å)	λ_{start} (Å)	λ_{end} (Å)	z(Lyα)
474	300	4600	4900	2.78 - 3.03
531	260	5180	5440	3.26 - 3.47
671	280	6580	6860	4.41 - 4.64
711	300	7000	7300	4.76 - 5.00

TABLE 2.4: System Throughput

	λ_{cent} (nm)			
Element	474	531	671	711
Fabry-Perot				
Blk Filter	0.73	0.80	0.79	0.77
Collimator	0.89	0.93	0.90	0.87
Etalon	0.85	0.85	0.85	0.85
Camera	0.89	0.93	0.90	0.87
Subtotal	0.49	0.59	0.54	0.50
CCD				
CCD Window	0.99	0.99	0.99	0.99
CCD QE	0.45	0.49	0.61	0.53
Subtotal	0.22	0.29	0.33	0.26
Telescope				
1° Mirror	0.80	0.80	0.80	0.80
Wynne Corr	0.96	0.96	0.96	0.96
Subtotal	0.17	0.22	0.25	0.20
Atmosphere	0.81	0.85	0.92	0.97
Total	0.14	0.19	0.23	0.19

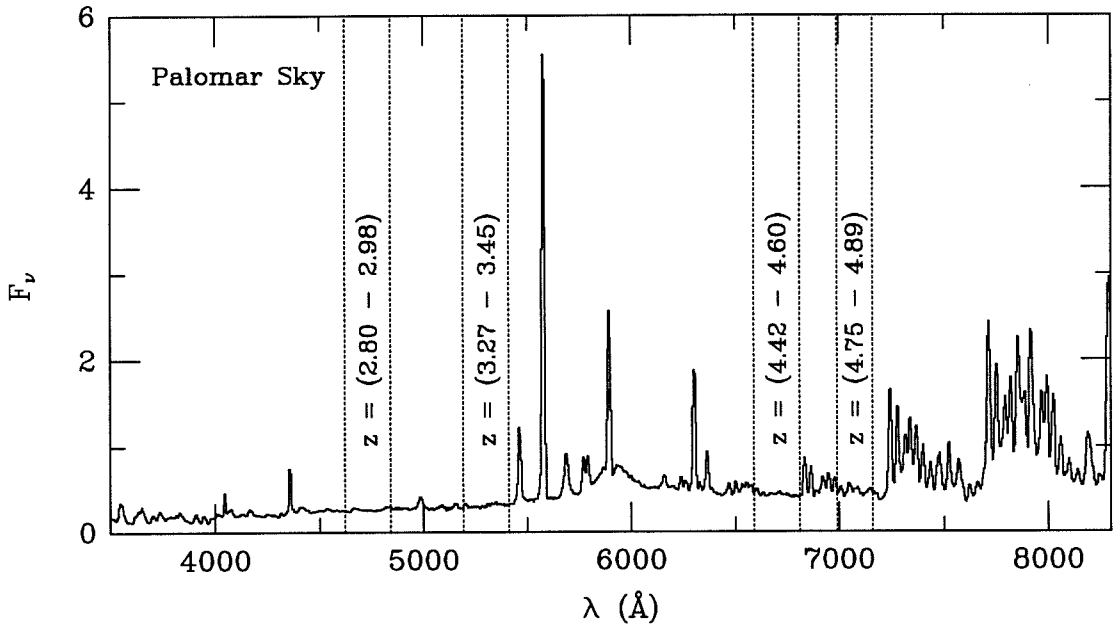

Figure 2.1: Fabry-Perot Survey Windows

The four spectral windows used in the Fabry-Perot survey are shown superimposed on a spectrum of the night sky from Palomar Observatory. The windows were chosen to avoid both natural and man-made emission-line features, and are labelled with the corresponding redshift ranges for the Lyα line. The flux scale is in arbitrary units.

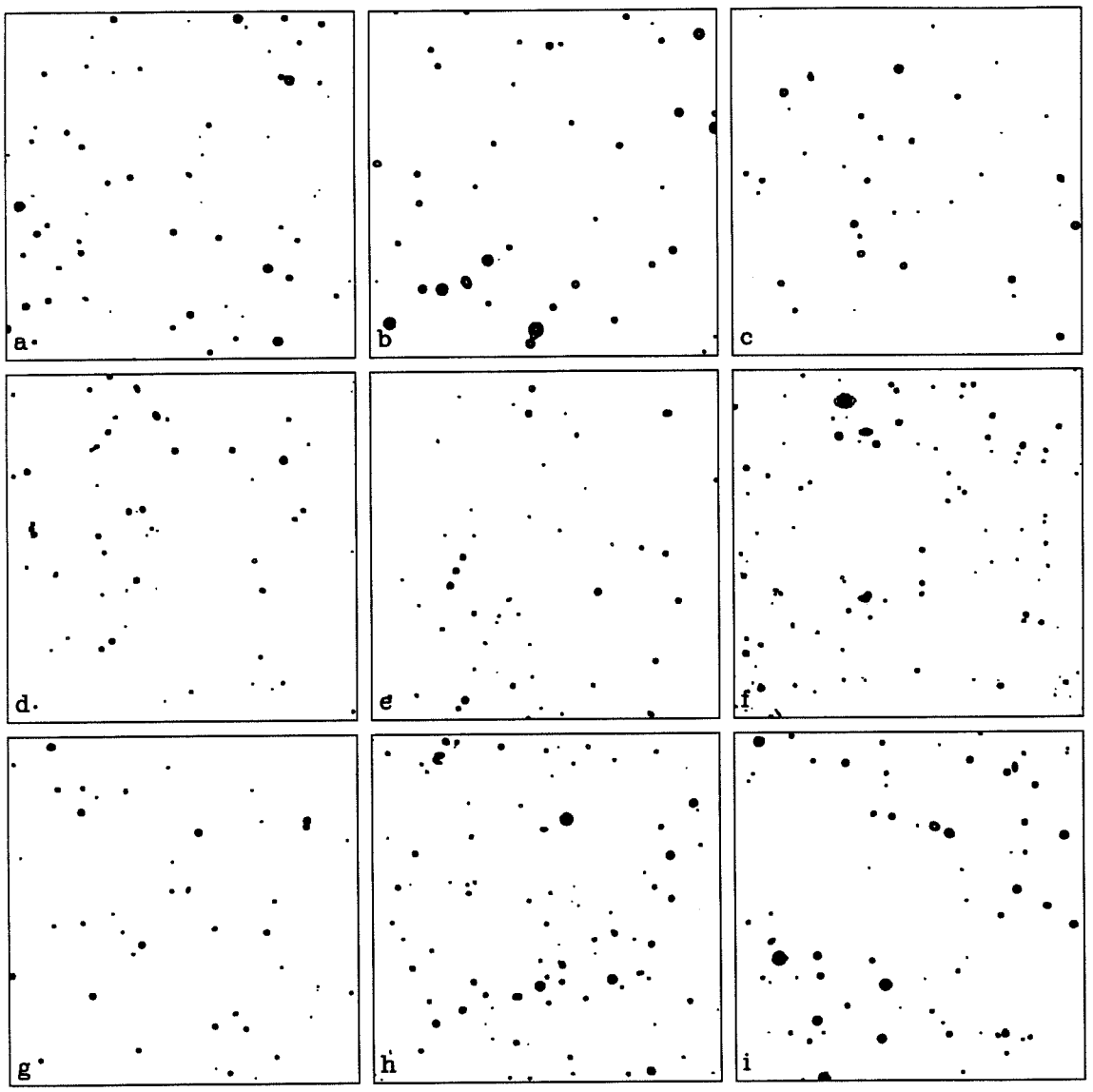

Figure 2.2: The Fabry-Perot Survey Fields

Finding charts for the 9 blank fields imaged in this survey. All fields are 4.5 arcmin square, centered on the survey data. North is up and east to the left, with the exception of FP0738, which has the coordinate system rotated 9.7 degrees clockwise from the other images. The fields are labelled in the lower left corner of each plot, and are identified as: a) FP0031, b) FP0738, c)FP1027, d) FP1254, e) FP1333, f) FP1454, g) FP1606, h) FP1623, and i) FP1656. Note that these plots are not contoured down to the noise, all plotted objects are real and these finding charts are presented here for field identification.

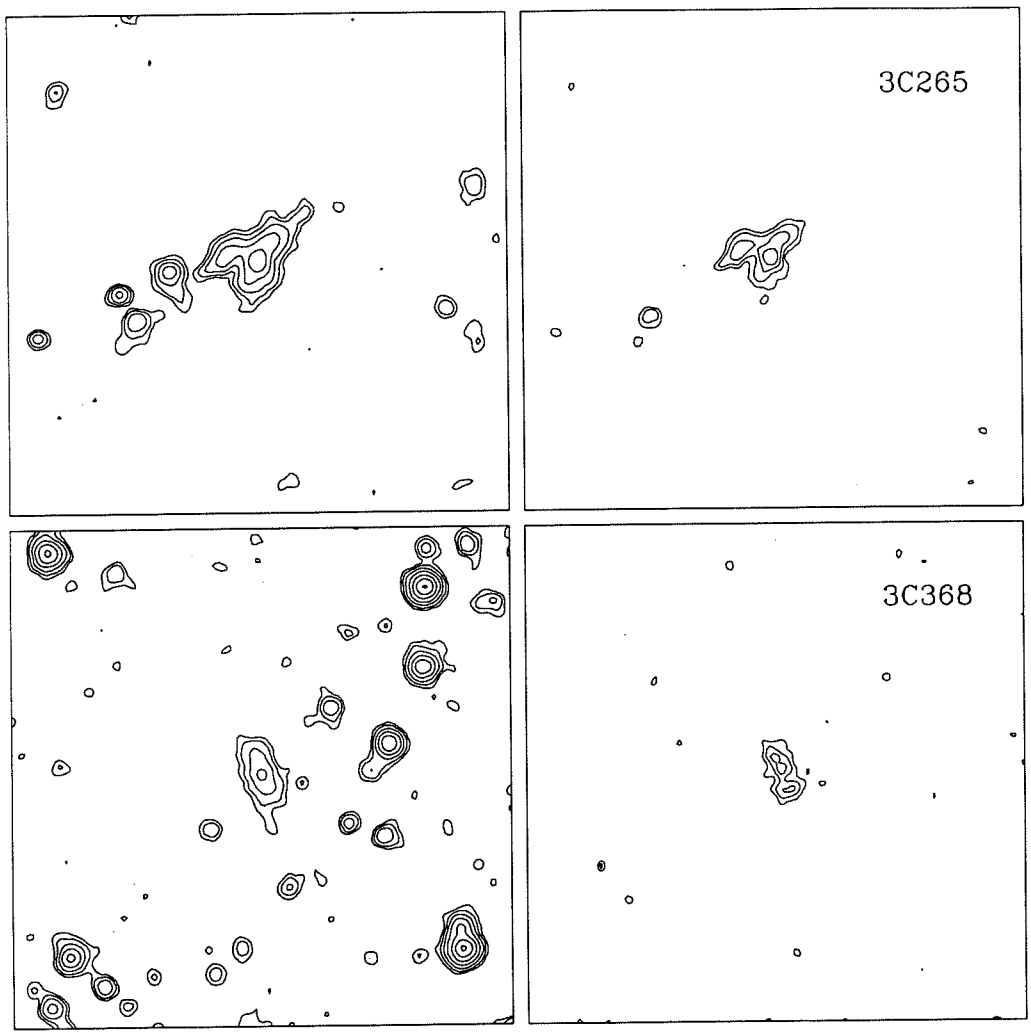

Figure 2.3: [O II] Images of Two Radio Galaxies

On-band [O II] $\lambda 3727$ images (left column) and continuum-subtracted [O II] residuals (right column) for two $z \simeq 1$ radio galaxies taken to test the survey's response to known, strong line emission sources. Top row: 3C265, bottom row: 3C368. All plots are N up, E to the left, and are 60 arcseconds square, centered on the line source. Note the strong, extended emission-line excess in both continuum-subtracted images.

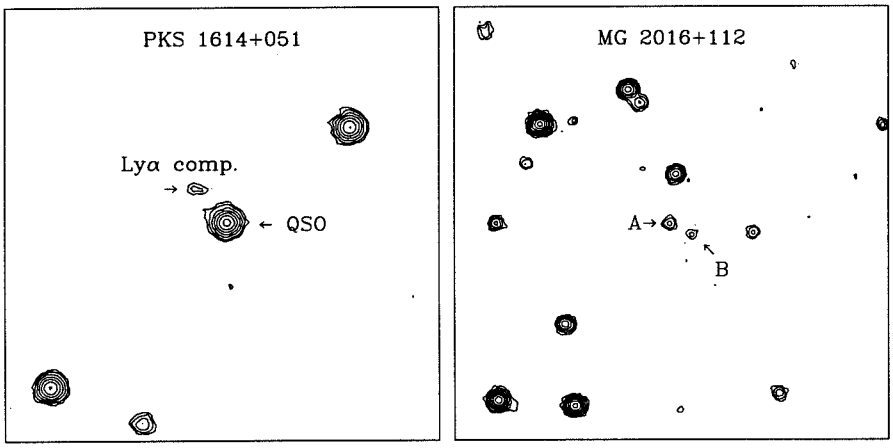

Figure 2.4: Lyα Images of Known High-z Sources

On-band Lyα images of the two known high-redshift Lyα emitters used to test the efficacy of this survey: PKS 1614+051 (left), and MG 2016+112 (right). Both contour plots have N up and E to the left, and are 60 arcseconds square. The Lyα objects are labelled (see text for details).

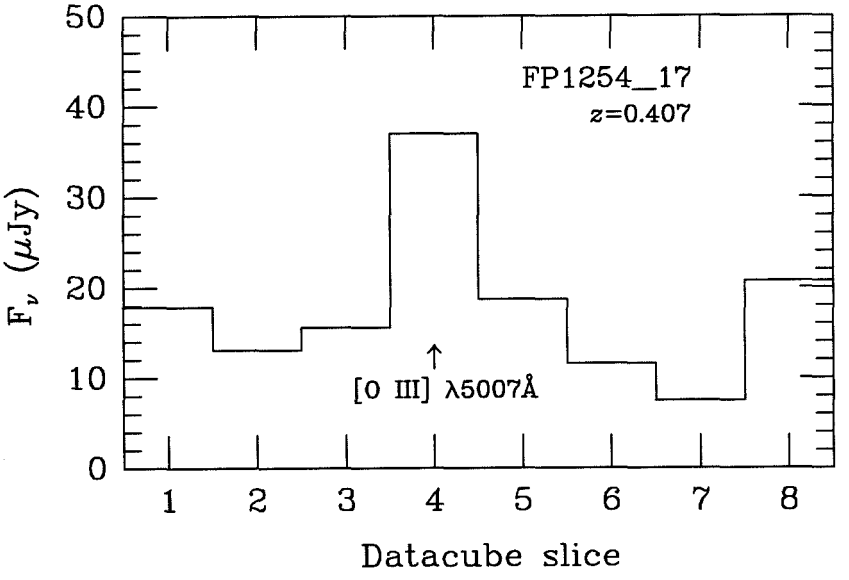

Figure 2.5: Example Fabry-Perot Spectrum

A Fabry-Perot spectrum for object FP1254_17, extracted and calibrated following the procedure outlined in the text. The strong emission line in the fourth bin was later confirmed spectroscopically to be [O III] λ5007, placing FP1254_17 at a redshift of 0.407.

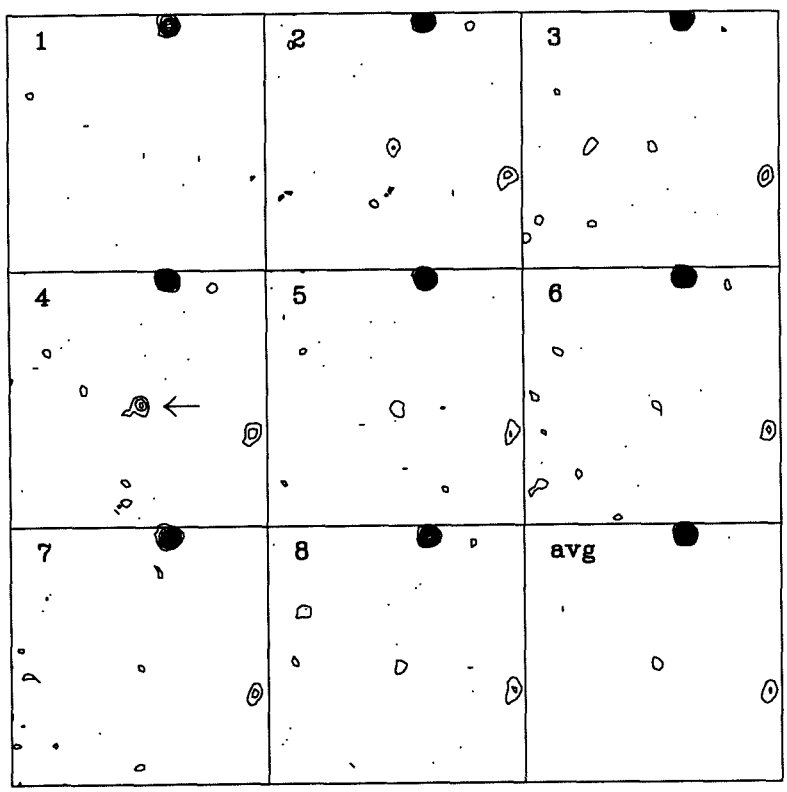

Figure 2.6: Example Fabry-Perot Datacube

An example datacube of a candidate emission-line object from the FP1254 field. The individual panels are 51 arcsecond square subregions extracted from each slice of the datacube, centered on the position of the candidate object. Note that the object, designated FP1254_17, appears brighter in the fourth image.

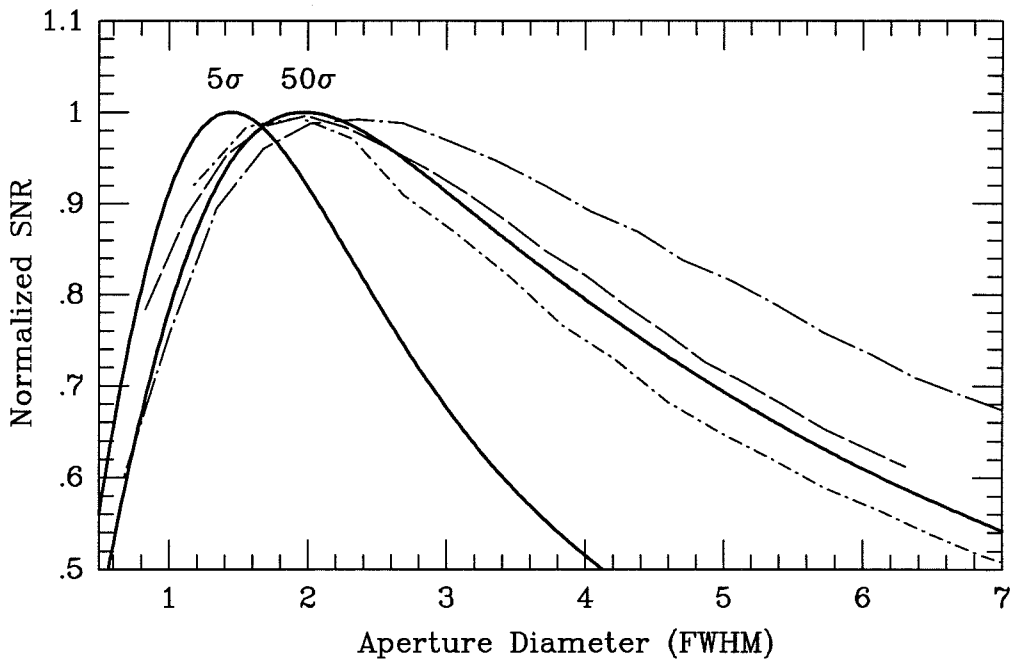

Figure 2.7: Optimal Apertures

A plot of optimal apertures, in units of the FWHM of the stellar images, vs. the signal-to-noise ratio for the photometry at that aperture. The data plotted are average curves for several well-detected stars in each field, and cover a range of seeing. The curves are from FP0031 (1.3 arcsec seeing, dot long-dash), FP1254 (1.6 arcsec seeing, long-dash), and FP1656 (2.2 arcsec seeing, dot short-dash). Note that all 3 curves peak near 2×FWHM. Two model curves are also plotted which are continuous integrations of a Gaussian PSF on a constant sky level approximating that of the FP survey data (CCD readout noise and dark current are both neglected for this model). Note that the optimal aperture for faint objects (5σ model) is smaller than for the brighter objects (50σ model).

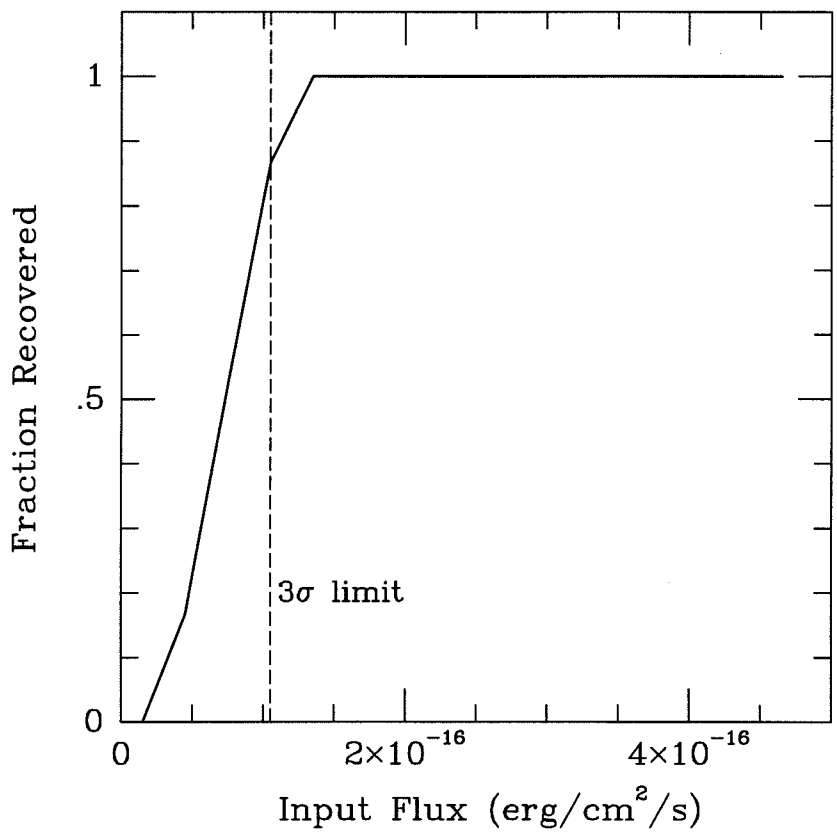

Figure 2.8: Completeness Curve

A completeness curve for this survey, determined from the recovery rate of test objects in simulated data (see section 3.1.4 for details).

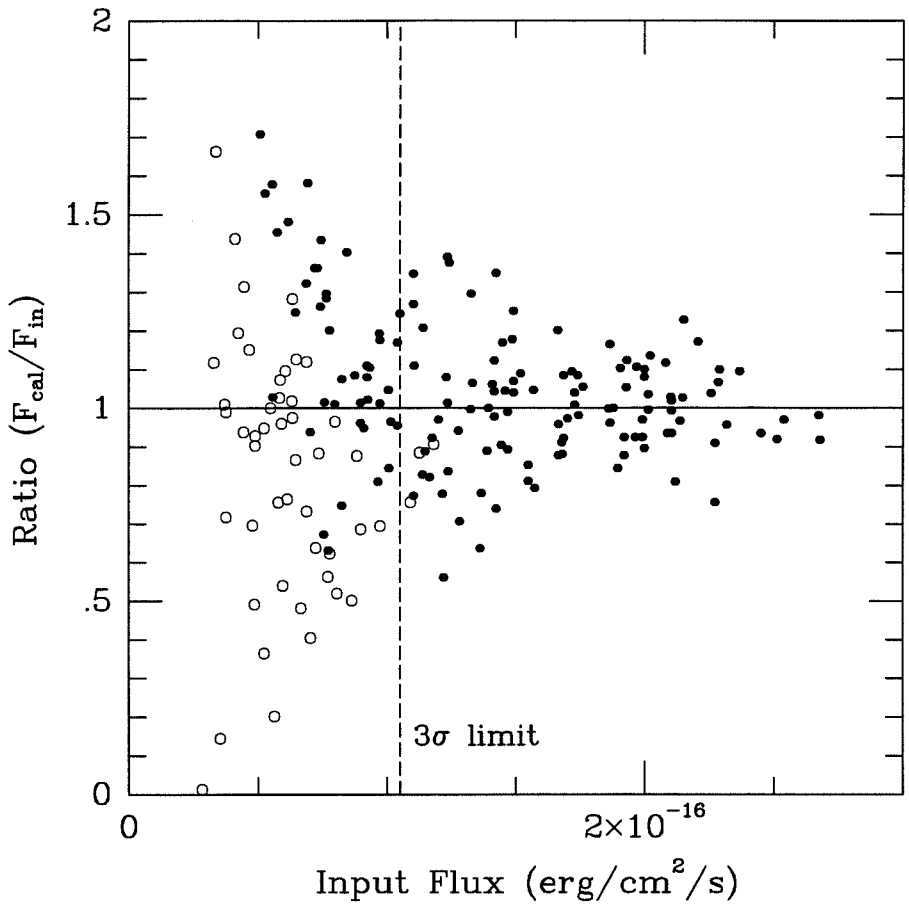

Figure 2.9: Flux Recovery Ratio

A plot of the ratio of recovered flux to input flux vs. the input flux for the test objects used to determine the survey completeness. Solid dots indicate successful recovery while open circles represent objects missed in the candidate selection process. The 3σ flux limit is indicated by the vertical dashed line. Note that the recovered flux is consistent with the input flux (ratio=1), modulo the noise introduced into the simulated data. Note also that a significant number of objects were successfully recovered below the 3σ limit, though these were typically scattered to higher recovered fluxes by the noise.

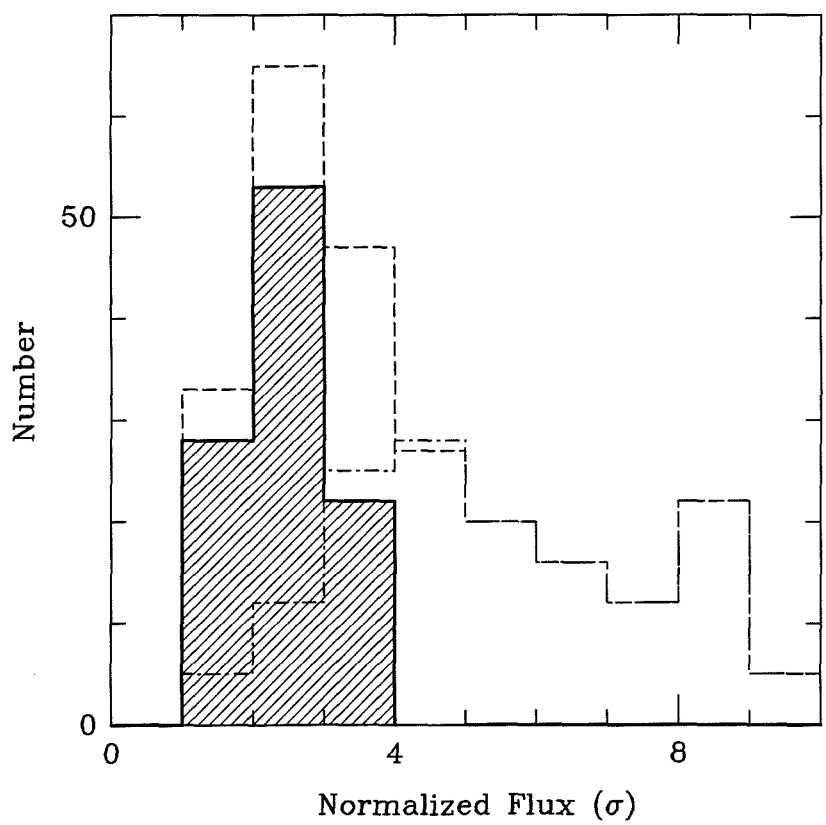

Figure 2.10: Excess Counts

Excess counts (hatched histogram) as a function of the normalized flux in units of sigma, where $1\sigma = 3.5 \times 10^{-17}$ erg cm^{-2} s^{-1} . Also plotted are the total number of objects in the final candidate list from the simulated datacube (short dash), and the number of test objects placed in the data (dot-short dash). The absolute number of the excess counts is not indicative of the counts in the survey data.

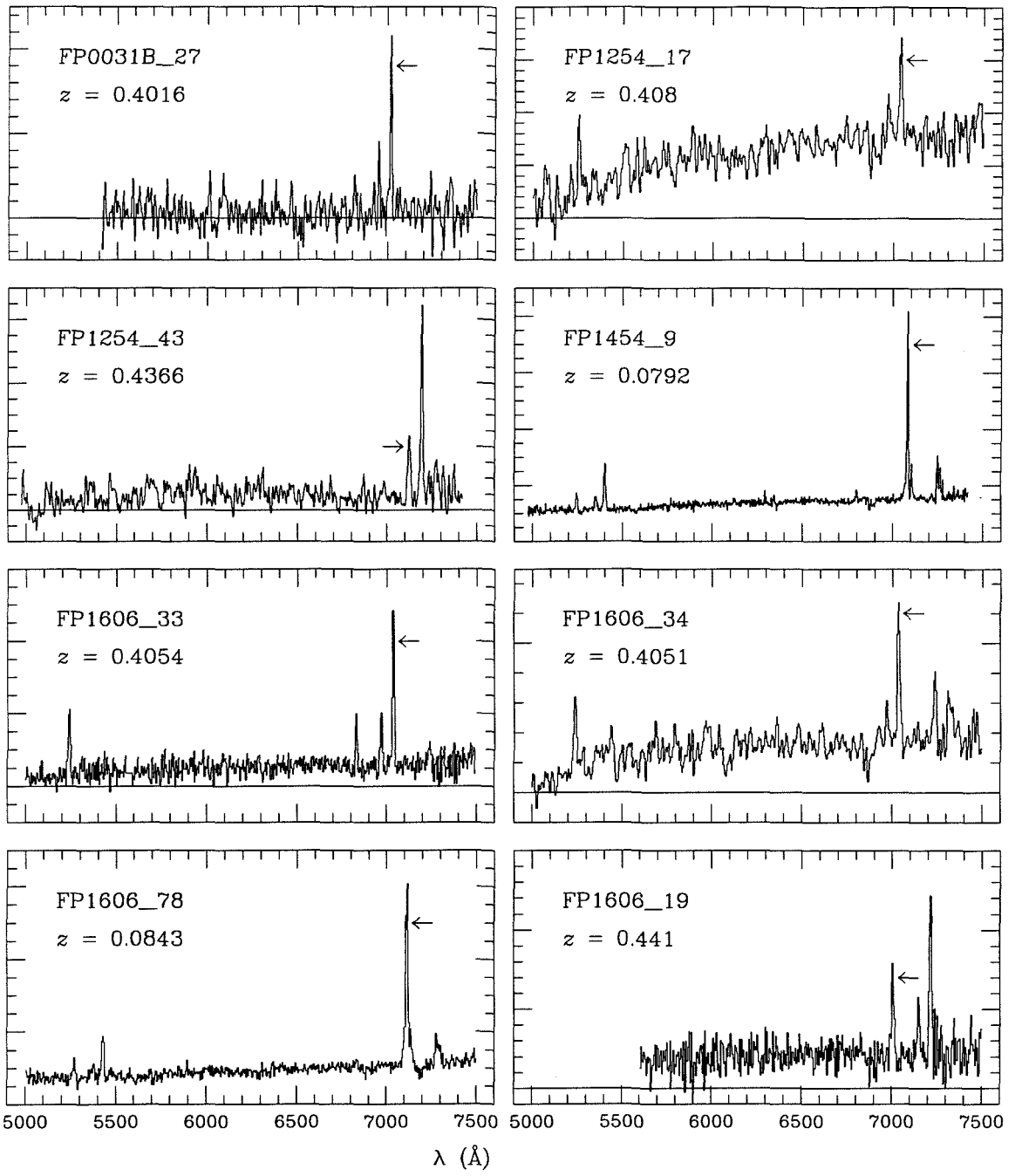

Figure 2.11: Example Follow-up Spectroscopy

Long-slit follow-up spectra of emission-line candidates selected from the FP data. The FP-selected emission line is indicated in each panel with an arrow. The wavelength range is the same in all eight panels, while the flux is in arbitrary units.

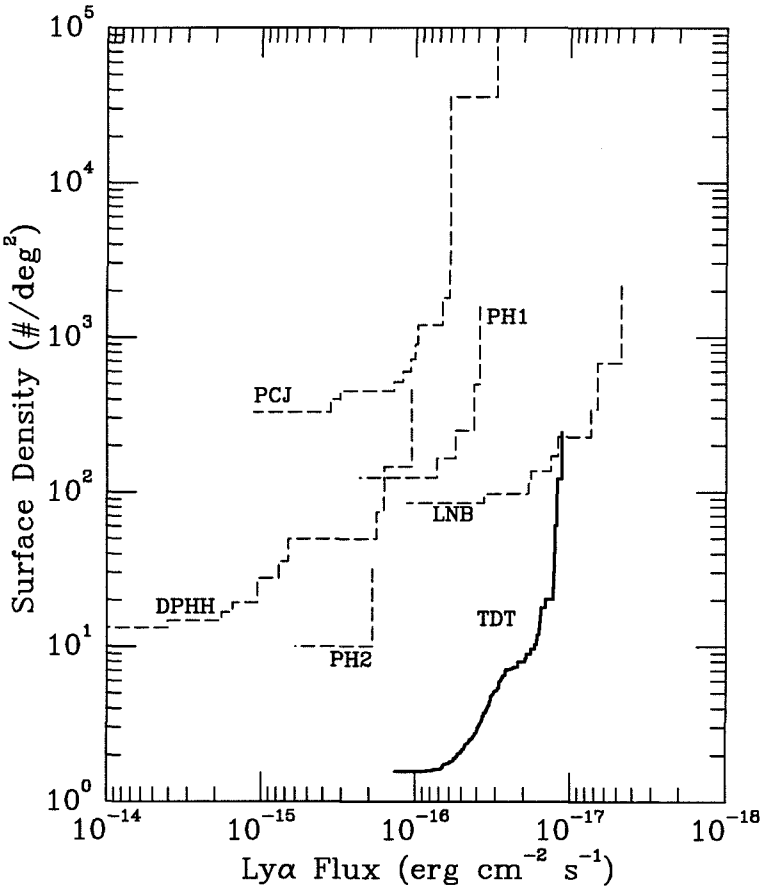

Figure 2.12: Observed-Frame Limits

Limits on the surface number density of Lyα PGs as a function of the limiting line flux. Note that there is *no* redshift information contained in this diagram! The surveys plotted span a range in redshift of 1.9–9.3, with Δz's in the range 0.02–0.20, depending on the width of the narrowband filters. Regions to the upper left of the limit lines are excluded by the surveys. Limits from several other Lyα surveys are plotted for comparison. All limits plotted are for a 1σ detection within an aperture equal to twice the seeing FWHM. Labels are the same as in figure 13, though some surveys are omitted for clarity. For comparison, the known radio galaxies and QSO companions typically have observed Lyα line fluxes of $10^{-15} - 10^{-16}$ erg cm^{-2} s^{-1} .

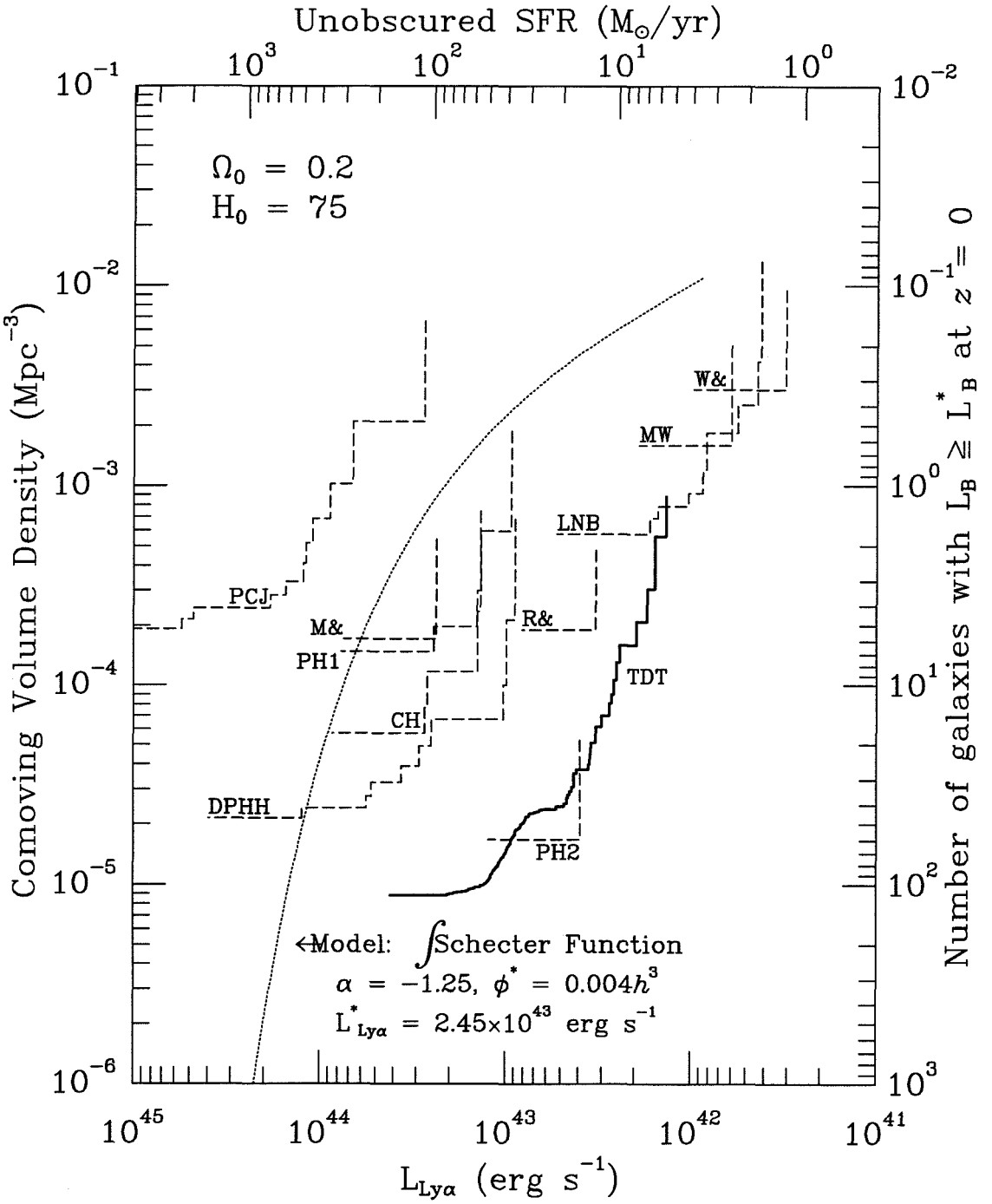
Unobscured SFR ($M_\odot$/yr)
10^3
10^2
10^1
10^0
Ω_0 = 0.2
H_0 = 75
W&
MW
LNB
R&
PCJ
M&
PH1
CH
DPHH
TDT
PH2
←Model: ∫Schecter Function
$\alpha = -1.25$, $\phi^* = 0.004h^3$
$L^*_{Ly\alpha} = 2.45\times10^{43}$ erg s^{-1}
Comoving Volume Density (Mpc^{-3})
10^{-1}
10^{-2}
10^{-3}
10^{-4}
10^{-5}
10^{-6}
Number of galaxies with $L_B \geq L^*_B$ at $z = 0$
10^{-2}
10^{-1}
10^0
10^1
10^2
10^3
10^{45}
10^{44}
10^{43}
10^{42}
10^{41}
$L_{Ly\alpha}$ (erg s^{-1})

Figure 2.13: Restframe Limits

Limits from Figure 12, with the observable coordinates translated into comoving volume number density and restframe Lyα luminosity, assuming $H_0 = 75$ km s^{-1} Mpc^{-1} and $\Omega_0 = 0.2$. The top x-axis shows the star formation rate corresponding to the Lyα luminosity on the bottom x-axis, while the right y-axis gives the number of $L \geq L^*_B$ galaxies expected within the comoving volume surveyed (normalized to the $z = 0$ space density of L* galaxies). As in Figure 12, regions to the upper left of the limit lines are excluded by the surveys, and the model PG luminosity function is as described in the text. Scaling to lower SFR moves the model to the right. The limits for several other Lyα-based surveys are plotted for comparison, and are identified as: CH = Cowie & Hu, in Cowie (1988); DPHH = De Propris et al. 1993; LNB = Lowenthal (1991); M& = Macchetto et al. (1993); MW = Møller & Warren (1993); PCJ = Parkes, Collins & Joseph (1994); PH1 = Pritchet & Hartwick (1987); PH2 = Pritchet & Hartwick (1990); R& = Rhee et al. (1989); TDT = this work; W& = Wolfe et al. (1992). Note that quasars lie in the lower left corner of this plot, with a peak space density of 3.5×10^{-7} Mpc^{-3} at $z = 2.3$ (Schmidt, Schneider, & Gunn 1991), and luminosities in the Lyα line of $\geq 10^{43}$ erg s^{-1}.

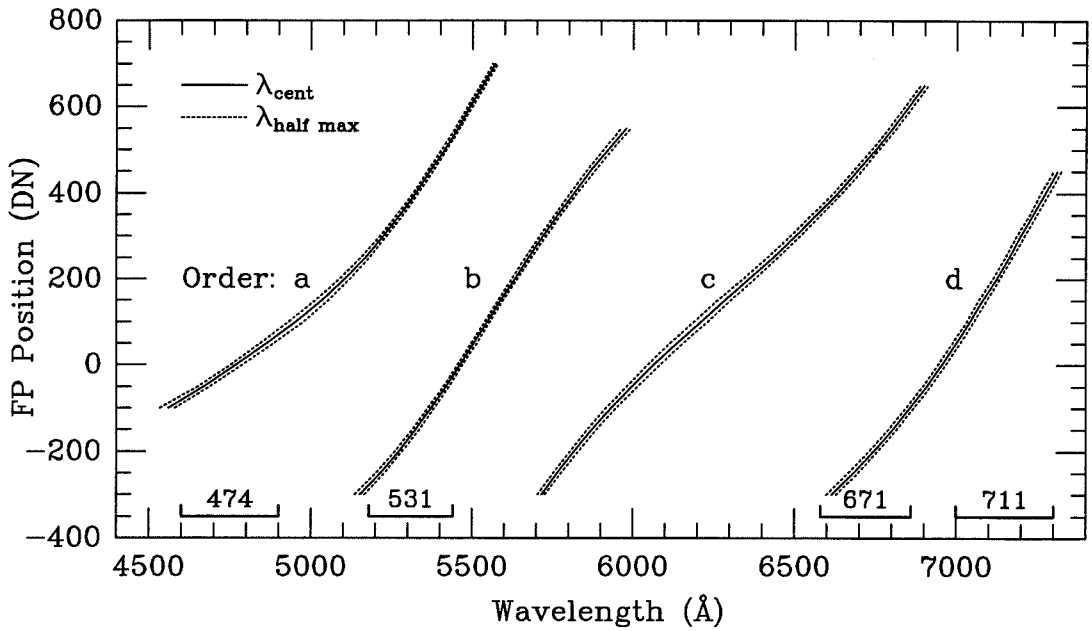

Figure 2.14: Calibration of the Fabry-Perot Etalon

Transmitted Fabry-Perot orders as a function of the computer position (DN) for the etalon used in this survey. Four orders are accessible in the visible window, with continuous coverage possible with appropriate blocking filters. The bandpasses for the four blocking filters obtained for this project are also indicated. The Fabry-Perot position (DN) is an arbitrary number the computer uses to indicate the relative spacing of the etalon plates, where larger DN = greater spacing.

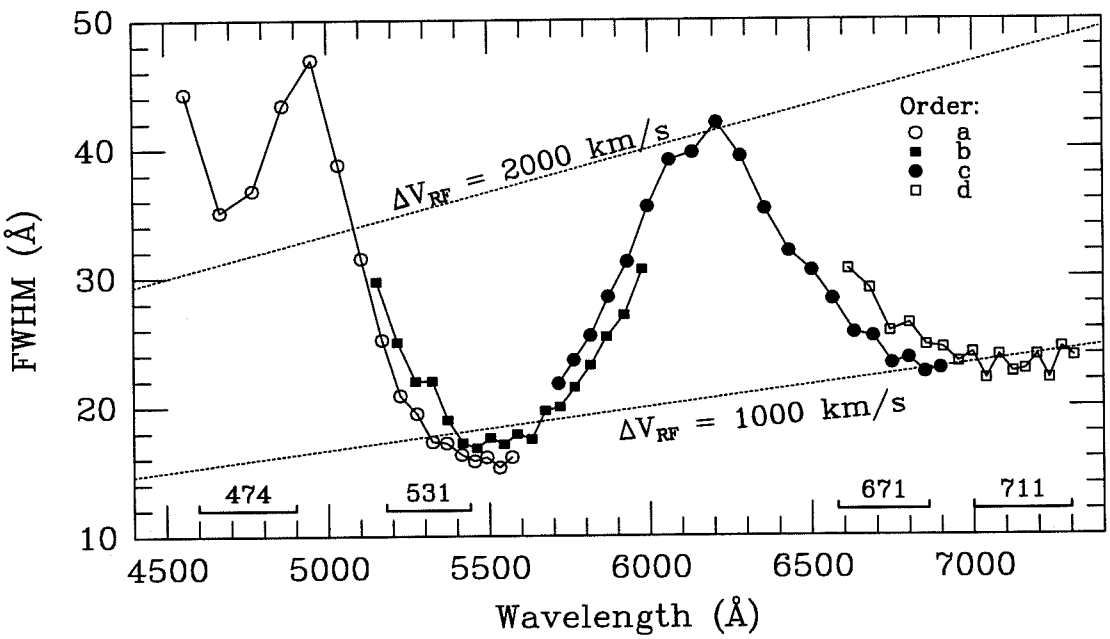

Figure 2.15: Etalon FWHM Variations

FWHM of the Fabry-Perot etalon as a function of the wavelength. The large variations are due to the phase shift on reflection in the etalon's broadband dielectric coatings. The bandpasses for the four blocking filters are again indicated, along with the restframe velocity width of the filter. Note that in regions where two orders overlap, the higher order line has a smaller FWHM.

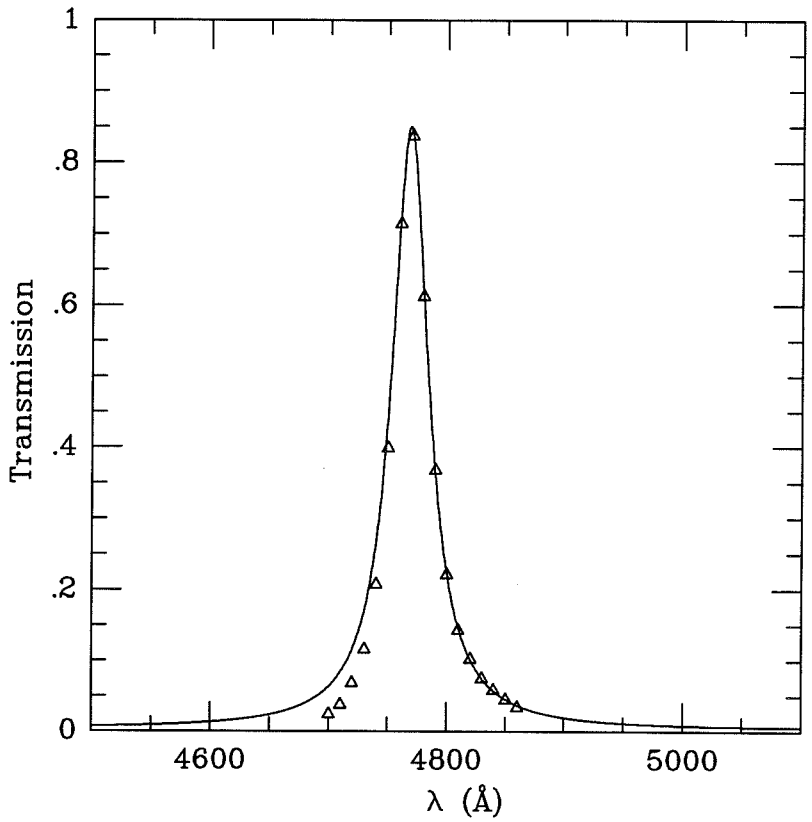

Figure 2.16: Airy Function Transmission Curve

An Airy function transmission curve (solid line) for comparison to our etalon's measured transmission curve (triangles) at λ_{cent} = 4769, FWHM = 34Å. The slight asymmetry of the actual bandpass on the blue side is a result of the rapidly changing FWHM at this wavelength (see Figure 15).

Chapter 3

The Serendipitous Long-Slit Spectroscopic Survey**

ABSTRACT

We present the results of a deep, serendipitous, long slit spectroscopy-based survey for Lyα emission at high redshifts. The data were obtained over the course of 6.75 years at Palomar Observatory, using the Double Spectrograph and 4-Shooter instruments on the Hale 200-inch telescope. A total of 421 independent spectroscopic frames, covering an area of 14.97 square arcminutes, was surveyed over a 2500Å span from 5000Å to 7500Å, with lesser areas surveyed across the entire optical passband. Out of 65 emission-line candidates found, we were able to determine firm redshifts for two quasars and 30 galaxies. An additional 20 galaxies have only tentative redshifts assigned, based on the identification of a single emission line as [O II]. The sample of galaxies with firm redshifts has a median redshift of 0.52, and reaches out to $z \sim 1$. The spectroscopic properties of these galaxies are consistent with the field galaxy populations identified in the deep spectroscopic surveys. No high-redshift tail is seen, consistent with the no-evolution models, though the majority of the data is not sensitive to [O II] beyond a redshift of 1. The remaining few objects are candidate Lyα galaxies at high redshift, with isolated, unidentified emission lines and little or no continuum. They require further spectroscopy to check on their nature. Assuming a Friedman cosmology with

** Adapted from a paper entitled "A Serendipitous Long-Slit Survey for Primeval Galaxies," by D. Thompson and S. Djorgovski, submitted to the Astronomical Journal.

$H_0 = 75$ km s^{-1} Mpc^{-1} and $\Omega_0 = 0.2$, we have surveyed a restframe comoving volume of 20,400 Mpc^3 to a limit sufficient to detect unobscured star formation at a rate of 10 $M_\odot$ yr^{-1}, and 102,600 Mpc^3 to a limit of 100 $M_\odot$ yr^{-1}. These volumes surveyed are sufficient to contain of order 20 and 100 galaxies with $L \geq L_*$, respectively, assuming the local space density of spheroids and elliptical galaxies and no density evolution. These limits are comparable to those achieved in narrowband imaging surveys, while probing a different region of the relevant parameter space. The lack of detection of a population of Lyα-luminous objects could be due to dust quenching of the Lyα line, higher redshift of formation than surveyed, short lifetimes in the Lyα-bright phase, or even masking of the star-formation emission-line signature by an active nucleus.

3.1 Introduction

Identification of the epoch of galaxy formation, i.e., the time when primeval galaxies (PGs) turn a good fraction of their gas into stars, is still one of the major outstanding problems in modern observational cosmology today. Despite a fair number of attempts to identify PGs, no clear population of such objects has turned up.

What a PG will look like is also subject to some debate. For this work, we assume PGs are high-redshift elliptical galaxies or massive spheroids, seen at the epoch when they are forming the majority of their stars. Objects containing or associated with an active nucleus are excluded from this definition, though it is indeed possible that *all* massive galaxies have an active nucleus at some stage of their formation (Terlevich 1992, Haehnelt & Rees 1993, Djorgovski 1994).

Modern PG searches have been reviewed recently by Djorgovski (1992), Djorgovski & Thompson (1992), and Pritchet (1994). The reader is referred to those works, as well as our Fabry-Perot-based narrowband imaging survey for PGs (Thompson, Djorgovski, & Trauger, 1995, hereafter TDT), for a discussion of the energetics of galaxy formation. Briefly, excluding the presence of an active nucleus, the dominant source of energy in a PG is expected to be from nuclear burning of hydrogen in stars. The formation of $\sim 10^{11}$ $M_\odot$ stars in $\sim 10^9$ years results in *average* star formation rates of order 100 $M_\odot$ /yr, with considerably higher peak formation rates being possible.

Several factors force us to the use of emission-line signatures as an aid in identifying PGs. The most obvious is in determining the redshifts for these objects, as the continuum is expected to be so faint ($m \gtrsim 23^m$) that direct spectroscopic observation of absorption-line signatures is currently not a feasible option for a systematic survey, though a single, relatively bright ($I = 20.0$) galaxy at $z = 2.35$ was recently identified through its absorption line signature by Cowie et al. (1994). Emission-line intensity ratios can be used as a diagnostic tool to help distinguish

active nuclei from pure stellar photoionization. The use of narrowband imaging or spectroscopic techniques also allows one to take advantage of the PG's effective increase in brightness in the emission lines (TDT, and references therein).

Fortunately, strong emission lines are an expected consequence of massive star formation, which must have taken place at some level as indicated by the significant metallicities seen in elliptical galaxies. This inference is relatively insensitive to the form of the stellar IMF since it is only the massive stars which both produce the UV ionizing radiation and ultimately enrich the interstellar medium with metals through supernovæ. One of the strongest emission lines is expected to be that of Lyα (Partridge & Peebles 1967), at a rest wavelength of 1215.7Å. The expected restframe Lyα luminosity from a star formation rate of 100 $M_\odot$ /yr is 2.45×10^{43} erg cm^{-2} s^{-1} (TDT and references therein), assuming no significant dust absorption. For objects at high redshifts, and for a range of standard cosmologies, the Lyα line can be expected to show an observable line flux in the range of $\sim 10^{-16\pm1}$ erg cm^{-2} s^{-1} . This is well within the current capabilities of CCDs on large telescopes.

We can make a second, independent estimate of the expected Lyα line fluxes using the galaxy population synthesis models by Bruzual (1983; and the more recent versions, kindly provided by Dr. Bruzual, priv. comm.). In Figure 3.1, we plot the results of integrating the ionizing flux produced by $\mu = 0.95$ Bruzual models, i.e., an exponential star formation rate with an e-folding time of 1/3 Gyr, assuming an initial baryonic mass of 10^{11} $M_\odot$ for two different redshifts of formation (5 and 10), and for both Scalo and Salpeter IMFs. These models should bracket the range of reasonable expectations for the Lyα emission line from PGs. As can be seen in the top panel, emission-line fluxes are comparable to our previous estimate of $\sim 10^{-16\pm1}$ erg cm^{-2} s^{-1} . In the bottom panel, we can also see that the observed equivalent width of the Lyα line remains high over the span of redshift which makes Lyα accessible to optical instruments.

Most PG surveys detailed in the literature (Pritchet & Hartwick 1987; Pritchet & Hartwick 1990; De Propris et al. 1993; Parkes, Collins & Joseph 1994; TDT; and see TDT for further references) have targeted the Lyα emission line using narrow-band imaging techniques to increase the signal to noise ratio of the candidates against the background of the night sky. Lyα remains the most viable emission line on which to base such surveys, as it is observable from the ground at cosmologically interesting redshifts ($1.9 \leq z \leq 7.2$) with sensitive, modern optical CCDs. These surveys probe a large area on the sky, but only a small interval of wavelength. Spectroscopic observations provide a complementary technique, probing deep in redshift space, but only covering a small area on the sky with each exposure. The two techniques can reach comparable line flux limits in portions of the night sky spectrum free of line emission. Only one spectroscopic survey for PGs is well documented in the literature (Lowenthal et al. 1990), but see also the work by Hu & Cowie (in Cowie 1988).

In this paper, we report on a serendipitous long-slit spectroscopic survey (SLSS) for Lyα line emission from possible high-redshift PGs. The main advantage in this project is that no dedicated telescope time had to be proposed for, with all of the data being obtained during the course of other projects. An early result in this effort was the chance discovery of an apparently normal galaxy at a redshift of 1.018 (Thompson & Djorgovski 1991). The viability of this type of survey is demonstrated by the fact that three high redshift quasars have been serendipitously discovered in long-slit spectroscopic data (McCarthy et al. 1988, z=4.406; LeBorgne et al. 1990, z=3.853; and Schneider, Schmidt, & Gunn 1994, z=4.210).

3.2 Observations and Data Reductions

All observations were obtained at the Hale 200-inch telescope at Palomar observatory, using the Double Spectrograph (DBSP, Oke & Gunn 1982), and the spectrograph on the 4-Shooter camera (4Sh, Gunn et al. 1987). The observations span a total of 6.75 years, from UT 1988 January 10 to UT 1994 September 2. A total of 30 nights of data from the DBSP and 39 nights of data from the 4Sh are included in this survey. These nights were typically shared with imaging, and were not completely dedicated to spectroscopy. Most of the data were obtained under less than photometric conditions, but were still useable for this project.

While the specific set-up of each spectrograph varied from run to run (and sometimes from night to night), a "typical" set-up for each spectrograph can be described. The majority (96.5%) of the DBSP data were taken through a 2"×128" slit. The blue camera would be set up with a 300 l/mm grating (λ_{blaze} = 3990Å), covering the wavelength range of ~3300Å - 5100Å at 2.16Å per 0.38" pixel and ~11Å resolution. The red camera used a 316 l/mm grating (λ_{blaze} = 7500Å), covering ~5000Å - 7500Å at 3.08Å per 0.56" pixel and ~11Å resolution. For the 4-Shooter, all of the data were obtained through a slit of 1.5 arcsec width and 96 arcsec length. A 300 l/mm transmission grating (λ_{blaze} = 5800Å) gives a dispersion of 4.56Å per 0.42" pixel and a resolution of ~16Å, covering the range of ~4950Å - 8600Å . Both spectrographs are equipped with TI 800 × 800 CCDs.

All data were bias subtracted and flatfielded using nightly bias and domeflat frames, following standard reduction procedures. Night sky spectral emission lines were subtracted out using a sliding window median filter routine which incorporates a sigma-clip, so that pixels which contain excess light from objects on the slit are ignored. It was found that this method was more efficient at removing the night sky features in our low-resolution spectra than other available routines. The brighter cosmic rays were also removed at this stage, using a small aperture median filter window and a relatively high clipping threshold. Multiple exposures at the

same slit position and position angle on the sky, and with similar spectrograph set-ups, were shifted appropriately and added together to effectively produce a longer exposure frame. Multiple exposures which could not be added together were removed from the sample so that each independent line of sight was only sampled once. Several DBSP red camera frames from one night were removed because of CCD read problems at the telescope, and one night of DBSP blue camera data was deleted due to poor flatfielding. Exposures less than 200 seconds in duration were also removed from further consideration, as well as those obviously taken in the galactic plane.

The final sample is composed of 190 frames of 4-Shooter data totalling 429691 seconds of exposure time (2261 s per frame average) and 231 frames of DBSP red camera data totalling 373572 seconds of exposure time (1617 s per frame average). There are also 206 frames of DBSP blue camera data totalling 349672 seconds. In particular, there are 97 frames (4Sh + DBSP-R) with exposure times of 1 hour or longer. Several factors contribute to the longer average exposure time of the 4Sh data: if conditions were not optimal for long spectrographic exposures, we would concentrate on imaging instead; and the 4Sh has the capability to take spectroscopic and imaging data simultaneously. A number of 1200-2000s exposures were obtained on random pointings while obtaining deep imaging data was the primary science driver. Also, because of the 4Sh capability of imaging the immediate vicinity of the spectrograph slit with a science-grade CCD, it was possible to "guide" the telescope for long periods with occasional manual adjustments based on short imaging exposures when no suitable guide star was present. A histogram of the exposure times of the survey sample (hereafter, references to the "sample" refers specifically to the 4Sh + DBSP red frames, with the DBSP blue camera data being considered as extensions to the red frames) is presented in Figure 3.2.

3.2.1 Selection of Candidates

The sky-subtracted spectroscopic frames were then inspected visually for candidate emission line objects in the clear regions along the slit. Areas near the ends of the slits, where the flatfielding and sky subtraction sometimes left strong residuals, were noted and dropped from inclusion in the survey, as was the area immediately surrounding any program objects to which the spectrograph was specifically pointed. In all, approximately 75% of the total slit area available was ultimately used, giving a total area surveyed of 53876 square arcseconds (~15 square arcminutes). All reasonable candidate emission lines were noted, including those which were obviously at relatively low redshift (e.g., the Hβ and [O III] lines around 5000Åare easy to recognize and typically at z~0.4), as well as very faint lines with no detectable continuum.

Frames containing candidate emission line objects were then re-inspected more carefully, to cull the list of the obviously spurious objects. It was important to consider the data from several steps along the processing trail, including the flatfield frame itself (to locate features which result from incomplete flatfielding), and the flatfielded frames which were sky subtracted using a simple median subtraction along entire rows (which located cosmic rays removed from the final sample frames, and helped to verify the candidate emission lines). The final frames were also squeezed by factors of 2 to 8 in the dispersion direction and smoothed, to help identify any faint continuum which may be present. Faint emission lines are much more believable if there is also a detectable continuum.

3.2.2 Extraction and Calibration of Spectra

The final list of candidate objects, 32 from the 4-Shooter data and 33 from the DBSP (red and blue cameras combined, objects which show lines in both cameras were only counted once), were then extracted along with the program objects,

arc lamps, and standard stars. Wavelength calibration was established using lines from Helium and Neon for the 4-Shooter data, and Helium, Neon, Argon, and Mercury for the DBSP. Fits to the arc lines show residuals of less than 1Å for all of the data, and are typically under 0.5Å r.m.s. We note, however, that the arc lamps were extracted at the same location as the standard stars and program objects, centrally located on the CCD. Due to a slight rotation of the CCD rows with respect to the slit, and the fact that the serendipitously detected objects can appear anywhere along the slit, the true error in wavelength calibration for the SLSS objects is a function of their position along the slit, and can be as high as ±10Å. This will have only a small effect on the derived redshift for the SLSS objects, and was not removed from the data.

Flux calibrations of the spectra were applied using typically two or more standard stars each night from the lists of Oke (1974), Oke & Gunn (1983), Stone (1974, 1977), Massey et al. (1988), and Massey & Gronwall (1990). While the majority of data were taken under non-photometric conditions, a check of the variations in the flux calibrations across the entire data set showed that ~70% of the data fall within ±20% of the few nights of photometric data available. The flux calibrations on the remaining ~30% of the data differ by no worse than a factor of two. The scatter is in the sense that *none of the data are scattered to significantly higher sensitivities*, i.e., the poorly calibrated data are not responsible for the faintest flux limits reached by this survey.

While the slit positions were accurately centered on the program objects, it is important to emphasize the fact that this is not the case for the SLSS objects. Random placement of the objects across the width of the slit should, on average, result in a factor of two underestimate of the line and continuum fluxes for these objects. This effect is lessened for point sources in excellent seeing, where the vignetting function is flat-topped, as well as for diffuse objects whose angular extent is comparable to or larger than the width of the slit. For the latter case,

the detected flux would be relatively independent of source position across the slit width, and consistently underestimated. No corrections to any of the data have been made to allow for this effect.

3.2.3 Calibration of Detection Limits

The identification of a faint emission line in spectroscopic data is similar to that of identifying emission line objects in narrowband imaging data in that the emission lines cover a finite area on the CCD, just as a galaxy would in an image. To optimize the detection of such objects against a background of noise, an aperture must be chosen which maximizes the signal-to-noise ratio of the emission line. This is something which the eye does naturally in selecting the candidates, but for purposes of establishing a flux-limit for this survey, we adopt an aperture of 1.4 $\times$ the seeing full-width at half-maximum (FWHM) by 1.4 $\times$ the spectroscopic resolution FWHM. As was shown in TDT (their Figure 7), this will maximize the SNR for a faint emission line point source in an image whose noise is dominated by sky photons. For extended sources, the noise limits would be about 40% higher than that for point sources.

Because of the presence of emission-lines in the spectrum of the night sky, the noise limit of any spectroscopy-based survey is a function of wavelength. We derive a measure of the r.m.s. noise (σ per pixel) appropriate for each row in the CCD frame using a robust, non-parametric estimate of σ from the difference of the quartile points of the distribution, a method which is not affected by the outlying points. This number was scaled up by the square root of the number of pixels within the aperture defined above, appropriate to that particular frame's seeing and spectral resolution, and saved as a "sigma-spectrum." These noise spectra were then wavelength and flux calibrated along with the object spectra, as described above. An example of a sigma-spectrum, converted to an emission-line flux scale, is shown in Figure 3.3. Frames with exposure times of 1 hour or

more typically reach 1-σ emission-line flux limits of 2.0×10^{-17} erg cm^{-2} s^{-1} or less over a significant portion of their wavelength span. These limits are 10 – 100 times fainter than the typical Lyα fluxes seen in radio galaxies (Djorgovski 1987, Djorgovski & Thompson 1992, and references therein).

3.2.4 Summary of Survey Coverage

The relevant parameter space for PG surveys has 3 axes: wavelength (or redshift), emission-line flux limit, and area surveyed. To date, the PG surveys have typically collapsed the redshift dimension and plotted survey limits on the surface density (= area^{-1}) vs. flux limit plane (TDT, and references therein). This survey, however, has continuous coverage over a very wide wavelength range: 3200Å to 9500Å, and so an attempt at preserving the true 3-dimensional PG parameter space was made.

Figure 3.4 presents two views of the limits datacube for this survey. It was constructed from the individual sigma-spectra by binning them to 10Å resolution, and summing up the areas covered by the individual exposures at all line fluxes equal to or greater than the line flux limits. The full datacube covers the wavelength range of 3200Å – 10000Å in 10Å steps, with 500 flux bins of 2.0×10^{-18} erg cm^{-2} s^{-1} width running from 2.0×10^{-18} to 1.0×10^{-15} erg cm^{-2} s^{-1} . The "mesa" running from 5000Å to 7500Å is due to the overlap between the typical 4Sh and DBSP set-ups.

Several cuts through the full datacube in the λ – area plane are presented in Figure 3.5. These curves give a more detailed view of the area surveyed as a function of the 1-σ emission-line flux limits. Emission line signatures from the night sky spectrum are visible in this plot, and demonstrate that there is a significant loss in sensitivity, and thus a loss of area surveyed at a given flux limit, in regions of the spectrum where the sky is significantly brighter. In fact, the sky is so bright

at the λ5577Å [O I] and λ5893Å Na I lines that essentially zero area was surveyed to a 1-σ emission-line flux limit of 1.0×10^{-17} erg cm^{-2} s^{-1} .

Cuts through the datacube perpendicular to this, in the flux limits – area plane, detail the rapid drop-off in area surveyed as a function of the sensitivity (Figure 3.6). A combination of CCD response, grating blaze wavelengths, and a nearly complete absence of emission lines in the night sky spectrum around 6700Å conserve to make this the most sensitive spectral region for this survey. In addition, all of the different spectrograph set-ups include this portion of the spectrum, so the full area of the survey (just short of 15 square arcminutes) was covered over this wavelength range.

3.3 Results and Discussion

Of the original sample of 65 SLSS objects extracted (this excludes other candidates which proved to be spurious on closer examination), we were able to obtain definite redshifts for 32. Determination of the redshifts was based on at least two confirming features in each spectrum. The presence of multiple emission lines was sufficient to determine a redshift for the majority of these objects. For some, absorption features such as the calcium H and K lines or a 4000Å break allowed the positive identification of a single emission line with [O II] λ3727. For a few objects with both a flat, weak continuum and a single emission line, we were able to identify the line as [O II] and rule out other possibilities by their lack of other expected emission lines. For these few objects, Lyα was not a viable interpretation due to the continuum extending well past what would have been the Lyman limit at 912Å.

Two quasars were detected in the sample, at redshifts of 1.669 and 2.29 (Figure 3.7). The former shows fairly strong, broad Mg II λ2798 and much weaker C III] λ1909. The latter has a strong and fairly narrow Lyα line, with weaker C III] λ1909 emission and possibly some C IV λ1549 emission (the latter line falls on the dichroic split in the DBSP data in which it was discovered, and so its presence is somewhat uncertain).

3.3.1 The Low Redshift Objects

The other 30 positive IDs span the redshift range of $0.031 \leq z \leq 1.018$ (representative spectra are given in Figure 3.8). We find a median redshift of 0.52 for this sample of objects (see Figure 3.9 for a histogram of the redshifts). Because of the specific spectrograph set-ups used in obtaining the majority of these data, [O II] lines at redshifts much greater than 1.0 would lie outside of the spectrograph bandpass for a large portion of the data. This may partially account for the lack

of detection of more than the one galaxy with a redshift over 1, despite finding four with redshifts above 0.9.

Spectroscopic R magnitudes span the range of $19 \leq R_{Spec} \leq 25$ (Figure 3.10), and were derived from the extracted spectra of the candidate objects. Magnitudes fainter than R $\sim$ 24 should be considered limits (R $\leq$ 24), as this is about as faint a continuum as can be detected in a 1 hour exposure with DBSP or 4Sh. Note that with a (B-R) color of $\sim$ 1.5, we are probing galaxies down to an equivalent B magnitude of $\sim$ 25.5, fainter than the deep field surveys by Broadhurst, Ellis, & Shanks (1988, $20.0 \leq b_J \leq 21.5$), Colless et al. (1990, $21 \leq b_J \leq 22.5$), and Colless et al. (1993, 22.5 $\leq$ B $\leq$ 24). They find a trend towards increasing median redshift towards increasing magnitude, with the faint samples having median redshifts of $\sim$ 0.5. This is consistent with the median redshift of 0.52 found in our sample, and suggests that our sample comes from the same population of objects as the galaxies in the deep field spectroscopic surveys.

Equivalent widths were determined for as many of the emission lines as possible, and are plotted versus redshift in Figure 3.11. The data have not been corrected by $(1+z)$, and there is no real trend towards increasing [O II] equivalent width with increasing redshift. This agrees with Koo & Kron (1992), who argue that there is no direct evidence for such a trend. We are, in fact, biased *against* high equivalent width [O II] lines at faint line fluxes, as we require some confirming feature in the spectrum, which for [O II] is typically a strong blue continuum or 4000Å break, before a definite redshift is assigned.

About 20 of the remaining objects were given tentative redshifts, all of which fall below $z = 1.2$. The isolated emission lines on extremely faint continuum appear to be real, but there is insufficient corroborating evidence to allow a definite redshift to be assigned. The most likely interpretation is that these are [O II] lines. Since the objects with a tentative identification of [O II] have equivalent widths typical of [O II] emission lines (W $\lesssim$ 100Å), it is likely that this interpretation is

correct (Figure 3.12). Of course, dust absorption in a high-redshift PG could allow Lyα to mimic the lower equivalent width [O II] lines, but it would be impossible to differentiate between the two without a considerable investment of time on a large telescope.

We can estimate the number of galaxies which should have been seen in this survey from faint R-band galaxy number counts (Metcalfe et al. 1994, Driver et al. 1994). After allowing for the distribution of exposure times in our sample (not all of the spectra go deep enough to see 24^m continuum), we estimate that of order 100 galaxies in the magnitude range of $19.5 \leq R \leq 24.0$ should have been located in the area covered by the spectrograph slits. About 60% of the galaxies in the Broadhurst, Ellis, & Shanks (1988) sample show emission, so this estimate is consistent with the number of emission-line candidates found in this survey.

Our sample of galaxies with certain or probable redshifts is thus consistent with mild evolution of field galaxies out to $z \sim 1$, implied by the results of the deep redshift surveys.

3.3.2 Candidate Lyα Galaxies

We were unable to assign even a tentative redshift to about a dozen candidate emission line objects. It is likely that many of these are [O II] galaxies for which there is simply not enough information to assign them even tentative redshifts. Some of these may be spurious, either poorly removed cosmic rays, bad pixels or columns, or features which printed through in flatfielding which slipped through the culling process described in section 3.1.2. One or two candidate objects appear to have single broad emission lines, but little or no detected continuum, and cannot be unambiguously identified. Some candidates may indeed be Lyα galaxies, and are interesting enough to warrant follow-up spectroscopy. The most interesting

candidates tend to be spatially extended over a few arcseconds, with a fairly uniform surface brightness across the width of the line and no detectable continuum, which leads to equivalent widths implausibly high for [O II].

A portion of the spectrum of one such emission-line candidate is shown in Figure 3.13. This object was found on a 1200 second 4Sh spectrum of a blank field near the high redshift quasar PC 1158+4635 ($z = 4.73$, Schneider, Schmidt, & Gunn 1989). We derive a line flux of 3.2×10^{-16} erg cm^{-2} s^{-1} , with a formal significance of 8.2σ. There is no continuum detectable from this object, giving a lower limit to the equivalent width of 230Å. The line lies in a particularly clean region of the night sky spectrum, at 6772Å, and there are no flatfield features at this location on the 4Sh CCD which could have printed through. The line possibly shows a velocity gradient of order 600 km s^{-1} . If this line is Lyα, it lies at a redshift of 4.57. The equivalent width limit, the line flux, and the velocity gradient all place it within the expected range of values for Lyα emission from a massively star-forming PG at this distance. Follow-up spectroscopy of the more interesting candidates will be reported on in a future paper.

3.3.3 Limits on High Redshift Lyα Emission

A much clearer picture of the limits obtained in PG surveys is presented when the observed coordinates of emission line flux limit and area surveyed are transformed into their corresponding restframe coordinates of limiting Lyα luminosity ($L_{\mathrm{Ly}\alpha}$) and comoving volume (V_{CM}) surveyed (Figure 3.14). A Friedman cosmology with $\mathrm{H}_0 = 75$ km s^{-1} Mpc^{-1} and $\Omega_0 = 0.2$ was assumed for the conversions. Here we must explicitly assume that none of our candidate Lyα objects actually are PGs. While the restframe datacube is similar in form to the observed-frame datacube of Figure 3.4, distortions are introduced in transforming to restframe coordinates such that the limiting restframe line luminosities reach to fainter levels

at the low redshift end because of less dimming with distance, while more volume is covered at higher redshifts for a given unit of area surveyed. The full datacube covers redshifts from 1.63 to 6.81 in steps of $\Delta z = 8.23 \times 10^{-3}$, with 500 flux bins of $\Delta \mathrm{Log}_{10}(L_{\mathrm{Ly}\alpha}) = 0.01$, from 10^{41} to 10^{46} erg s^{-1}.

Several cuts through the full datacube in the z – V_{CM} plane detail the restframe limits reached at different 1-σ limiting restframe luminosities (Figure 3.15). Note that the comoving volume plotted in this figure is *per 10Å bin*; the *total* comoving volume surveyed is the sum over all of the redshift bins. Integrating the datacube along the redshift axis shows the total comoving volume sampled by this survey as a function of restframe line luminosity (Figure 3.16). A comoving volume of 20400 Mpc^3 was surveyed to a level sufficient to detect an unobscured 10 $M_\odot$ yr^{-1} SFR, while a total of 102,600 Mpc^3 was surveyed to 100 $M_\odot$ yr^{-1} SFR (1-σ). These numbers are directly comparable to the limits achieved in the narrowband surveys (Figure 3.17), although the two surveys are complementary, probing different regions of the PG parameter space.

3.3.4 Possible Reasons for the Absence of Lyα-Luminous PGs

Dust obscuration is still the most reasonable explanation for the lack of any positive detection of a population of PGs (Djorgovski & Thompson 1992, Pritchet 1994, and references therein). Resonant scattering of the Lyα line can greatly attenuate this line, though the available evidence for this is somewhat conflicting (TDT). One way around this problem is to look for emission-line signatures from lines which are much less affected by dust, such as [O II], [O III], or the Balmer lines, which are also expected to be seen strongly in emission in star-forming PGs. Several projects, completed or in progress, seek to address this question with infrared arrays (Thompson, Djorgovski, & Beckwith 1994, Mannucci, Beckwith, & McCaughrean 1994, Pahre & Djorgovski 1995).

Other causes of the lack of PG detection in the modern surveys include the possibility that all PGs undergo an active nucleus phase (Terlevich 1992, Haehnelt & Rees 1993, Djorgovski 1994 and references therein), in which case PGs may be identified with high-redshift radio galaxies and quasars. If the epoch of galaxy formation were to occur at even higher redshifts, then it would push any observable signature of PGs out of the optical passband. Parkes, Collins, & Joseph (1994) address this possibility with a near-infrared narrowband survey around 1.1 μm ($z \sim 9$ for Lyα). Another possibility is that the Lyα-bright phase of galaxy formation could be quite short, effectively decreasing the space density of Lyα-luminous galaxies to below the levels probed by the modern surveys.

3.3.5 Concluding Remarks

In summary, we have presented a deep, serendipitous, long-slit spectroscopy-based survey for Lyα emission at high redshifts. A total of almost 15 square arcminutes was surveyed over a 2500Å span from 5000Å to 7500Å, with lesser areas surveyed across the entire optical passband. A significant area was surveyed to a 1-σ limiting emission-line flux limit of 1.0×10^{-17} erg cm^{-2} s^{-1} , with larger areas covered at lower flux limits. In restframe coordinates, a total comoving volume of 102600 Mpc^3 was surveyed to a 1-σ limiting restframe Lyα line luminosity of 2.45×10^{43} erg s^{-1}, with smaller volumes covered to lower line luminosity limits. Assuming no density evolution, this is a sufficient volume to contain $\sim 100L \geq L^*$ galaxies, and would have been able to detect unobscured star formation at the rate of 100 M$_\odot$ yr^{-1}. No PGs were unambiguously identified, but several promising candidates were found which require further observations. The results of the follow-up spectroscopy on these objects will be presented in a future paper. Serendipitous surveys such as this are efficient, require no direct initial allocation of telescope time, and are both competitive with and complementary to narrowband imaging surveys.

3.A Appendix: A Normal Galaxy at z = 1.018 †

3.A.1 Introduction

Study of galaxy evolution at large look-back times is one of the principal tasks of modern observational cosmology. However, normal galaxies at large redshifts are notoriously difficult to find. Many examples of powerful radio galaxies and emission-line galaxies near quasars are now known at high redshifts, but the presence of active nuclei in or near them makes the interpretation of their properties in terms of "normal" galaxies somewhat uncertain (see, e.g., Djorgovski et al. 1987, McCarthy et al. 1987, Steidel et al. 1991, etc.; or the reviews by Spinrad 1986, and Djorgovski 1988). On the other hand, deep imaging surveys (e.g., Tyson 1988, Cowie et al. 1988, Lilly et al. 1991; see also the reviews by Tyson 1990, and Cowie and Lilly 1990) have certainly detected galaxies at large redshifts, but to date unambiguous redshifts greater than a few tenths have not been obtained for any of them.

In this *Letter*, we report on the discovery of an apparently normal field galaxy at $z = 1.018$, found in the course of an unbiased long-slit survey for high-redshift objects. This galaxy, designated G0333+3208, is one of the first examples of galaxies at $z > 1$ which are not associated in any way with an active nucleus. It may be representative of an actively evolving, normal galaxy population at a look-back time of about a half of the present epoch. Other possible examples of such

† Adapted from a paper entitled "Discovery of a Normal Galaxy at $z = 1.018$," by D. Thompson and S. Djorgovski, which appeared in the Astrophysical Journal Letters: 1991, ApJ, 371, L55.

objects include some recently found galaxies, associated with quasar absorption-line systems (Bergeron 1990; Wolfe et al., in preparation).

3.A.2 Data and Results

A long–slit spectrum of the quasar NRAO 140 (0333+321) and its stellar companion at PA = 100° was obtained on UT 1988 September 08 as part of a program to search for possible gravitational lens candidates. The Four–Shooter spectrograph at the Cassegrain focus of the Palomar Observatory Hale 200–inch telescope was used with a 300 lines/mm grism and a TI 800×800 CCD detector, giving a dispersion of 4.09Å per pixel and a resolution of ∼15Å. The exposure time was 1200 seconds and covered the wavelength range 4760–8010Å. After bias subtraction and flatfielding using standard procedures, the CCD frame was cleaned of cosmic ray hits and the night sky emission lines were straightened and subtracted so that it could be checked as part of an ongoing serendipitous long–slit survey for faint emission–line objects.

A possible emission line was detected at 7523Å, at a separation of 32 arcseconds from the quasar. A deeper, confirming spectrum of 3000 seconds duration was obtained on UT 1990 September 19, again with the Four–Shooter, and with a similar set up, covering the wavelength range 4790–8450Å. The emission line was again detected. A third spectrum of the emission–line object was obtained on UT 1990 October 18 with the Double Spectrograph (Oke and Gunn 1982) at the Hale 200–inch telescope, looking for other emission lines at the blue end. The slit was set to the optimum parallactic angle, but since all three spectra were taken at low airmass, atmospheric dispersion should not be significant. A 300 lines/mm grating gave a dispersion of 2.05Å per pixel, resolution of ∼10Å, and a wavelength coverage of 3950–5580Å. An exposure time of 4000 seconds failed to detect any other convincing emission lines, but does show a weak continuum extending

down to approximately 4000Å. Exposures of standard stars from Oke and Gunn (1983) were used for the flux calibration. A coaveraged spectrum of G0333+3208 is shown in Figure 3.18.

Imaging in the Gunn–Thuan g, r, and i bands was done on the night of UT 1990 October 17 with the 4-Shooter on the Hale 200–inch telescope. Exposure times totalled 700 seconds each in r and i, and 400 seconds in the g band. The images were flux calibrated with the standard star BD+28°4211 (Kent 1985). Magnitudes of the object are $g = 23.5 \pm 0.2$, $r = 23.5 \pm 0.2$, and $i = 22.6 \pm 0.2$. The i band magnitude is undoubtedly affected by the strong emission line, which falls at the peak of the i filter transmission curve. A coadded contour plot of the region is shown in Figure 3.19.

Assuming the radio position for NRAO 140 from Perley (1982), and the offsets from the quasar in our CCD images, we obtain for the position of G0333+3208:

$$\alpha_{1950} = 03^h\ 33^m\ 24.89^s, \quad \delta_{1950} = +32^\circ\ 08'\ 31.3'' ,$$

with the net estimated uncertainties of about 0.5 arcsec in each coordinate.

3.A.3 Discussion

There is only a single emission line in the optical spectrum of G0333+3208, which we interpret as [O II] λ3727 at $z = 1.018 \pm 0.001$. This line is commonly seen in high-redshift galaxies, and is one of the strongest. Other possibilities are much less likely: Hα and [O III] λ5007 can be ruled out due to the absence of other expected strong emission lines, e.g., Hβ or [O II] λ3727. If the detected line were Mg II λ2798, it would have an unusually large equivalent width, and we would expect to see either C II] λ2326 or C III] λ1909. Lyα at $z = 5.2$ is ruled out both from the lack of continuum depression across the line, which at that redshift may be as much as a factor of 5, extrapolating from the known quasars at $z > 4$

(Schneider et al. 1989), and by the presence of a detectable continuum blueward of the corresponding Lyman limit at 5641Å.

No absorption lines due to Mg II λ2798 at the galaxy redshift are detected in the spectrum of the quasar NRAO 140 ($z = 1.258$), though this is not surprising since the narrow absorption lines would perhaps be lost in our low–resolution spectrum, and at $z = 1.018$ the separation of 32 arcsec on the sky represents a projected comoving separation of $\sim 300h^{-1}$ kpc, for a reasonable range of Ω_0.

The distance modulus in a standard $\Lambda_0 = 0$ Friedmann cosmology with $H_0 = 100$ km s^{-1} Mpc^{-1}, for a redshift of 1.018, is in the range of 42.8 ($\Omega_0 = 1$) to 43.3 ($\Omega_0 = 0$). Thus, the inferred luminosity of G0333+3208 is consistent with that of an approximately L_* galaxy, undergoing a relatively mild evolution.

There is no morphological or spectroscopic sign of an active nucleus in this object. The velocity dispersion of the emission line is $\sim 160 \pm 30$ km s^{-1}, typical for normal galaxies. The emission is also marginally extended (spatially resolved) on the slit, suggesting an *in situ* ionization mechanism, such as the young stars. If the line is indeed [O II] λ3727, then the ionization is fairly low; witness, e.g., the complete absence of the Mg II λ2798 line. There is no radio emission detected from this object to 200 μJy rms at λ20cm (Perley and Murphy, private communication). We thus conclude that G0333+3208 does not contain an active nucleus, and that the line emission is probably powered by star formation.

The integrated emission line flux is 1.5×10^{-16} erg cm^{-2} s^{-1}. In the models by Stasinska (1982), the [O II] λ3727 to Hβ flux ratio is constant to within a factor of 2 or so over three orders of magnitude in density, over the range 30,000°K to 53,000°K in the temperature of the exciting star, and the metallcity range of 0.1 – 1.0 times solar. Adopting the value of 1.65 for this ratio, and using the theoretical value of 2.87 for the Hα/Hβ flux ratio gives us a conversion to Hα flux of: L(Hα) = 1.74 × L([O II]). Kennicutt (1983), using a nearly Salpeter IMF, gives a conversion to the integrated star formation rate as: SFR = L(Hα)/(1.12×10^{41}

erg s^{-1}) $M_\odot$ yr^{-1}. From this we derive the estimate for the star formation rate in G0333+3208 of about $3.5h^{-2}$ $M_\odot$ yr^{-1}. An independent estimate by N. Scoville (private communication), using a somewhat different approach, gives nearly the same result. This SFR is comparable to that of actively star forming, normal galaxies at low redshifts, and it is at least an order of magnitude smaller than the rates inferred (using similar reasoning) for the powerful radio galaxies at comparable or larger redshifts, or to the ultraluminous IRAS galaxies at low redshifts.

The [O II] restframe equivalent width in G0333+3208 is $W_\lambda = 106 \pm 10$Å, which is several times smaller than the values typically found in powerful radio galaxies at similar or larger redshifts (McCarthy 1988, and references therein). It is also at the high end of the distribution found for the field galaxies from the field surveys with typical limiting magnitudes of $B \sim 21 - 22$, and median redshifts of $z \sim 0.2 - 0.4$ (Ellis 1988, Colless et al. 1990). This difference may be indicative of an evolution of the average SFR in galaxies over the corresponding time interval.

The optical continuum shape in G0333+3208 is broadly similar to the flat spectrum or blue galaxies found in large numbers at comparable magnitude levels in the deep field surveys by Tyson (1988), Cowie et al. (1988), Lilly et al. (1991), etc. This population is generally interpreted as actively evolving normal galaxies at $z > 1$, which may be responsible for a substantial part of the energy and metals generation in the universe. The only constraint on the typical redshift of these galaxies is the absence of the Lyman limit in the U and B bands, suggesting that most of them are at $z < 3$ (Guhathakurta et al. 1990). G0333+3208 may be a representative member of this faint galaxy population.

Finally, we note that there are several other galaxies in the field, which have blue or neutral colors similar to G0333+3208, possibly signifying the presence of a loose cluster. We will be following these up with spectroscopic observations in the future.

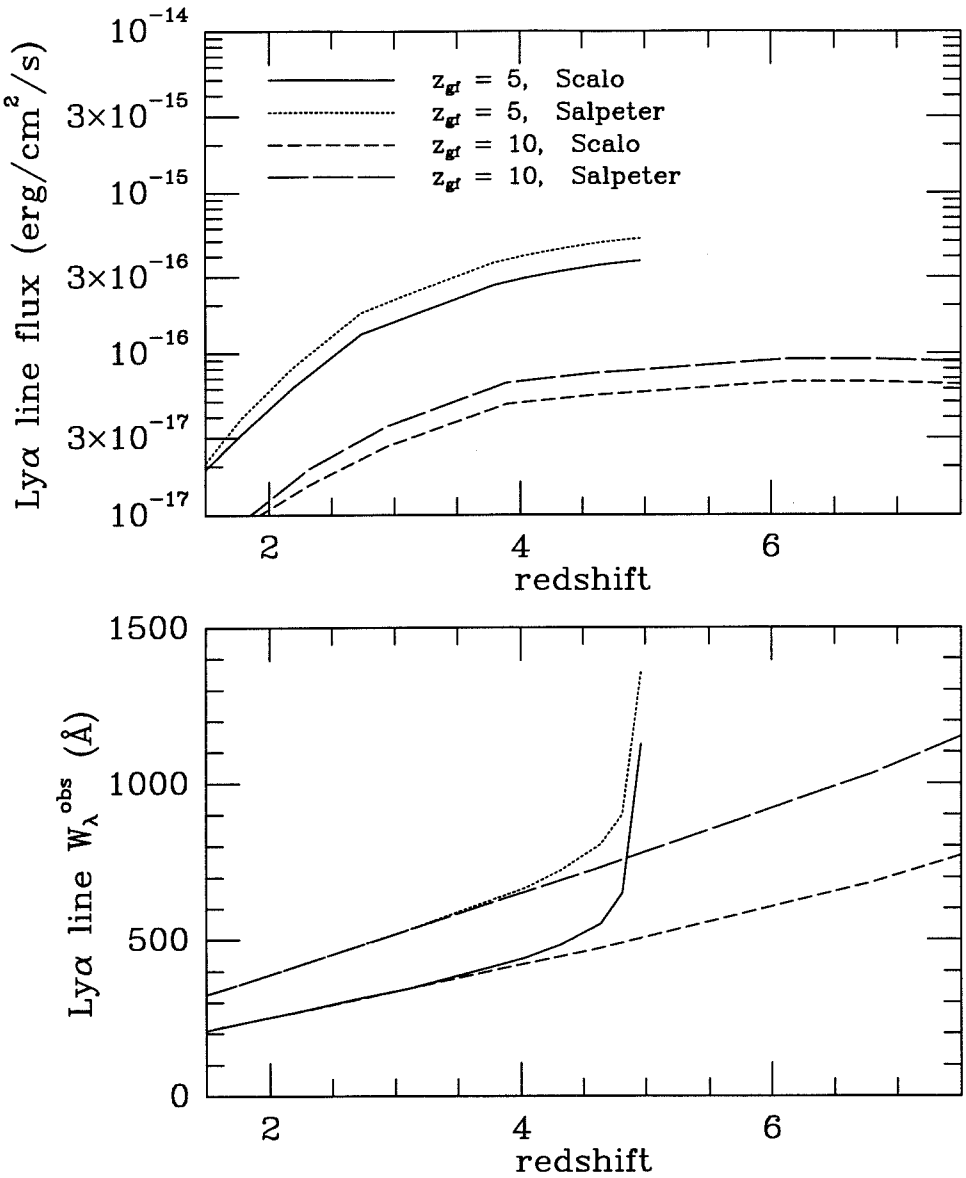

Figure 3.1: Modeling Primeval Galaxies

Bruzual $\mu = 0.95$ with an initial baryonic mass of 10^{11} $M_\odot$. Both Scalo and Salpeter IMFs are plotted for two different redshifts of formation (5 and 10). These models should bracket the range of reasonable expectations for the Lyα emission line from PGs. The top panel shows the range of emission-line fluxes expected from PGs, while the bottom panel shows the observed equivalent width expected to result from such models.

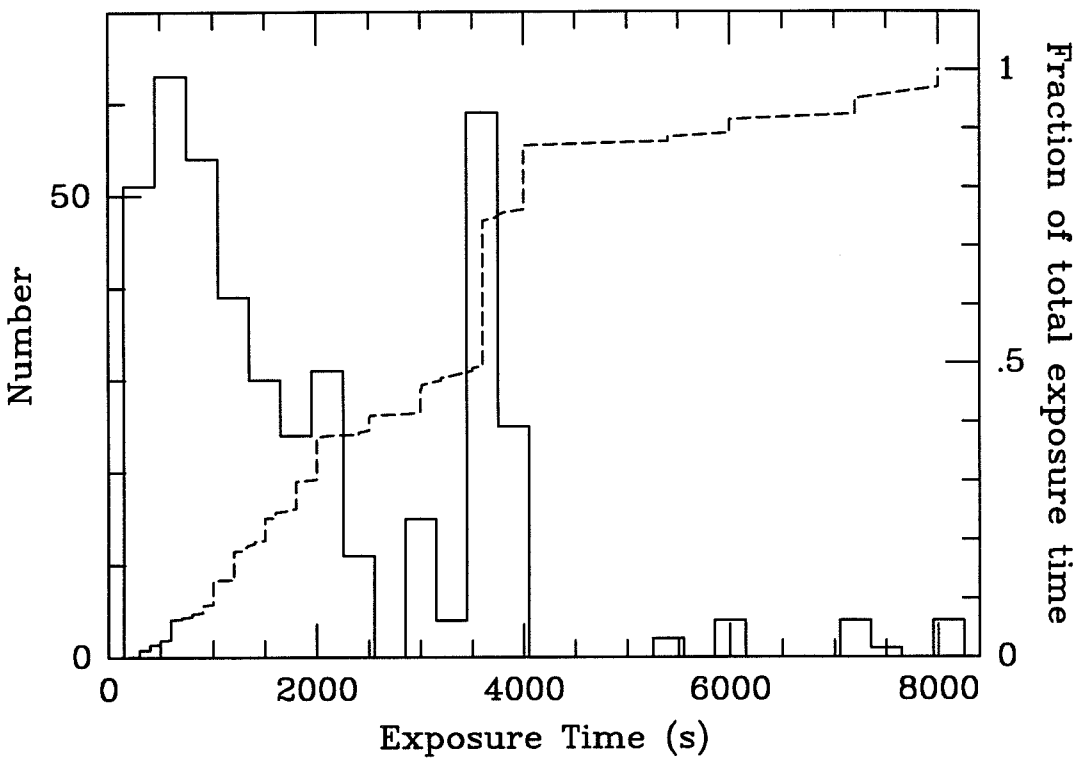

Figure 3.2: Exposure Time Histogram

A histogram of the 4-Shooter and DBSP red camera exposure times included in this survey. The dotted line is the integrated exposure time as a function of the exposure time of the individual frames, expressed as a fraction of the total time in the survey. While the area surveyed is weighted towards low exposure times, 38% of the spectra included here have exposure times of 2000 seconds or more. Fully half of the total exposure time is from spectra of 1-hr or longer exposure time, and 70% of the total time is from exposures of 2000s or longer. The DBSP blue camera frames are not included in this diagram, as they basically duplicate the red frames and serve to increase the effective wavelength coverage of the red frames.

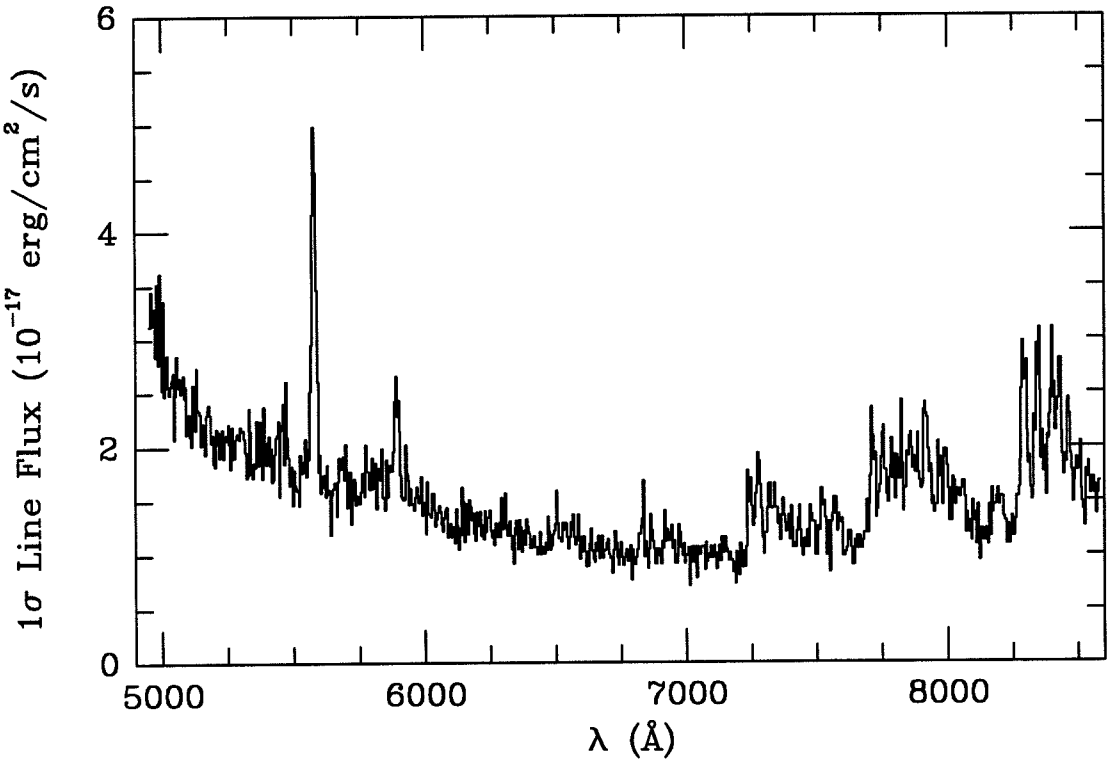

Figure 3.3: Emission Line Flux Limits

A sigma-spectrum from a 1-hour exposure with the 4Sh spectrograph. Note the increase in noise at the 5577Å [O I], 5893Å sodium lines, and in the OH forest lines, particularly longward of 7245Å. The upturn at the blue end of the spectrum is due primarily to the falloff in the sensitivity of the spectrograph below 5000Å.

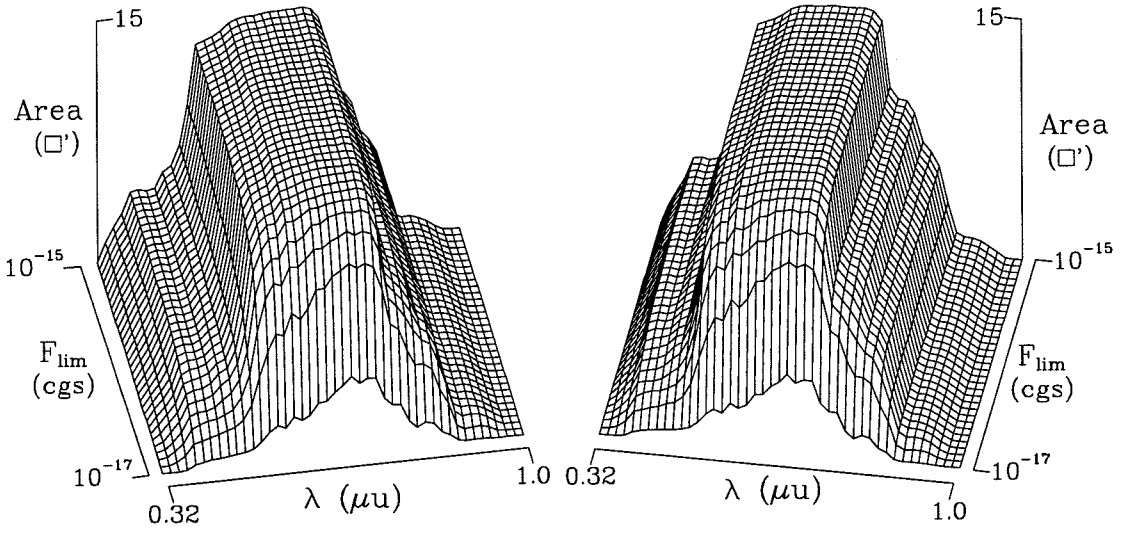

Figure 3.4: Observed-Frame Limits Datacube

A 3-dimensional representation of the limits achieved in this survey, expressed as cumulative area on the sky surveyed as a function of both the wavelength of observation and the emission-line flux limit reached. The strong "mesa" which runs from 5000Å to 7500Å represents the overlap region between the 4Sh and DBSP data, where the full survey area was sampled. Smaller areas were covered outside of this range, spanning the full optical spectral range visible from the ground, because only a portion of the spectra obtained cover these wavelengths. The full datacube was binned by a factor of 15 in both the wavelength and flux dimensions to produce this plot.

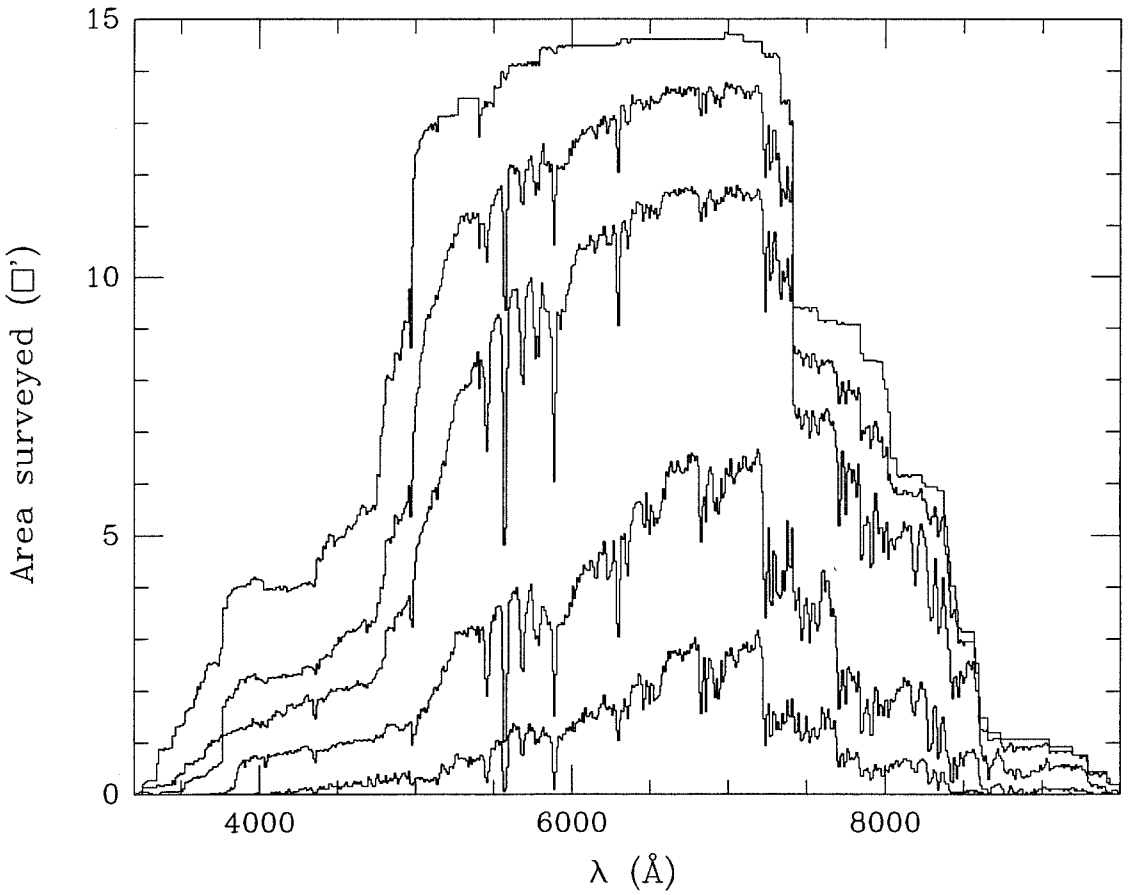

Figure 3.5: Observed-Frame Limits Detail: Wavelength vs. Area

Cuts through the datacube of Figure 4 in the λ – area plane, detailing the areas surveyed as a function of wavelength for several different flux limits. From bottom to top, the 5 curves represent 1-σ emission-line flux limits of 1.0×10^{-17}, 2.0×10^{-17}, 5.0×10^{-17}, 1.0×10^{-16}, and 1.0×10^{-15} erg cm^{-2} s^{-1} .

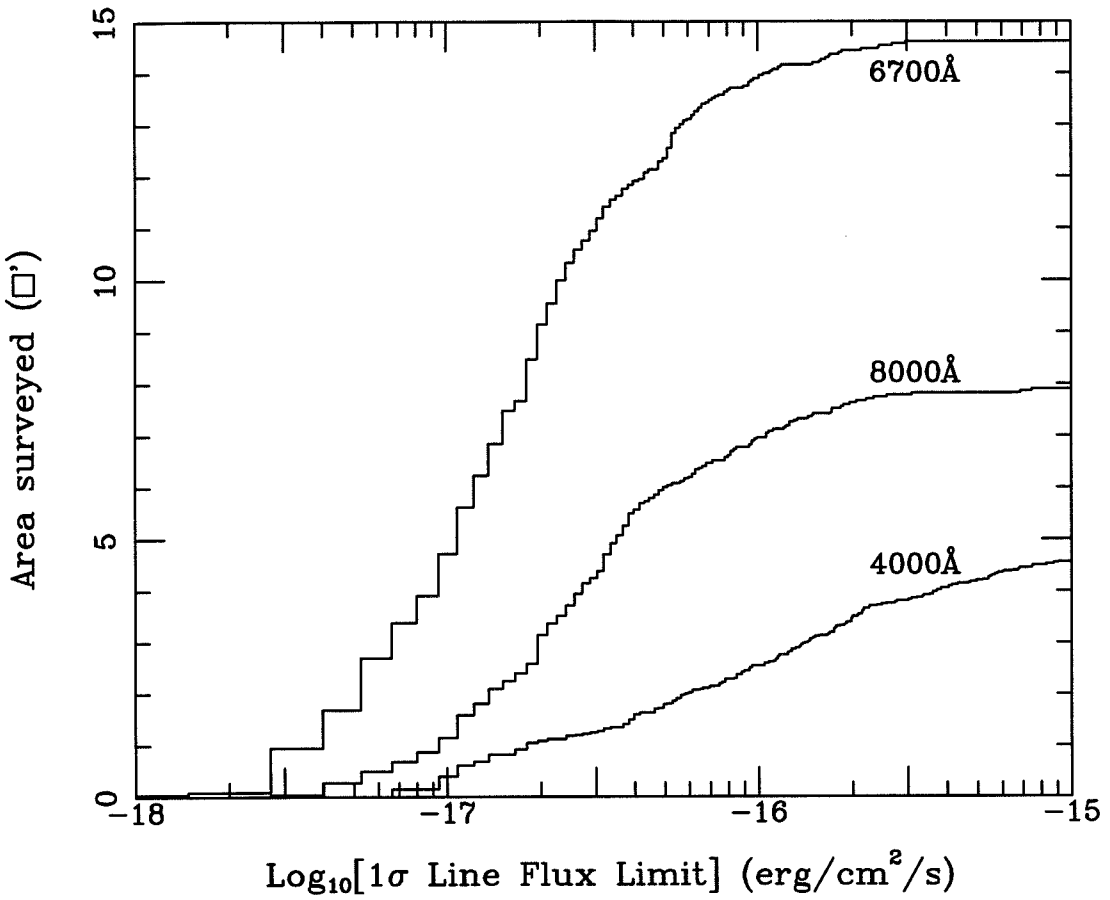

Figure 3.6: Observed-Frame Limits Detail: Line Flux vs. Area

Cuts through the datacube of Figure 4 in the line flux – area plane, showing the rapid drop-off in area surveyed at fainter flux limits. The 6700Å region of the night sky spectrum is free of emission lines, and is the region of greatest sensitivity in this survey. Cuts at 4000Å and 8000Å are also plotted to show that smaller areas were surveyed at the extremes of the optical spectrum due to the fact that only a portion of the spectrograph set-ups sample these spectral regions.

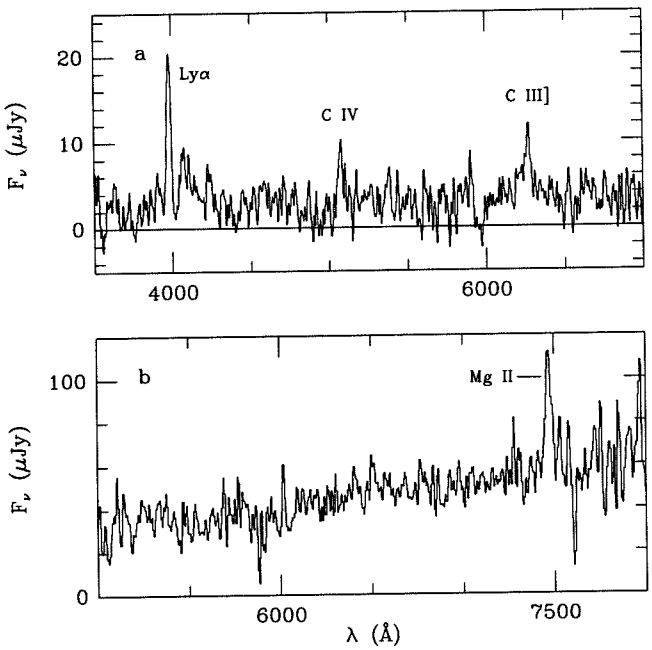

Figure 3.7: Quasar Spectra

Spectra of the two quasars discovered during this survey. a) Q0856+406, a $z = 2.29$ quasar with a strong, narrow component to the Lyα line. b) Q1233+4749 $z = 1.669$ quasar. A broad C III] λ1909 line is faintly visible on the spectroscopic CCD frame of this QSO, though it does not show in this spectrum.

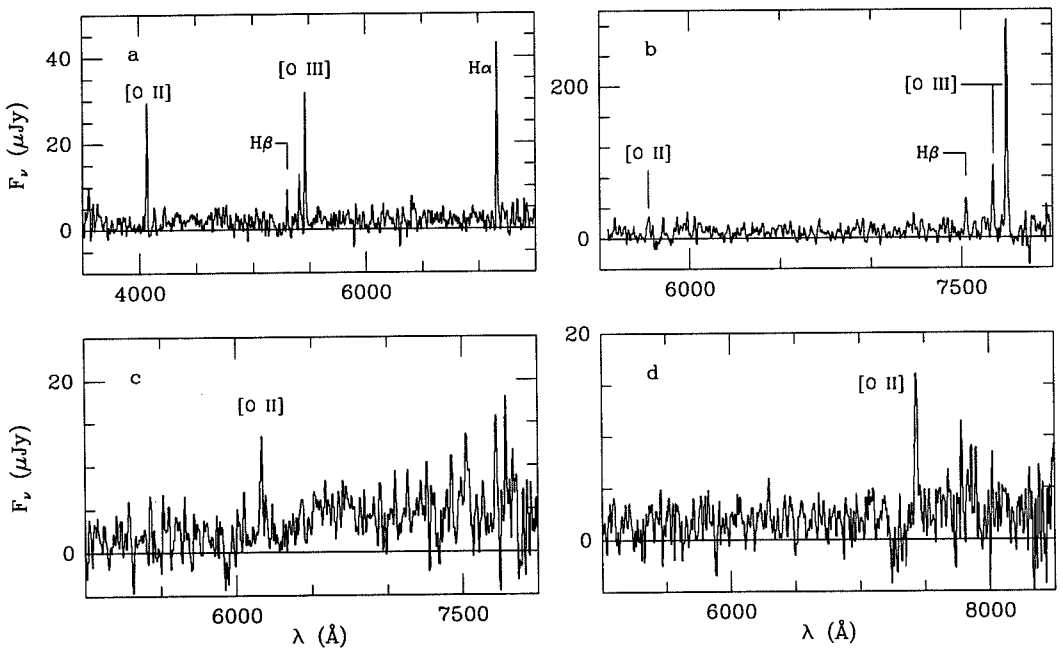

Figure 3.8: Example Spectra of Serendipitous Objects

Example spectra of 4 of the serendipitously discovered galaxies from this survey. They are identified as a) a $z = 0.091$ galaxy with strong [O II], [O III], and Balmer emission lines, found in the field of the radio galaxy B3 0123+402; b) a $z = 0.548$ galaxy in the field of PC 1233+4752, with strong [O III] and Hβ, but only weak [O II]; c) a $z = 0.654$ galaxy from the FP 1454+34 (TDT, Fabry-Perot survey field), where the 4000Å break confirms that the single line is [O II]; and d) a $z = 0.995$ galaxy found in the FP 0031+23 field (TDT). For the latter case, a weak 4000Å break and strong blue continuum blueward of the emission line, as well as an absence of other emission lines, confirms the identification of the isolated emission line as [O II].

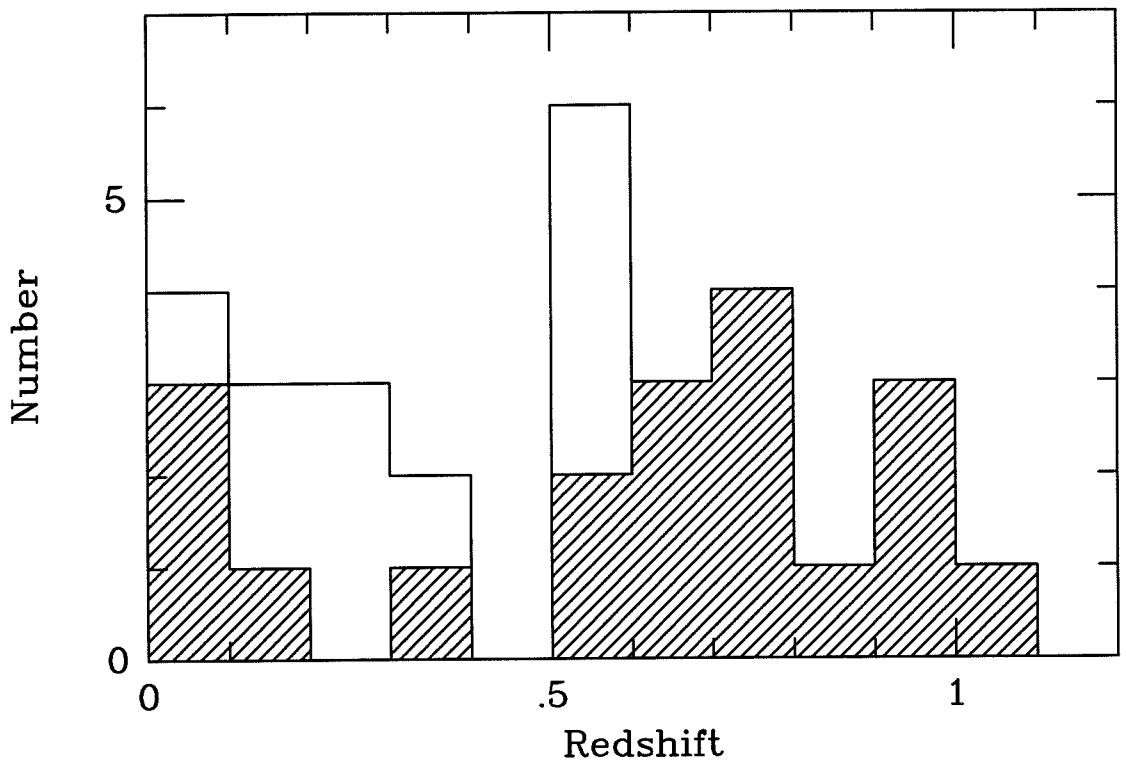

Figure 3.9: Redshift Histogram

Redshift histogram for the 30 galaxies for which we were able to derive a firm redshift. The hatched area applies to the [O II] λ3727 lines only. There is a curious lack of objects detected in the range of $0.4 < z < 0.5$, given that objects at this redshift are particularly easy to recognize, with [O II], [O III], and Hβ all falling within the wavelength region sampled by essentially every spectrum in this survey.

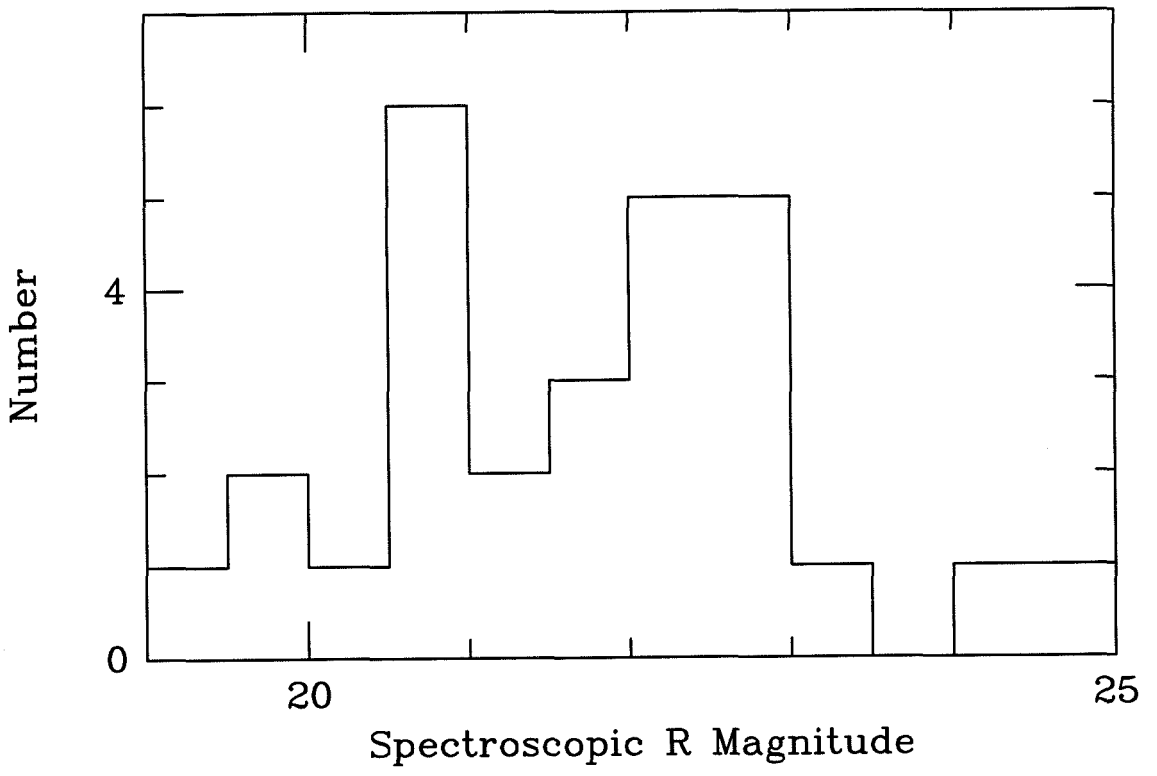

Figure 3.10: R Magnitude Histogram

Number counts for the galaxies with firm redshifts for which we were able to determine a spectroscopic R magnitude. Note that the galaxies with $R \geq 24$, equivalent to $B \geq 25$, should be considered limits at $R \geq 24$ rather than accurate determinations of the continuum magnitudes, as it is exceedingly difficult to detect continuum below this level.

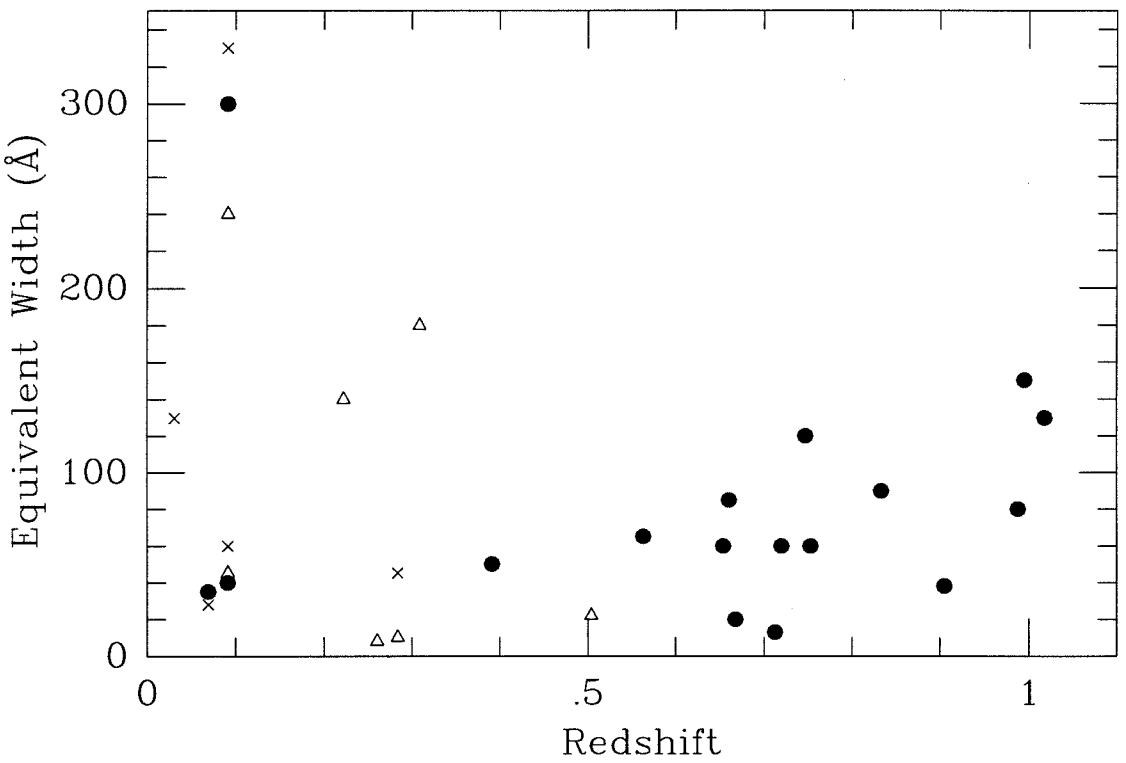

Figure 3.11: Observed Equivalent Widths vs. Redshift

Observed equivalent widths (not corrected for 1+z) of the identified lines as a function of redshift. Filled circles are [O II] λ3727, open triangles are [O III] λ5007, and crosses are for Hα. There are no correlations within the data, and the [O II] equivalent widths are consistent with those found in the deep field spectroscopic surveys.

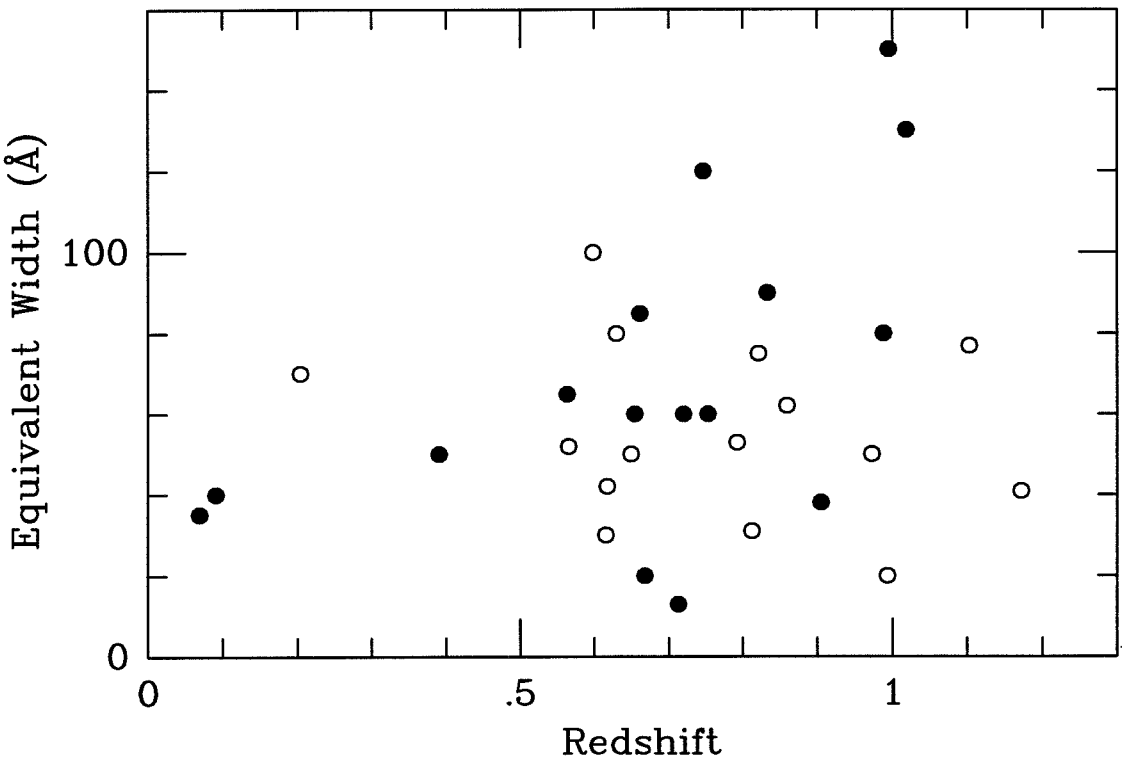

Figure 3.12: [O II] Equivalent Width vs. Redshift

Equivalent widths of the [O II] λ3727 lines as a function of redshift. Filled circles are from the objects for which we were able to determine a firm redshift, while the open circles are for the objects with only tentative redshifts assigned, assuming the detected line was [O II]. The similar distribution of the two samples suggests that the [O II] identification of the lines in the second group is a reasonable interpretation.

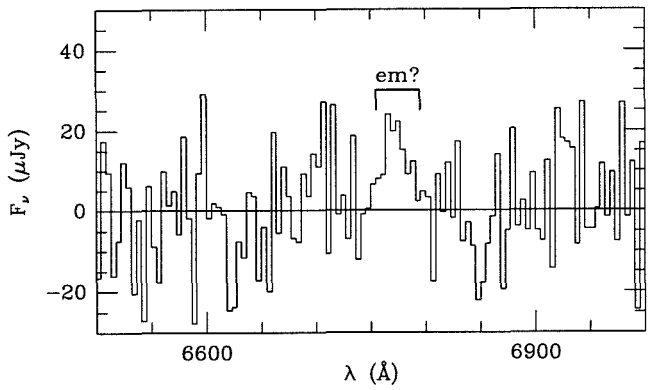

Figure 3.13: Candidate Lyα Emission

A portion of the spectrum containing the emission line of the Lyα candidate from the PC 1158 field. The formal significance of the line is 8.2σ, determined as described in the text, and has an integrated line flux of 3.2×10^{-16} erg cm^{-2} s^{-1} . It lies in a portion of the night sky spectrum free of emission lines, and is not associated with any features on the flatfield frame which might have printed through.

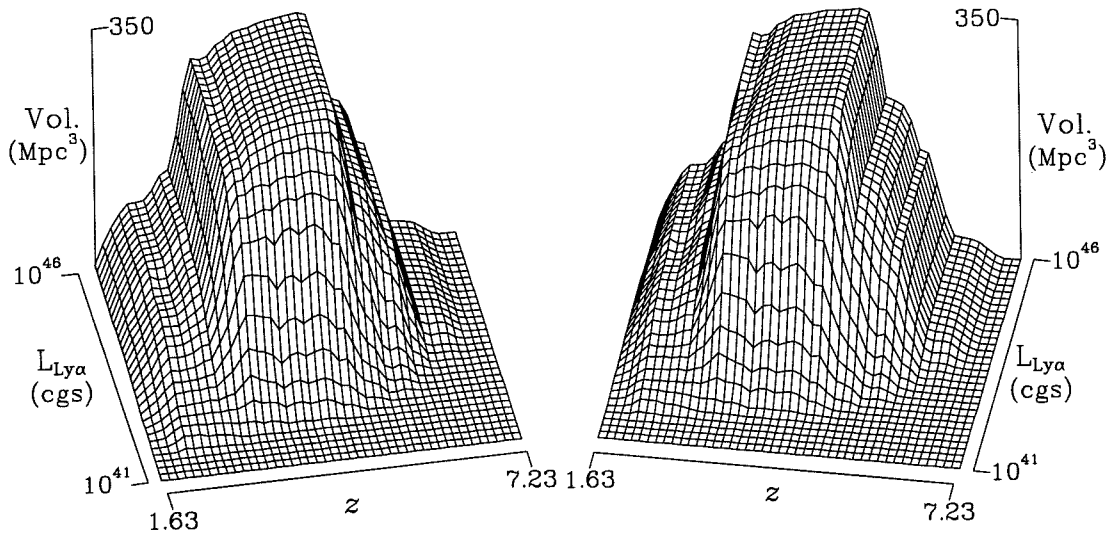

Figure 3.14: Restframe Limits Datacube

A 3-dimensional representation of the restframe comoving volume surveyed, expressed as a function of both the redshift of Lyα and the Lyα emission-line luminosity limit. The flat-topped "mesa" of Figure 4 appears slanted here because more volume is surveyed at higher redshifts for a given unit of area on the sky. The datacube has been rectified, such that lines of constant line luminosity are straight. The lines of constant line flux from Figure 5 would otherwise be curved in this figure, as a given line flux limit samples to much fainter line luminosities at lower redshifts. The full restframe datacube was binned by a factor of 15 in both the wavelength and flux dimensions to produce this plot, and a cosmology of $H_0 = 75$ km s^{-1} Mpc^{-1} and $\Omega_0 = 0.2$ was assumed for the conversion from observed coordinates.

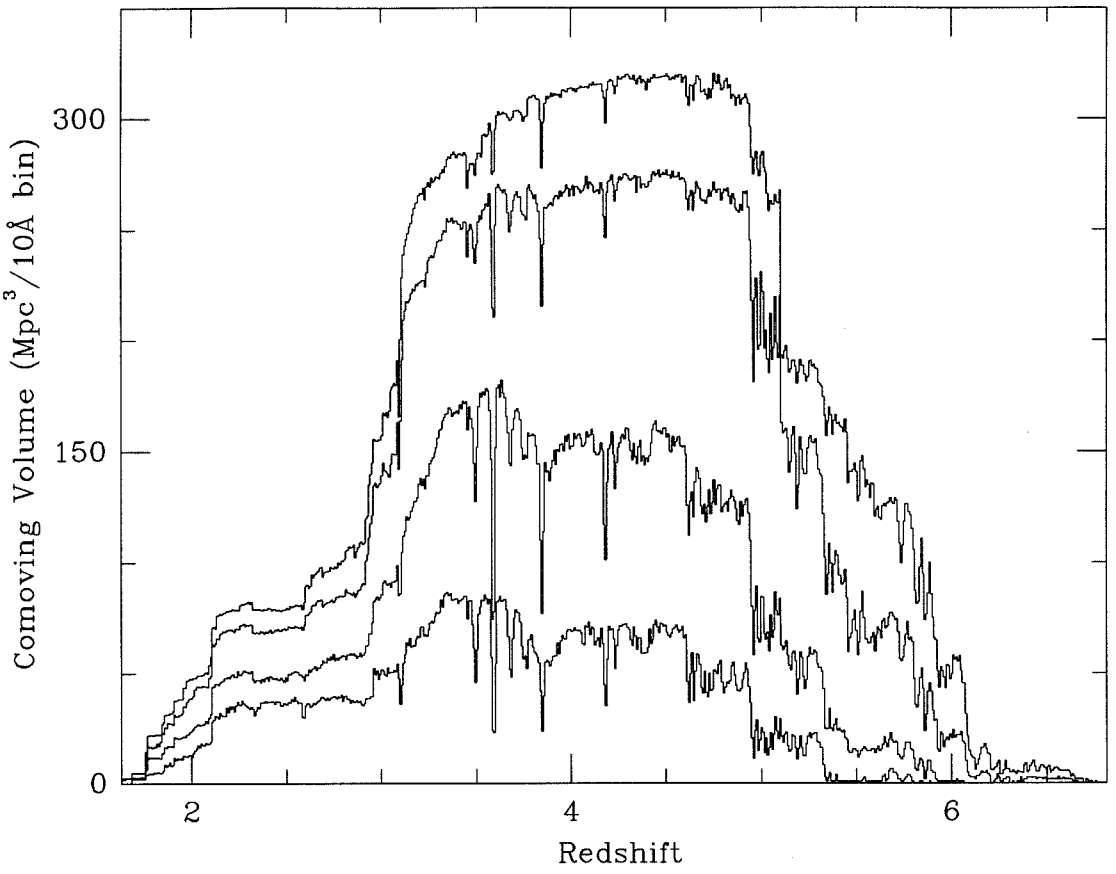

Figure 3.15: Restframe Limits Detail: Volume vs. Redshift

Cuts through the restframe datacube in the redshift – volume plane, detailing the volume surveyed at different line luminosity limits. From bottom to top, the 4 curves represent the comoving volume surveyed *per 10Å bin* to a 1-σ limiting restframe Lyα line luminositiy of 2.45×10^{42}, 4.90×10^{42}, 1.23×10^{43}, and 2.45×10^{43} erg s^{-1}, equivalent to unobscured star formation rates of 10, 20, 50, and 100 $M_\odot$ yr^{-1}. Note that the total volume surveyed at a given luminosity is the integral under these curves. The volume surveyed at the equivalent SFRs of 10, 20, 50, and 100 $M_\odot$ yr^{-1} are, respectively, 20400, 44800, 83600, and 102600 comoving Mpc^3. $H_0 = 75$ km s^{-1} Mpc^{-1} and $\Omega_0 = 0.2$ were assumed for the cosmology.

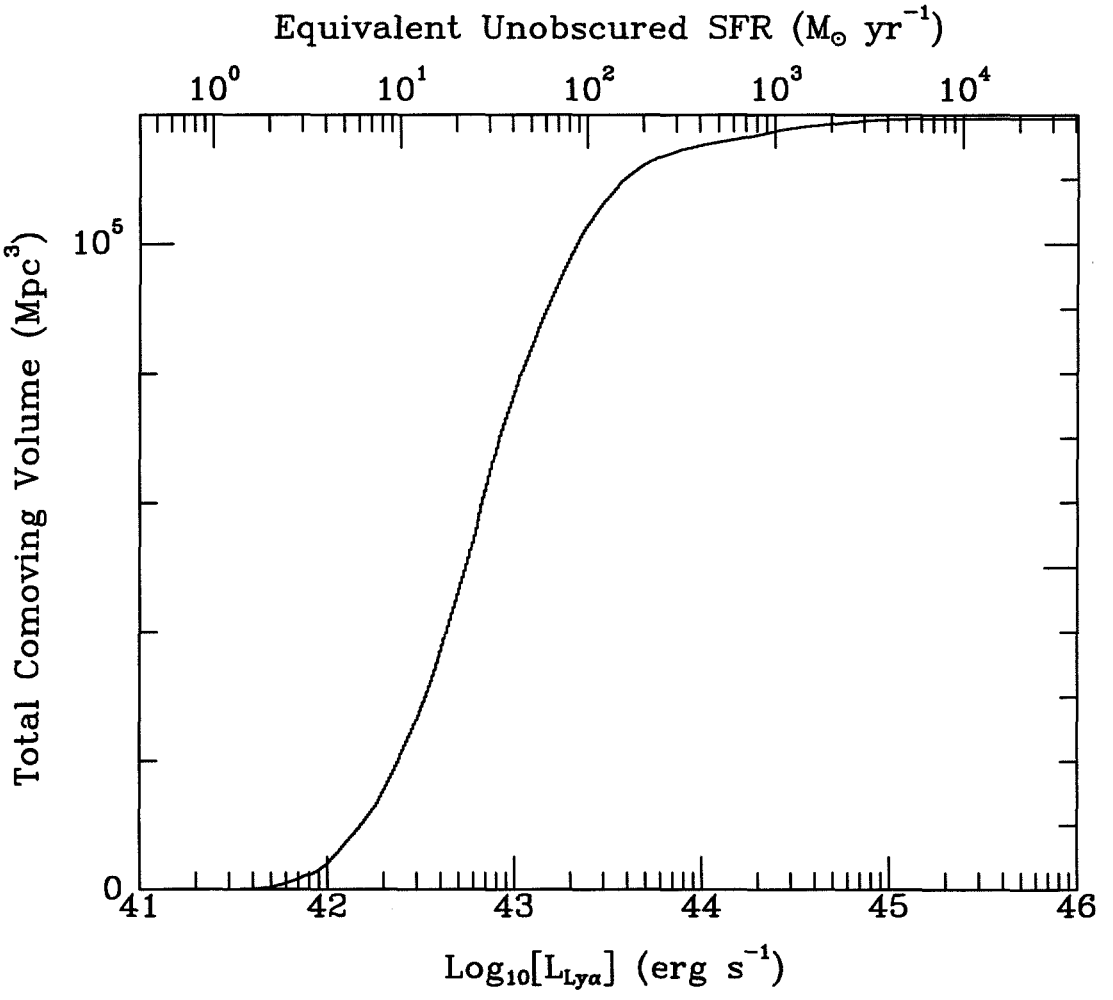

Figure 3.16: Total Comoving Volume Surveyed

Integrating the restframe datacube along lines of constant luminosity gives the total comoving volume surveyed as a function of the Lyα emission-line luminosity. This removes the redshift information, but allows for a comparison with the limits achieved in other PG surveys. Equivalent unobscured star formation rates corresponding to these line luminosities are shown on the top axis.

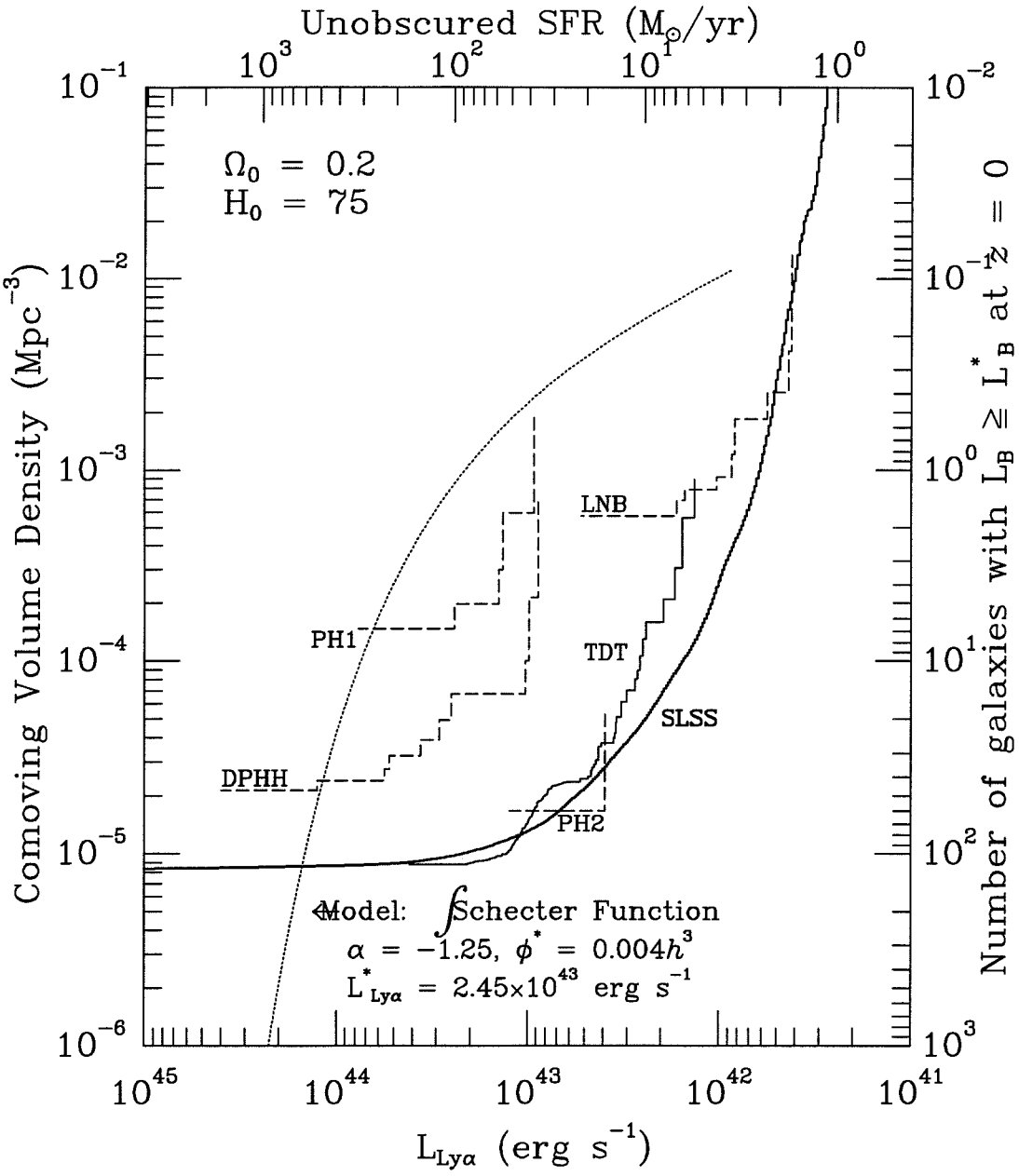
Unobscured SFR ($M_\odot$/yr)
10^3
10^2
10^1
10^0
Ω_0 = 0.2
H_0 = 75
LNB
PH1
TDT
SLSS
DPHH
PH2
Model: ∫Schecter Function
$\alpha = -1.25$, $\phi^* = 0.004h^3$
$L^*_{Ly\alpha} = 2.45\times10^{43}$ erg s^{-1}
Comoving Volume Density (Mpc^{-3})
10^{-1}
10^{-2}
10^{-3}
10^{-4}
10^{-5}
10^{-6}
Number of galaxies with $L_B \geq L^*_B$ at $z = 0$
10^{-2}
10^{-1}
10^0
10^1
10^2
10^3
10^{45}
10^{44}
10^{43}
10^{42}
10^{41}
$L_{Ly\alpha}$ (erg s^{-1})

Figure 3.17: Restframe Limits: Comparison with Other Surveys

A restframe limits diagram showing the comoving volume number density surveyed as a funtion of the limiting 1-σ Lyα luminosity. A cosmology of $H_0 = 75$ km s^{-1} Mpc^{-1} and $\Omega_0 = 0.2$ were assumed in converting the observed limits to restframe coordinates. This plot is the same as Figure 13 of TDT, with the addition of the SLSS limits. The other surveys, plotted for comparison, are DPHH = De Propris et al. 1993; LNB = Lowenthal (1991); PCJ = Parkes, Collins & Joseph (1994); PH1 = Pritchet & Hartwick (1987); and PH2 = Pritchet & Hartwick (1990). The top x-axis shows the star formation rate corresponding to the Lyα luminosity on the bottom x-axis, while the right y-axis gives the number of $L \geq L^*_B$ galaxies expected within the comoving volume surveyed (normalized to the $z = 0$ space density of L^* galaxies). Regions to the upper left of the limit lines are excluded by the surveys, and the model PG luminosity function is as described in the text. Scaling to lower SFR moves the model to the right. The model Lyα emission line luminosity function is an integral of the $z = 0$ Schechter function (i.e., assuming no density evolution), with a normalization appropriate for spheroids today: $\phi^* = 0.004h^3$ and $\alpha = -1.25$ (Baron & White 1987). We also assume a characteristic luminosity of $L^*_{Ly\alpha} = 2.45 \times 10^{43} h^{-2}$ erg s^{-1} (TDT, their equation 4), corresponding to an unobscured star formation rate of 100 $M_\odot$ yr^{-1}.

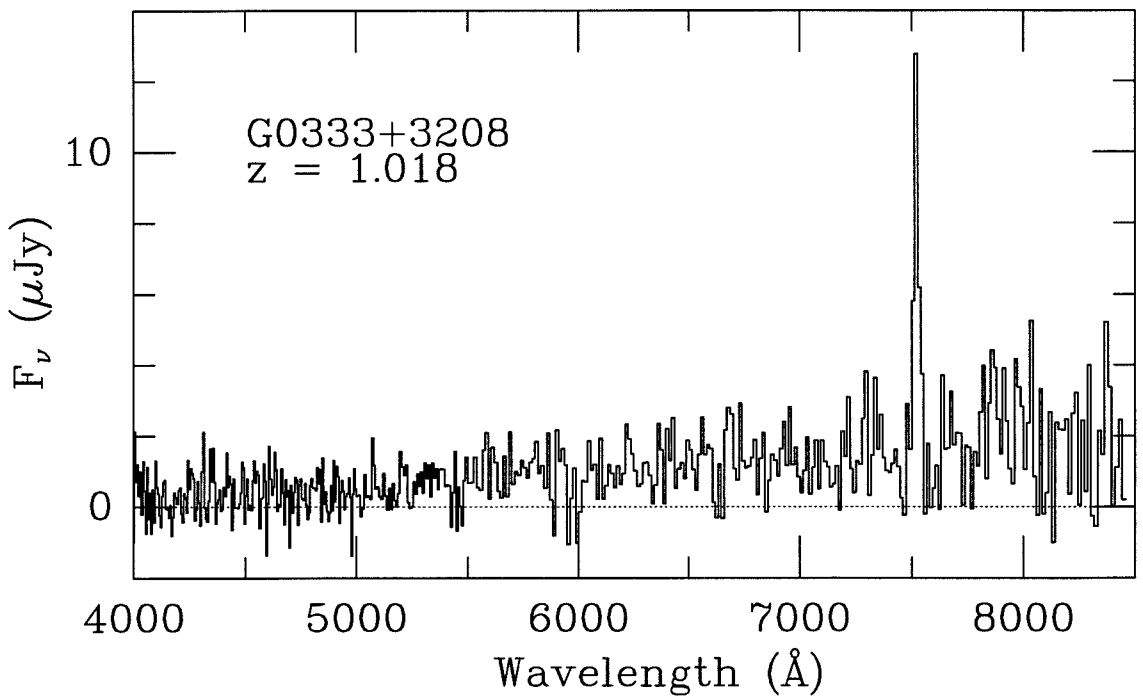

Figure 3.18: Spectrum of G0333+3208

A spectrum of the $z = 1.018$ galaxy G0333+3208, coaveraged from all three of our observations. The absolute flux calibration is accurate to about 30%, based on a comparison with the broadband magnitudes. The strong emission line at 7523Å is interpreted as [O II] λ3727 at $z = 1.018$.

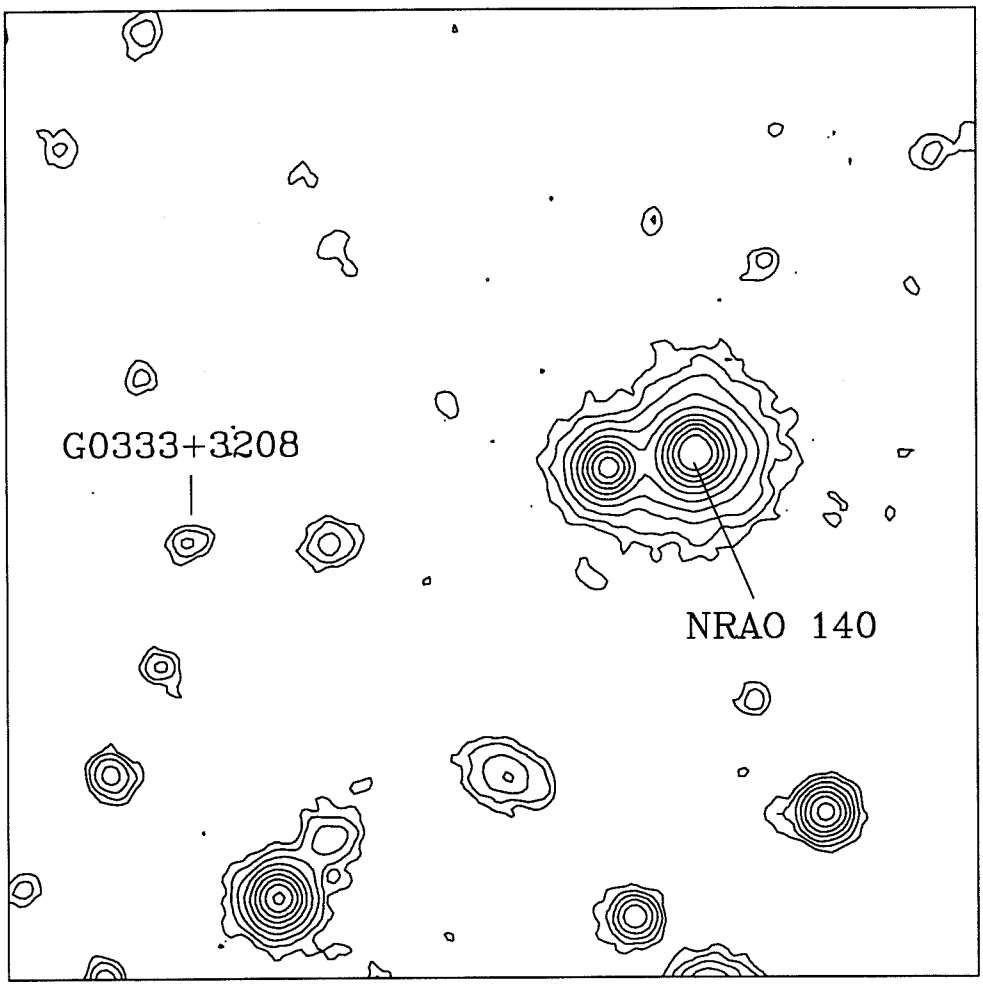

Figure 3.19: Broadband Image of G0333+3208

Coadded Gunn g, r, and i CCD frames of the field of G0333+3208, obtained at Palomar. North is at the top, east to the left, and the field size is 60 arcsec square. The emission–line object and the quasar are indicated. The object just east from the quasar is a foreground Galactic star. Contours have an arbitrary zero-point, and are spaced by a factor of 2 in intensity.

Chapter 4

The Preliminary Infrared Narrowband Imaging Survey‡

ABSTRACT

We discuss the feasibility of detecting the progenitors of normal elliptical galaxies (PGs) undergoing their first massive starbursts at large redshifts using narrowband imaging in the near infrared. Four strong emission lines are plausible tracers of such objects, viz., [O II] λ3727, Hβ λ4861, [O III] λ5007, and Hα λ6563, spanning the redshift range $z \sim 1 - 5.5$ in the standard JHK bands. The expected line fluxes are in the range $F \sim 10^{-16\pm1.5}$ erg/cm^2/s, depending on the star formation history, emission line, amount of dust present, redshift, and cosmology. The brighter end of this flux range is already within the reach of existing technology. We estimate the expected surface density of protogalaxies on the sky and several other related quantities.

We report on the results of a pilot project done at Palomar to search in the K band for [O II] λ3727 emission line galaxies in the fields of three $z > 4$ quasars, using a narrowband ($\Delta z = 0.013$) imaging technique. The total area surveyed is 0.72 arcmin^2, with a limiting line flux (90% confidence limit) in the range $F \sim (4 - 10) \times 10^{-16}$ erg/cm^2/s. The total comoving volume covered is $V \sim 100$ Mpc^3, down to limiting restframe line luminosities in the range $L \sim$

‡ Adapted from a paper entitled "Searches for Primeval Galaxies in the Near Infrared," by D. Thompson, S. Djorgovski, and S. V. W. Beckwith, which appeared in the Astronomical Journal: 1994, AJ, 107, 1.

$(0.3 - 30) \times 10^{43}$ erg/s, or implied unobscured star formation rates (SFR) in the range $SFR \sim (30 - 15000)\ M_\odot/\mathrm{yr}$, for a Friedman cosmology with $H_0 = 75$ km/s/Mpc, $\Omega_0 = 0.2$, and $\Lambda_0 = 0$. No viable candidate protogalaxies were found, though this was not entirely unexpected given our limited field size and line flux limits, but the limits achieved are an improvement over previously published surveys. Forthcoming experiments should be able to extend these limits by two or more orders of magnitude in comoving volume coverage and one or two orders of magnitude in limiting flux, and could detect young ellipticals if our calculations are representative of their emission-line properties.

4.1 Introduction

How galaxies were assembled is one of the central questions of cosmology. Identification of the population of progenitors to normal galaxies is similarly important for many fields of astrophysics. Young galaxies at high redshifts are expected to be faint and difficult to observe, and no such population has been unambiguously identified despite considerable effort (cf., e.g., Djorgovski & Thompson 1992, or Djorgovski 1992 for recent reviews).

We will refer to young ellipticals or bulges undergoing their first major burst of star formation at large redshifts as *primeval galaxies*, hereafter PGs. This is an observational definition: massive star formation and, if present, active galactic nuclei (AGN) are probably the principal sources of energy in young galaxies leading to observable manifestations in the visible and infrared bands (cf. Djorgovski 1992 for a more detailed discussion). Assembly of the dark halos, although theoretically quite important, is currently thought to be unobservable, unless it leads to star formation or other dissipative phenomena, and we do not include it in the discussion which follows.

There should have been early populations of massive stars. The presence of metallic lines in the spectra of quasars out to $z \sim 5$, i.e., when the universe was at most $\sim$ 1 Gyr old, indicates that massive starbursts occurred early in some objects (Haman & Ferland 1993, Matteucci & Padovani 1993). More generally, average metallicities of elliptical galaxies comparable to the solar value or greater probably occurred very early (cf. Matteucci 1993), and at least cluster ellipticals appear to be an old, homogeneous population of such objects (Bower et al. 1990, de Carvalho & Djorgovski 1992). We are, therefore, looking for a *population* of objects which may be identified as progenitors of the present-day normal, early-type galaxies.

Progenitors of normal disks probably have been found in the form of damped Lyman alpha (Lyα) absorbers (cf. Wolfe 1993, and references therein). Their

formation probably extends over a good fraction of the Hubble time, and is thus a rather different phenomenon from the early formation of ellipticals, at least in clusters.

We believe that the high-redshift objects found to date, including radio galaxies, quasars, and their companions (Djorgovski et al. 1985; McCarthy et al. 1987; Djorgovski 1988; Rowan-Robinson et al. 1991; etc.) derive the bulk of their luminosity from AGN. This does not actually exclude them from being PGs, even according to our definition, but it has thus far been impossible to unambiguously measure the SFR and, therefore, establish their connection to the formation of the galaxies themselves. For this reason, we seek a population of young galaxies whose luminosities derive principally from star formation and constitute clear examples of PGs.

Most searches for "normal" PGs so far have been based on the use of Lyα line emission as a detectable signature; recent examples include the surveys by De Propris et al. (1993), or Thompson et al. (1992, 1993). The modern searches have reached the necessary sensitivity and area coverage (cf. Djorgovski et al. 1993 for a recent summary of limits), but no obvious population of PGs has been seen so far.

There are two standard explanations for the failure of Lyα searches thus far. The first is that PGs were obscured by dust which effectively extinguished the Lyα line emission. Complete obscuration of the young galaxies by dust is excluded by the limits on distortions of the cosmic background spectrum (Mather et al. 1993); enough energy should have been generated in the old, metal-rich stellar populations around us to produce a detectable sub-mm background (cf., e.g., Djorgovski & Weir 1990, and references therein). But mild obscuration can strongly depress Lyα relative to longer-wavelength lines without seriously distorting the cosmic background. The second is that PGs released the bulk of their energy at very high redshifts, so that the Lyα emission lies beyond the visible band, the band to

which almost all previous searches are limited, $2 < z_{PG} < 5$. If either $z_{PG} > 5$, or PGs were slightly dusty, a good way to detect young, star-forming galaxies at large redshifts would be through their hydrogen or oxygen emission lines, now redshifted into the near IR. These possibilities are the motivation for the present work.

4.2 Line Fluxes and Other Parameters

Given the meager information contained in broadband colors, some emission-line signature of PGs is necessary, both as a redshift indicator and as a probe of physical conditions in the object. Strong line emission is expected from objects powered by massive star formation, i.e., PGs as mega - H II regions. The strongest lines on which a search could be based include [O II] λ3727, Hβ λ4861, [O III] λ5007, or Hα λ6563, or perhaps even Lyα λ1216 at high (but for ellipticals still plausible) z_{PG}. For example, in the K-band window, this corresponds to the redshift ranges 4.42 – 5.44 for [O II], 3.16 – 3.94 for Hβ, 3.03 – 3.79 for [O III], 2.08 – 2.66 for Hα, and perhaps somewhat unlikely, 15.5 – 19 for Lyα. In the J-band window, Lyα occurs in the range $z_{PG} = 8 - 10$. Observable redshift intervals for each line in the JHK bands are indicated in Figure 4.1.

It is noteworthy that in the redshift intervals $\Delta z \sim 1.3 - 1.7$, $\Delta z \sim 2.1 - 2.6$, and $\Delta z \sim 3.1 - 3.8$, more than one line can be observed using different bands, thus making the redshifts easier to measure and verify. These redshift intervals may be the optimal hunting grounds for PGs, although pursuit of objects at $z > 4$ using the [O II] λ3727 line alone certainly seems attractive.

We estimate the star-formation powered line luminosities by using Kennicutt's (1983) ratio of $H\alpha$ emission to SFR to estimate the $H\alpha$ strength: $1 M_{\odot}$/yr of star formation produces an extinction corrected $H\alpha$ line luminosity of 1.12×10^{41} erg/s. Other line strengths are normalized to $H\alpha$ using values from the literature for objects powered by star formation. Table 4.1 lists these line ratios. There is a large spread in predicted ratios, and we list our best guesses at the end of Table 4.1. These guesses are only a guideline; real variations in star-forming galaxies are to be expected, e.g., due to variations in the initial mass function. Incidentally, the Case B recombination value for the Lyα to Hα ratio without obscuration is $\sim$ 8. We neglect here the possible contributions of shock excitation, e.g., due

to protogalactic infall and merging, and to supernovæ; the [O II] λ3727 line in particular would be enhanced due to such processes.

To estimate the line fluxes, we assume an $SFR = 100\ M_{\odot}/\mathrm{yr}$, which may be a characteristic value for a PG and is comparable to the SFR seen in ultraluminous starburst galaxies at low redshifts. Thus, for the $H\alpha$ line $L_{H\alpha} = 1.12 \times 10^{43}$ erg/s, and for the other lines scaled according to the last row of Table 4.1. The observed line flux F, corresponding to the restframe line luminosity L, is given by:

$$F = \frac{L}{4\pi D^2 (1+z)^2} \ , \tag{1}$$

where D is the proper distance given by:

$$D = \left(\frac{2c}{H_0}\right) \frac{\Omega_0 z + (\Omega_0 - 2)[(1+\Omega_0 z)^{1/2} - 1]}{\Omega_0^2 (1+z)} \ . \tag{2a}$$

for $\Omega_0 > 0$, or by:

$$D = \left(\frac{c}{H_0}\right) \frac{z(1+z/2)}{(1+z)} \ . \tag{2b}$$

for $\Omega_0 = 0$. Using our adopted average line ratios and corresponding luminosities, in Figure 4.1 we plot the expected line fluxes for an "average" Friedman model cosmology with $H_0 = 75$ km/s/Mpc, $\Omega_0 = 0.2$, and $\Lambda_0 = 0$. The effect of changing Ω_0 is illustrated in Figure 4.2; the scaling with H_0 is in the sense that for a given restframe line luminosity, the observed line fluxes scale as $(H_0/75\mathrm{km/s/Mpc})^2$.

Line fluxes of the order of $\sim 10^{-16}$ erg/cm^2/s can be readily detected with present-day technology, and the forthcoming generation of 8 to 10-meter class telescopes should extend this another order of magnitude. Note that Hβ, [O III] λ5007, or Hα emission line fluxes detected from powerful radio galaxies at high redshifts ($2 < z < 3.8$) are typically of order $\sim 10^{-16}$ erg/cm^2/s (Eales & Rawlings 1993, and references therein), although their line emission is very likely powered by an active nucleus rather than by star formation. Similarly, the Hα + [N II] emission line flux detected from the peculiar object IRAS 10214 ($z = 2.286$) is $\sim 10^{-14}$ erg/cm^2/s (Soifer et al. 1992).

Of course, the presence of dust would lower these fluxes, while the presence of an early AGN would make them higher. We illustrate the possible attenuation effects due to restframe dust extinction in Figure 4.3 using a simple dust screen model and the Galactic extinction curve from Seaton (1979). In reality, variations in the geometry of dust and its chemical composition can be expected to cause some variations, which are difficult to model; this diagram is simply meant to be indicative. In any case, these lines are *much* less vulnerable to extinction than the Lyα line: the ratio of extinction at 1216 Å to that in the V band is $A_{1216}/A_V \simeq 3.1$ (both in magnitudes!), for the Galactic extinction curve.

Finally, we estimate the number density of PGs per unit solid angle and unit redshift interval as follows. We integrate the standard Schechter luminosity function:

$$\frac{dN}{dV} = \Phi_* \int_{L_{min}/L_*}^{\infty} \left(\frac{L}{L*}\right)^{\alpha} \exp\left(\frac{-L}{L*}\right) d\left(\frac{L}{L*}\right) , \qquad (3)$$

where we have assumed $\alpha = -1.25$ and $\Phi_* = 0.020\ h^3$ (Huchra 1988). Down to $L_{min} = L_*$, we obtain a fiducial comoving number density of objects of 0.00172 per comoving Mpc^3 for $H_0 = 75$ km/s/Mpc, and 0.0212 per comoving Mpc^3 down to $L_{min} = 0.1L_*$. These integration boundaries are arbitrary, and simply meant to indicate the range expected for the progenitors of normal galaxies today. We also neglect the possible effects of density evolution, which probably goes in the direction of there being more fragments of lower luminosity at higher redshifts. Again, our purpose here is to provide an order-of-magnitude estimate only.

The comoving volume sampled by a solid angle of 1 square arcmin, for a $\Lambda_0 = 0$ Friedman cosmology, is given by the formula:

$$\Delta V = \frac{4\pi D^2 c \Delta z}{\omega H_0 (1+z)(1+\Omega_0 z)^{1/2}} , \qquad (4)$$

where z is the central redshift of the shell, $\omega = 1.4851 \times 10^8$ is the number of square arcmin on the sphere, and D is the distance given by eqs. (2ab). Figure 4.4 shows the expected numbers of objects down to a luminosity of L_* or 0.1 L_*,

in the comoving volumes corresponding to a solid angle of 1 arcmin^2 (a typical detector size) and a redshift depth of $\Delta z = 0.01$ (a typical narrowband filter width). In order to have a fair chance of intercepting at least one object, coverage corresponding up to either some tens of arcmin^2, and/or a few tenths of the redshift depth are needed. Basically, you want to cover a comoving volume of space large enough to contain at least a few L_* galaxies, then image to as faint a level (i.e., as far down the luminosity function) as time will allow. The situation is more favorable for the lower density universes in that more volume is available, but the observable fluxes would also be lower in such models. Without a greater understanding of PGs and galaxy formation, it is difficult to differentiate between cosmologies when deciding on an observational strategy. The effect of a positive cosmological constant would be in the same direction as lowering Ω_0.

We thus conclude that PG searches in the near-IR are plausible, albeit by no means trivial, with existing technology.

4.3 A Preliminary Search at Palomar

We have conducted a pilot experiment at Palomar Observatory, to search for PGs using narrowband imaging in the near-IR. This experiment was intended as a testbed for future searches for primeval galaxies in the IR. We chose to use known high redshift objects as markers of possible protoclusters rather than attempt a completely unbiased search, since the purpose is to uncover *any* PG candidates, not an unbiased sample. The same rationale applies to optical searches (Djorgovski et al. 1991, Smith et al. 1993, and references therein).

These observations targeted [O II] λ3727 emission in the K-band window near three, $z > 4$ quasars. Table 4.2 lists the objects, while their coordinates, finding charts, and other data are given by McCarthy et al. (1988) and Schneider et al. (1989, 1991). The observations were also sensitive to the other three strong lines

at the corresponding lower redshifts: every one of our narrowband frames samples four independent redshift slices in the same pointing direction.

The instrument used was the Cassegrain IR Camera at the 200-inch Hale telescope, with a continuously variable interference filter (CVF) in the K-band. The resolution of the CVF corresponds to $\Delta z \simeq 0.013$, or ~ 4000 km/s in the rest-frame, which is well matched to galaxy cluster or supercluster sizes in redshift space. The detector is a 58×62 pixel InSb device with 0.313 arcsec square pixels, giving a total field size of 18.2×19.4 arcsec$^2 \simeq 0.1$ arcmin^2. The seeing ranged from 0.9 to 1.5 arcsec FWHM. The data were first corrected for nonlinearity and flatfielded using dome flats and sky frames, then sky-subtracted and median stacked to form the final image. Multiple exposures of bright, flat-spectrum IR flux standard stars were used to establish the flux limits in our narrowband frames. Broadband K exposures are used as a comparison; in one case, (PC 1247+3406), we also have off-line narrowband exposures. We look for objects which stand out in the narrowband exposures relative to the comparison band.

We shifted the telescope between sets of exposures to cover a larger area and facilitate flatfielding and sky subtraction. Thus, the flux limits are given at up to three levels corresponding to different depths covered. Unfortunately, it was impossible to align many of the frames subsequently to improve sensitivity owing to problems with recording accurate telescope offsets and the lack of bright objects in the fields on which to centroid. The flux limits reached are shown in Figure 4.5, and are listed in Table 4.3. Detection limits are at the 90% confidence level; our estimates of these fluxes are probably on the conservative side.

In the QSO 2203+29 field, the data taken in the two separate runs covered somewhat different areas, with some overlap. The deepest limits are from the overlap region of the two runs, which contains the quasar itself (data set a); the remaining "core" overlap areas for the two runs have comparable limiting flux (data set b); finally, the union of the boundary areas which were less well exposed

is even shallower (data set c). In the PC 1247+3406 field, there are data for two CVF settings, one centered on the [O II] line at the nominal quasar redshift, and one slightly redward, sampling the quasar continuum (or the [O II] line at a higher redshift). For the former, the core area of the mosaic (data set a) reaches the deepest limits; the less well exposed boundary region around it (data set b) has a higher flux threshold; and the entire data set (c) taken at the larger wavelength has a comparable depth. Finally, in the case of PC 2331+0216, we could not mosaic the data at all, and use the union of areas on four deep exposures for the search (data set a). The wavelength is in the wings of the K band filter, and the atmospheric absorption is also partly responsible for the relatively high flux thresholds achieved.

Tables 4.4a – 4.4d list the comoving volumes and limiting line luminosities for each data set, for the four strong lines of interest here. The total comoving volume covered in all four lines is $V \simeq 100$ Mpc^3, which should contain at least one $0.1L_*$ galaxy, and has only a $\sim 10 - 20\%$ probability of containing a single L_* galaxy. We also give the corresponding unobscured star formation rates, according to the calibration given in Section II under a Friedman model cosmology with $H_0 = 75$ km/s/Mpc, $\Omega_0 = 0.2$, and $\Lambda_0 = 0$. The limiting star formation rates around these targets appear to be rather too large; however, comparable or larger star formation rates have been quoted for the peculiar object IRAS 10214, i.e., $SFR \sim 3000$ to 10000 $M_\odot$/yr (Rowan-Robinson et al. 1991). For the lower redshift lines, $H\alpha$ in particular, the limiting star formation rates are closer to the "typical" PG, although the volumes covered are too low to make the detection probability high.

Figure 4.6 plots the joint limits for all four strong lines in terms of the total comoving volume sampled (at different redshifts!) at a given limiting line luminosity, or the inferred star formation rate according to the calibration described in Section II with the Friedman model quoted above. In the volume needed to

capture at least one L_* galaxy, only objects with $SFR \sim 1000\ M_\odot/\mathrm{yr}$ would have been seen.

These limits are still too poor to conflict with current notions of galaxy formation, given the relatively small volume sampled and the relatively bright flux limits. The comoving volume covered for the [O II] line alone is only $\sim 28\ \mathrm{Mpc}^3$ for $H_0 = 75$ km/s/Mpc and $\Omega_0 = 0.2$; only strong biasing effects could have greatly enhanced the number density of PG candidates near the quasars. However, these limits are fainter than those of previously published IR surveys, viz., those by Boughn et al. (1986) and Collins & Joseph (1988) which used only broadband images; we converted their limits to line fluxes assuming a 100% efficiency factor.

One initially convincing candidate object was found near QSO 2203+29, but was not confirmed by follow-up observations. We were unable to explain this through any instrumental or other effects. This illustrates the potential pitfalls in pushing the observing technology to its limits; any viable PG candidates must be independently confirmed before they can be believed.

4.4 Prospects for the Future

The purpose of the experiment was largely exploratory. We did not expect to see many candidates at this stage, given the relatively small volume sampled and the relatively bright flux limits. According to our estimates, surveys at least an order of magnitude deeper, and/or covering an order of magnitude larger volumes, are needed in order to have a reasonable chance of detecting PGs. Improvements in both directions are feasible with the instruments and telescopes now coming on line.

One strategy is to maximize the volume covered, e.g., by increasing the area covered per detector field, even if only at a moderate flux level. The intent here would be to capture the brighter PGs, if they are indeed present in the expected

numbers. The optimum redshift intervals for such a survey may be $\Delta z \sim 2.1 - 2.6$, and $\Delta z \sim 3.1 - 3.8$, where the expected line fluxes are higher. Either targeted or unbiased field surveys could be performed in this way. Such a survey could well be done on a 4-meter class telescope and is already underway using the wide-field camera MAGIC, developed by the Max-Planck-Institute für Astronomie for use at the Calar Alto observatory (Mannucci & Beckwith 1994). The instrument has a square field of view 3.5 minutes of arc on a side ($0.8''$ pixels) and can reach flux levels around 10^{-16} erg s^{-1} cm^{-2} using narrowband filters.

A complementary approach is to reach deeper flux levels, even if not covering a large solid angle or comoving volume. Surveys reaching fainter than $F \sim 10^{-17}$ erg/cm^2/s could detect [O II] emission from PGs with $SFR \sim 100\ M_\odot$/yr or less, at $z > 4$ or 5, and would also be sensitive to the Hβ, [O III], and Hα emission from mildly obscured and/or less active PGs at lower redshifts. If the areas covered are small, targeted surveys, e.g., centered on the known high-z quasars, may be the preferred strategy. Such surveys are planned, using the NIRC instrument at the Keck telescope. This instrument has a field of view of only $\sim$ 40 arcsec square, but it should go very deep: preliminary data suggest that line fluxes approaching $F \sim 10^{-18}$ erg/cm^2/s may be reachable in several hours of integration, in good conditions.

TABLE 4.1. Line Intensity Relative to Hα

[O II]	Hβ	[O III]	Source	Reference
	0.35		Case B recomb.	Brocklehurst 1971
0.18			local [O II] em.	Kennicutt 1992
0.14	0.36	0.70	I Zw 18	Campbell 1990
0.89			local blue galaxies	Gallagher, et al. 1989
		0.91	NGCs 4214 & 4670	Huchra, et al. 1983
0.44	0.35	2.20	Orion H model	Shields 1990
0.62	0.35	0.35	Orion L model	Shields 1990
0.09	0.30	0.61	I Zw 18	Dufour, et al. 1988
0.18	0.35	0.60	Adopted ratio	

TABLE 4.2. Observations

Date	Field	z_{QSO}	λ_{obs} (μm)	t_{exp} (sec)
18 Mar 92	PC 1247+3406	4.897	2.197	3300
18 Mar 92	PC 1247+3406	4.897	2.237	3000
20 Jul 92	PC 2331+0216	4.093	1.897	600
21 Jul 92	QSO 2203+29	4.399	2.012	3200
07 Sep 92	QSO 2203+29	4.399	2.012	3400

TABLE 4.3. Areas and Flux Limits

Field	Data set	Area arcsec^2	Flux limit erg cm^{-2} s^{-1}
QSO 2203+29	a	167	4×10^{-16}
QSO 2203+29	b	173	5×10^{-16}
QSO 2203+29	c	340	1×10^{-15}
PC 1247+3406	a	324	8×10^{-16}
PC 1247+3406	b	376	3×10^{-15}
PC 1247+3406	c	725	3×10^{-15}
PC 2331+0216	a	490	3×10^{-15}

TABLE 4.4a. Restframe Coverage for the [O II] Line.

Field	Data Set	z_{em}	log V Mpc^3	log L erg/s	SFR $M_\odot$/yr
QSO 2203+29	a	4.399	0.24	43.46	1400
	b	4.399	0.26	43.55	1800
	c	4.399	0.55	43.85	3500
PC 1247+3406	a	4.897	0.54	43.89	3900
	b	4.897	0.60	44.46	14000
	c	5.002	0.89	44.49	15000
PC 2331+0216	a	4.093	0.70	44.24	8700
Total log Volume			1.44		

TABLE 4.4b. Restframe Coverage for the Hβ Line.

Field	Data Set	z_{em}	log V Mpc^3	log L erg/s	SFR $M_\odot$/yr
QSO 2203+29	a	3.139	0.20	43.04	280
	b	3.139	0.22	43.14	350
	c	3.139	0.51	43.44	710
PC 1247+3406	a	3.520	0.51	43.48	780
	b	3.520	0.57	44.08	3000
	c	3.602	0.86	44.08	3100
PC 2331+0216	a	2.902	0.66	43.82	1700
Total log Volume			1.40		

TABLE 4.4c. Restframe Coverage for the [O III] Line.

Field	Data Set	z_{em}	log V Mpc^3	log L erg/s	SFR $M_\odot$/yr
QSO 2203+29	a	3.019	0.20	42.99	140
	b	3.019	0.21	43.09	180
	c	3.019	0.51	43.39	360
PC 1247+3406	a	3.388	0.50	43.44	410
	b	3.388	0.57	44.04	1500
	c	3.468	0.86	44.04	1600
PC 2331+0216	a	2.789	0.65	43.77	870
Total log Volume			1.40		

TABLE 4.4d. Restframe Coverage for the Hα Line.

Field	Data Set	z_{em}	log V Mpc^3	log L erg/s	SFR $M_\odot$/yr
QSO 2203+29	a	2.066	0.12	42.54	31
	b	2.066	0.14	42.63	38
	c	2.066	0.43	42.93	76
PC 1247+3406	a	2.348	0.44	42.99	87
	b	2.348	0.50	43.59	320
	c	2.409	0.79	43.59	350
PC 2331+0216	a	1.890	0.57	43.31	180
Total log Volume			1.33		

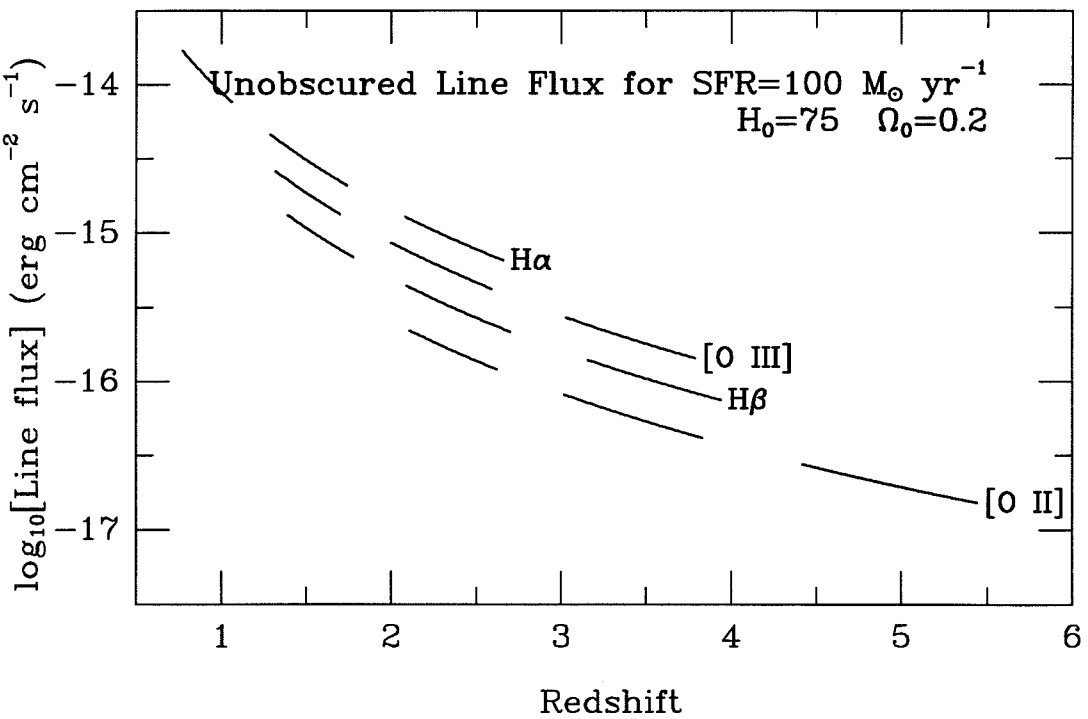

Figure 4.1: Expected Emission-Line Fluxes

The expected line fluxes from a protogalaxy powered by an unobscured star formation rate of $100M_{\odot}$/yr, assuming the calibration as described in the text, for a Friedman cosmology with $H_0 = 75$ km/s/Mpc, $\Omega_0 = 0.2$, and $\Lambda_0 = 0$. The three curve segments for each emission line correspond to the standard JHK bands, at about the 60% of peak transmission level.

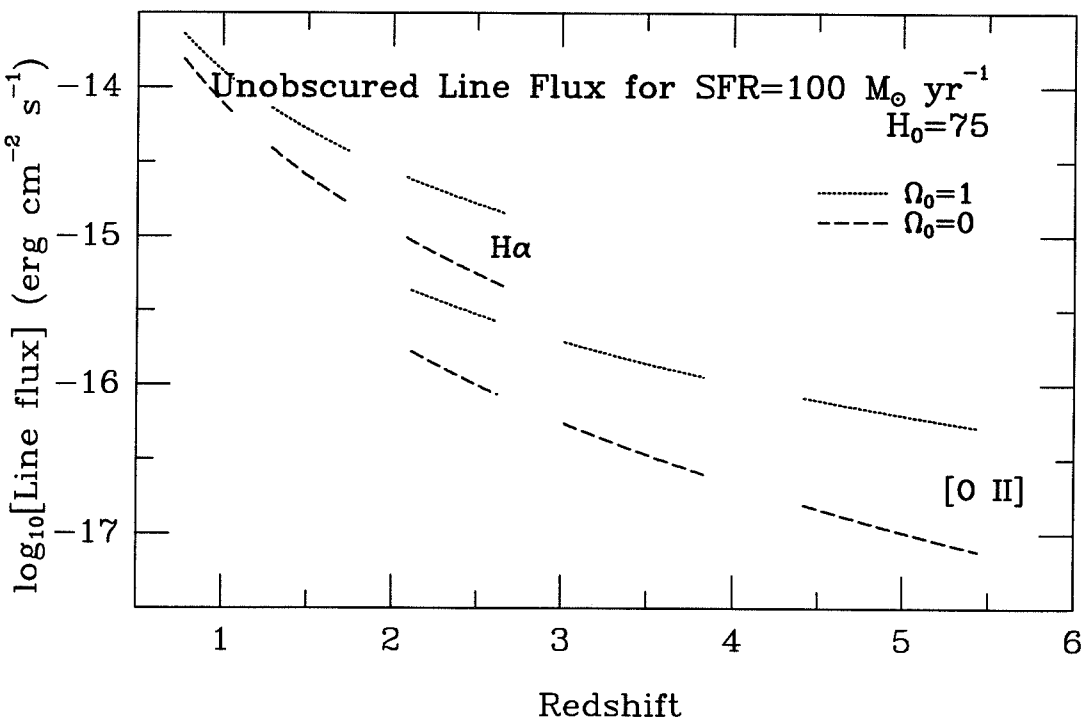

Figure 4.2: Cosmology Efects on Line Flux

Similar to Figure 4.1, but for the [O II] λ3727 and Hα λ6563 lines only, illustrating the effect of changing cosmology.

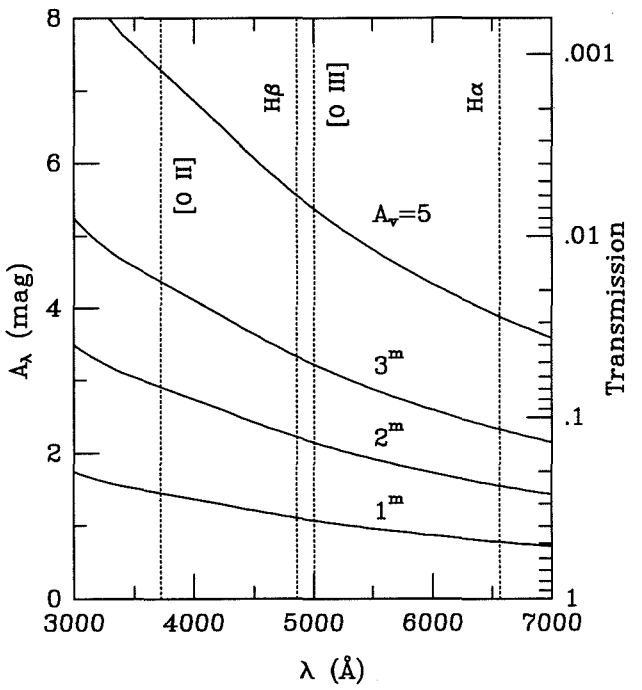

Figure 4.3: Dust Extinction Curves

Extinction curves for different amounts of total extinction in the V band, as labeled. The extinction is assumed to be a simple slab of dust in the protogalaxy restframe, and the Galactic extinction curve for $A_V/E_{B-V} = 3.1$, from Seaton (1979). The wavelengths of the four strong emission lines are indicated as dotted lines.

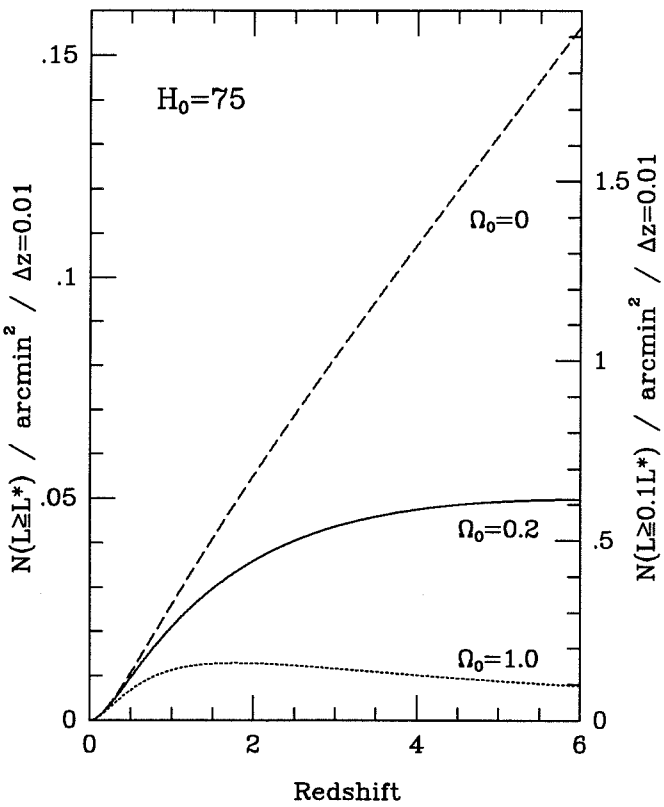

Figure 4.4: Galaxies Within Survey Volume

The expected numbers of galaxies with $L \geq L_*$ (left scale) or with $L \geq 0.1L_*$ (right scale), in a data slice covering 1 arcmin^2 and a thickness of $\Delta z = 0.01$, for the three Friedman cosmologies, as labeled. We assumed a standard Schechter function and no density evolution.

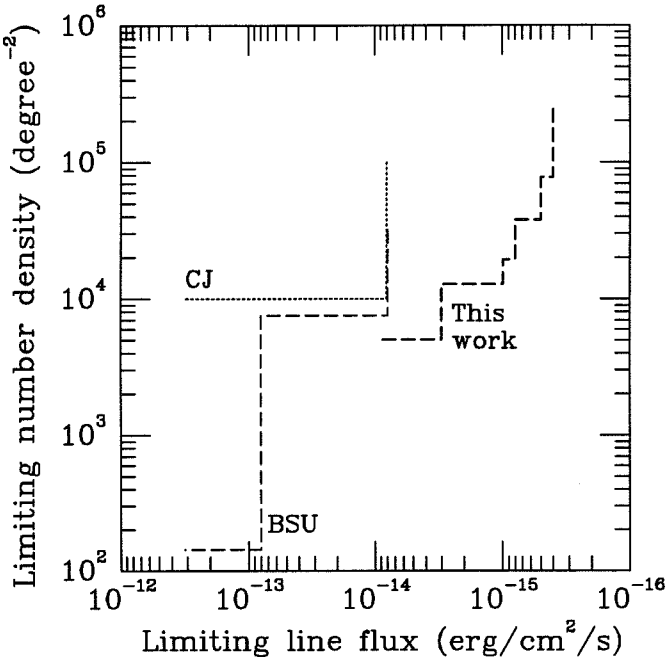

Figure 4.5: Observed-Frame Survey Limits

90% confidence limits on the surface density of PGs as a function of the [O II] λ3727 emission line flux. The areas to the upper left of the limit lines are excluded. The solid line gives the current limits from the Palomar survey. Dotted and dashed lines represent the limits from the surveys by Collins & Joseph (1988, CJ) and Boughn et al. (1986, BSU), respectively. Their continuum magnitudes have been converted to line fluxes by assuming that all of the light would be in the emission line.

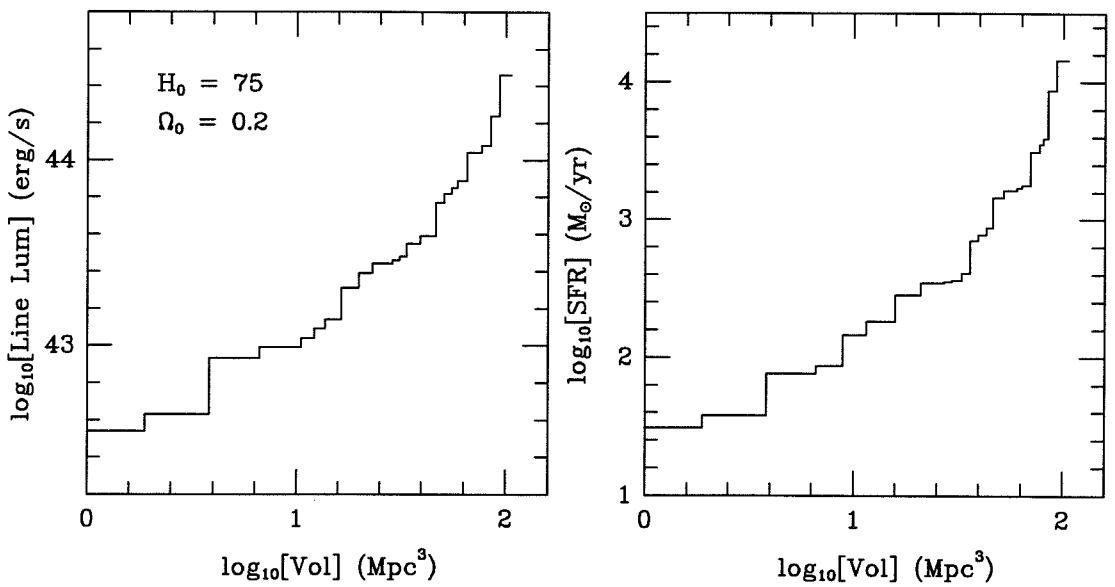

Figure 4.6: Restframe Cumulative Survey Limits

Cumulative limits of the Palomar experiment for all four strong lines, in terms of the limiting line luminosity at the given comoving volume sampled (left), and the corresponding unobscured star formation rate (right), for a Friedman cosmology with $H_0 = 75$ km/s/Mpc, $\Omega_0 = 0.2$, and $\Lambda_0 = 0$.

Chapter 5

Conclusions

Of order 10^5 comoving Mpc^3 were surveyed in *each* of the two optical PG searches presented here, to a level sufficient to detect the Lyα flux from unobscured star formation at a rate of 100 $M_\odot$ yr^{-1}. Using the space density of spheroidal systems as given by Baron & White (1987), and assuming no density evolution to the redshifts surveyed, the volume sampled by each survey should contain $\sim$ 100 – 200 galaxies with L $\gtrsim$ L* (Figures 5.1, 5.2). Smaller, though still significant, volumes are surveyed to flux limits an order of magnitude lower than this. To a limiting SFR of 10 $M_\odot$ yr^{-1}, a volume was surveyed sufficient to contain $\sim$ 40 galaxies with L $\gtrsim$ L*. No obvious population of PGs was discovered, though there remain a number of candidate emission-line objects which require follow-up spectroscopy.

The limits set by these surveys are, individually, some of the most stringent limits on high-redshift Lyα emission to date. We are in conflict with simple but reasonable models of galaxy formation by one to two orders of magnitude in *both* restframe Lyα luminosity and in space density. Taken together, the joint limits of all of the recent PG surveys are in even stronger conflict with these models.

There are a number of mechanisms which may account for the fact that a population of PGs has not been seen. The most obvious of these is dust extinction. Combined with resonant scattering of the Lyα photons, a small amount of dust is all that is needed to quench the Lyα line. There is, however, conflicting empirical

evidence on exactly how strong this mechanism is (section 2.4.2). At least some star formation must take place in a relatively dust-free environment, though, as the *first* generation of stars must form out of gas with primordial metal abundance.

PGs may also be extended. Models of galaxy formation predict everything from extended red objects (Baron & White 1987) to compact blue objects (Meier 1976). The limits plotted for different surveys (Figures 2.13 and 3.17) are generally expressed as those applying to point-sources. If the PGs were extended, the limiting flux for the surveys would have to be increased in proportion to their larger size. Pritchet (1994) shows that these two factors (dust obscuration and angular extent) can, at least in principle, account for the lack of detection of a population of PGs in the surveys.

If PGs have only a short lifetime in their Lyα-bright phase, then this would effectively lower the space density of PGs. The models by Charlot & Fall (1993), as well as work by Valls-Gabaud (1993), indicate that the Lyα emission from short, intense bursts of star formation can be rapidly overwhelmed by Lyα absorption in the atmospheres of cooler stars as the hotter stars evolve off the main sequence.

The lack of detection of a population of PGs may simply be a matter of recognition. That PGs may be masquerading as radio galaxies or quasars has already been mentioned. Clearly, though, the majority of massive galaxies we see in the local universe are not harboring strongly active nuclei, and thus AGN were excluded from our definition of a primeval galaxy. However, it is possible that unusual populations of stars, such as the Wolf-Rayet WN or WC stars, could add atypical lines of C or N to the predicted spectra of PGs, much as the He II λ4686Å line appears in the optical. In addition, the P Cygni line profiles from these stars with exceptionally strong stellar winds are unusual features in the spectra of typical star-forming regions. There are examples of anomalous abundance quasars (e.g., Q0358-28, Osmer 1980) which show relatively strong emission lines of nitrogen.

PGs may also be hiding in the population of objects known as "one liners," detected in the SLSS or other deep spectroscopic surveys. Both [O II] and Lyα can appear as strong, isolated emission lines over long spans in wavelength. Without sufficient signal to noise ratio in the continuum of such objects, it would be relatively easy to confuse the much lower redshift [O II] lines with Lyα (Turnshek et al. 1991).

Proto-spheroids may collapse at higher redshifts than are surveyed by the majority of the PG searches. The presence of some collapsed objects at high redshifts, e.g., radio galaxies and quasars out to $z = 4.9$, argues that at least some galaxy formation must have taken place at $z > 5$. This would push the Lyα line into the atmospheric OH lines beyond 7245Å, where the brightness of the sky makes sensitive observations more difficult. However, it is possible to choose narrowband filters which lie in dark portions of the night sky emission line spectrum to circumvent this problem. Pritchet & Hartwick (1990) used this technique to push Lyα-based surveys to $z \sim 6.5$, while Parkes, Collins, & Joseph (1994) chose filters in the near infrared J band, looking for Lyα at $z \sim 9$.

An alternative technique, explored in chapter 4, is to look in the infrared for restframe *optical* emission lines, such as those from [O II] λ3727Å, Hβ λ4861Å, [O III] λ5007Å, and Hα λ6563Å. These lines, redshifted into the near-infrared, cover the redshift range of $1 \leq z \leq 5.5$. This is similar to the optical Lyα-based surveys, but has the added advantage of suffering from much less extinction than Lyα. With the development of large infrared arrays, narrowband surveys based on these emission lines can now cover sufficient area at the necessary sensitivities to make such surveys feasible (section 4.2). Such surveys are currently underway by at least two groups (Mannucci & Beckwith 1994, Pahre & Djorgovski 1995).

It would seem that the last word on Lyα-based surveys has yet to be said. If indeed some portion of the PG phase of galaxy formation was at least slightly dusty, and PGs are extended objects, then perhaps PG surveys are only starting

to push into the regime where we might expect to detect significant numbers of objects, as suggested by Pritchet (1994). These surveys might best be conducted with the next generation of optical cameras which seek to "pave" large areas in the focal plane with CCD detectors. The significantly larger fields of view afforded by these cameras would allow larger volumes of the PG parameter space to be probed while perhaps also pushing to fainter flux limits.

An alternative approach is to use the techniques developed in chapter 4. Success in near-IR surveys such as this also depend on the new, large format infrared arrays to cover large volumes in the PG parameter space with reasonable amounts of telescope time. Both lines of research should be pursued, as the identification of a population of primeval galaxies has such important consequences to cosmology.

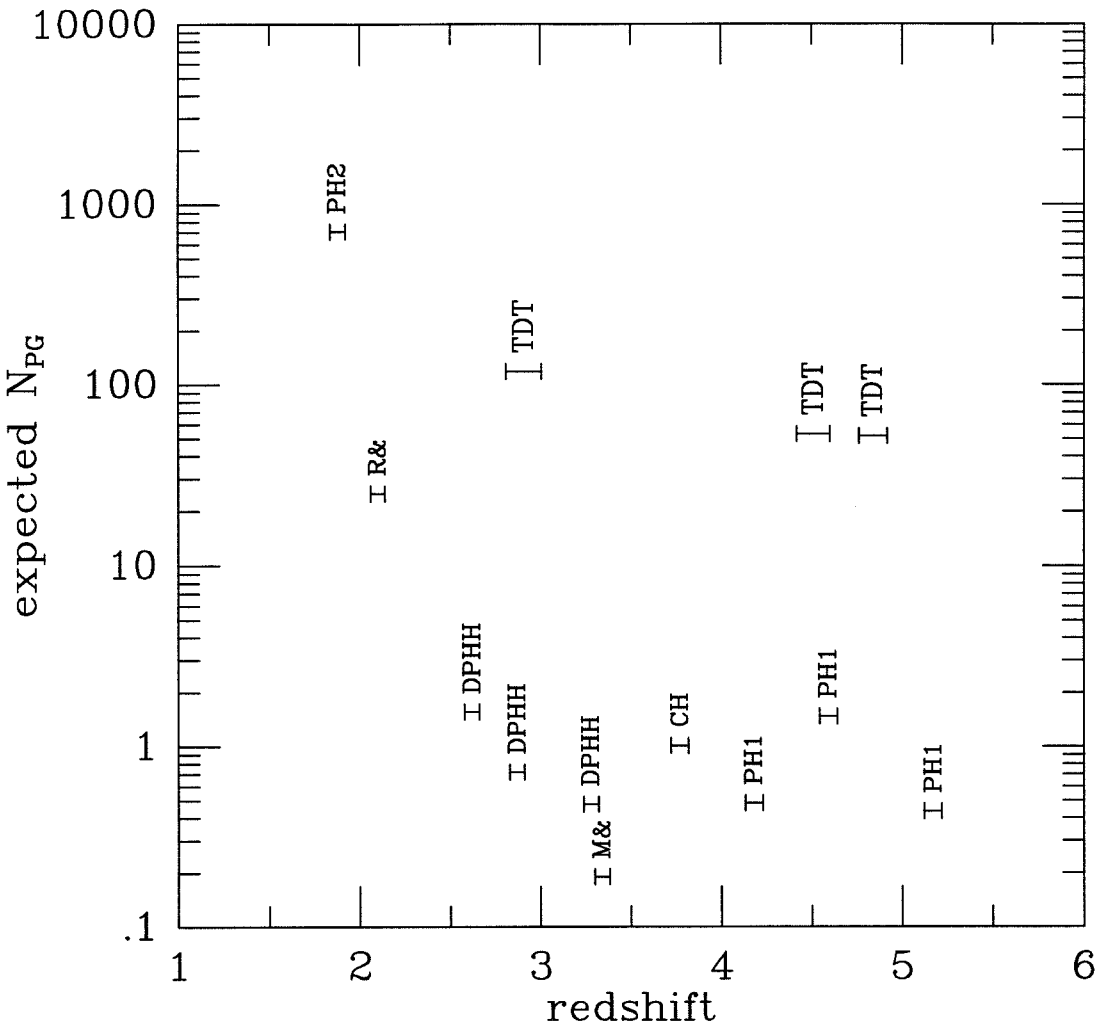

Figure 5.1: Expected Numbers of Galaxies: Imaging Surveys

The estimated number of galaxies which lie above each survey's limiting Lyα line luminosity. These estimates were obtained by integrating a non-evolving Schecter function with the assumption that 1% of the bolometric luminosity is in the Lyα line. The narrowband imaging surveys with $\Delta z \geq 0.03$ are included in the plot, and all published limits were converted to an $H_0 = 75$ km s^{-1} Mpc^{-1}, $\Omega_0 = 0.2$ cosmology for comparison. The surveys are identified as: CH = Cowie & Hu, in Cowie (1988); DPHH = De Propris et al. 1993; M& = Macchetto et al. (1993); PH1 = Pritchet & Hartwick (1987); PH2 = Pritchet & Hartwick (1990); R& = Rhee et al. (1989); and TDT = Thompson, Djorgovski, & Trauger (1995, chapter 2). The width of the survey lines indicates the redshift range covered.

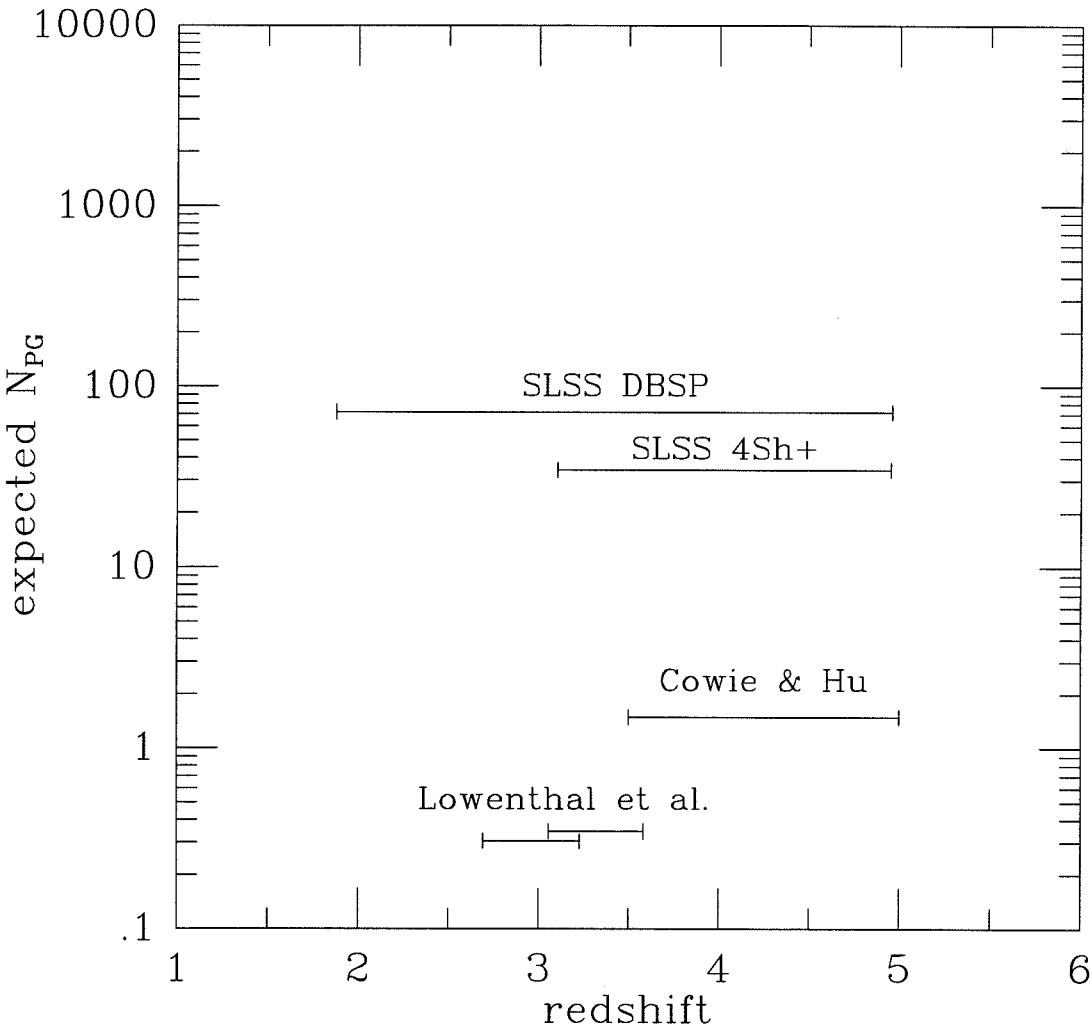

Figure 5.2: Expected Numbers of Galaxies: Spectroscopic Surveys
Same as Figure 5.1, but for the spectroscopic Lyα surveys. The widths of the survey lines indicates the redshift range covered, but the expected numbers of PGs is integrated over the entire survey volume. The surveys are identified as: Cowie & Hu, in Cowie (1988); Lowenthal et al. (1990); SLSS = Thompson, & Djorgovski (1995, chapter 3).

Bibliography

Baron, E., & White, S. D. M. 1987, ApJ, 322, 585

Bergeron, J. 1990, ESO Messenger #62

Blain, A. W. & Longair, M. S. 1993, MNRAS, 265, L21

Boughn, S. P., Saulson, P. R., & Uson, J. M. 1986, ApJ, 301, 17

Boulanger, F., & Perault, M. 1988, ApJ, 330, 964

Bower, R. G., Ellis, R. S., Rose, J. A., & Sharples, R. M. 1990, AJ, 99, 530

Bower, R. G., Lucey, J. R., & Ellis, R. S. 1992, MNRAS 254, 601

Broadhurst, T. J., Ellis, R. S., & Shanks, T. 1988, MNRAS, 235, 827

Brocklehurst, M. 1971, MNRAS, 153, 471

Bruzual, G. 1983, ApJ, 273, 105

Calzetti, D., & Kinney, A. L., 1992, ApJ, 399, L39

Calzetti, D., Kinney, A. L., & Storchi-Bergmann, T. 1994, ApJ, 429, 582

Campbell, A. 1990, ApJ 362, 100

Chambers, K. C., Miley, G. K., & van Breugel, W. J. M. 1990, ApJ, 363, 21

Charlot, S. & Fall, S. M. 1993, ApJ, 415, 580

Colless, M., Ellis, R. S., Taylor, K., & Hook, R. N. 1990, MNRAS, 244, 408

Colless, M., Glazebrook, K., Ellis, R. S., & Broadhurst, T. J. 1993, in Observational Cosmology, G. Chincarini et al. (eds.), ASPCS, 51, 328

Collins, C. A., & Joseph, R. D. 1988, MNRAS, 235, 209

Cowie, L. L. 1988, in Post-Recombination Universe, N. Kaiser, & A. Lasenby (eds.), p. 1, Dordrecht: Kluwer

Cowie, L. L., & Lilly, S. J. 1990, in Evolution of the Universe of Galaxies, Kron, R. G. (ed.), ASPCS 10, 212

Cowie, L. L., Lilly, S. J., Gardner, J., & McLean, I. S. 1988, ApJ 332, L29

Cowie, L. L., Songaila, A., Hu, E. M., Egami, E., Huang, J.-S., Pickles, A. J., Ridgeway, S. E., Wainscoat, R. J., & Weyman, R. J. 1994, ApJ, 432, L83

de Carvalho, R., & Djorgovski, S. 1992, ApJ, 389, L49

Deharveng, J. M., Joubert, M., & Kunth, D. 1985, in Star-Forming Dwarf Galaxies and Related Objects, D. Kunth et al. (eds), p. 431, Gif sur Yvette: Editions Frontières

De Propris, R., Pritchet, C. J., Hartwick, F. D. A., & Hickson, P. 1993, AJ, 105, 1243

Djorgovski, S. 1987, in Starbursts and Galaxy Evolution, Thuan, T. X., Montmerle, T., & Tran Thanh Van. J. (eds.), p. 401, Gif sur Yvette: Editions Frontières

Djorgovski, S. 1988, in Towards Understanding Galaxies at Large Redshift, Kron, R. G., & Renzini, A. (eds.), p. 259, Dordrecht: Kluwer

Djorgovski, S. 1992, in Cosmology and Large-Scale Structure in the Universe, R. de Carvalho (ed.), ASPCS 24, p. 73

Djorgovski, S. 1994, in Mass-Transfer Induced Activity in Galaxies, I. Shlosman (ed.), p. 452, Cambridge: Cambridge University Press

Djorgovski, S., Smith, J. D., & Thompson, D. 1991, in The Space Distribution of Quasars, D. Crampton (ed.), ASPCS, 21, 109

Djorgovski, S., Smith, J. D., & Thompson, D. 1991, in The Space Distribution of Quasars, D. Crampton (ed.), ASPCS, 21, 325

Djorgovski, S., Spinrad, H., McCarthy, P., & Strauss, M. A., 1985, ApJ, 299, L1

Djorgovski, S., Spinrad, H., Pedelty, J., Rudnick, L., & Stockton, A. 1987a, AJ, 93, 1307

Djorgovski, S., Strauss, M. A., Perley, R. A., Spinrad, H., & McCarthy, P. J. 1987b, AJ, 93, 1318

Djorgovski, S., & Thompson, D. 1992, in The Stellar Populations of Galaxies, B. Barbuy & A. Renzini (eds.), IAU Symp #149, p. 337, Dordrecht: Kluwer

Djorgovski, S., Thompson, D., & Smith, J. D. 1993, in First Light in the Universe, B. Rocca-Volmerange et al. (eds.), p. 67, Gif sur Yvette: Editions Frontières

Djorgovski, S., Thompson, D., & Smith, J. D. 1993, in Texas/PASCOS'92: Relativistic Astrophysics and Particle Cosmology, eds. C. Akerlof & M. Srednicki, Ann. N.Y. Acad. Sci., 688, 515

Djorgovski, S., & Weir, N. 1990, ApJ, 351, 343

Driver, S. P., Phillips, S., Davies, J. I., Morgan, I., Disney, M. J. 1994, MNRAS, 266, 155

Dufour, R. J., Garnett, D. R., & Shields, G. A. 1988, ApJ, 332, 752

Eales, S. A., & Rawlings, S. 1993, ApJ, 411, 67

Eisenhardt P., & Dickinson, M. 1992, ApJ, 399, L47

Ellis, R. S. 1988, in Towards Understanding Galaxies at Large Redshift, Kron, R. G., & Renzini, A. (eds.), p. 147, Dordrecht: Kluwer

Elston, R., McCarthy, P. J., Eisenhardt, P., Dickinson, M., Spinrad, H., Jannuzi, B. T., & Maloney, P. 1994, AJ, 107, 910

Gallagher, J. S., Bushouse, H., & Hunter, D. A. 1989, AJ, 97, 700

Giavalisco, M., Steidel, C. C., & Szalay, A. S. 1994, ApJ, 425, L5

Guhathakurta, P., Tyson, J. A., & Majewski, S. R. 1990, ApJ, 357, 9

Gunn, J. E. et al. 1987, Optical Engineering, 26, 779

Gunn, J. E., & Westphal, J. A. 1981, Proc. SPIE, 290, 16

Haehnelt, M. G., & Rees, M. J. 1993, MNRAS, 263, 168

Hamann, F., & Ferland, G. 1993, ApJ, 418, 11

Hartmann, L. W., Huchra, J. P., Geller, M. J., O'Brien, P., & Wilson, R. 1988, ApJ, 326, 101

Hecht, E. 1987, Optics (2nd Edition), Addison-Wesley Pub. Co., pp. 363-372

Howell, S. B. 1989, PASP, 101, 616

Hu, E. M. & Cowie, L. L. 1987, ApJ, 317, L7

Hu, E. M., Songaila, A., Cowie, L. L., & Stockton, A. 1991, ApJ, 368, 28

Huchra, J. P., 1988, in The Minnesota Lectures on Clusters of Galaxies and Large Scale Structure, ed. J. M. Dickey, ASPCS, 5, 41

Huchra, J. P., Geller, M. J., Gallagher, J., Hunter, D., Hartmann, L., Fabbiano, G., & Aaronson, M. 1983, ApJ, 274, 125

Jannuzi, B. T., Elston, R., Schmidt, G. D., Smith, P. S., & Stockman, H. S. 1994, ApJ, 429, L49

Kennicutt, R. C. 1983, ApJ 272, 54

Kennicutt, R. C. 1992, ApJ 388, 310

Kent, S. M. 1985, PASP 97, 165

Koo, D. C. 1986, in Spectral Evolution of Galaxies, Chiosi, C. & Renzini, A. (eds.), p. 419, D. Reidel

Koo, D. C., & Kron, R. K. 1992, ARAA, 30, 613

Kormendy, J. 1993, in The Nearest Active Galaxies, J. Beckman et al. (eds.), Madrid:CSIS

Kormendy, J. & Sanders, D. B. 1992, ApJ, 390, L53

Le Borgne, J. F., Pelló, R., Sanahuja, B., Soucail, G., Mellier, Y., & Breare, M. 1990, A&A, 229, L13

Lilly, S. J., Cowie, L. L., & Gardner, J. P. 1991, ApJ, 369, 79

Lowenthal, J. D. 1991, Ph.D. Thesis, University of Arizona

Lowenthal, J. D., Hogan, C. J., Green, R. F., Caulet, A., Woodgate, B. E., Brown, L., & Foltz C. B. 1991, ApJ, 377, L73

Lowenthal, J. D., Hogan, C. J., Leach, R. W., Schmidt, G. D., & Foltz, C. B. 1990, ApJ, 357, 3

Macchetto, F., Lipari, S., Giavalisco, M., Turnshek, D. A., & Sparks, W. B. 1993, ApJ, 404, 511

Mannucci, P., & Beckwith, S. V. W. 1994, in preparation

Mannucci, F., Beckwith, S. V. W., & McCaughrean, M. J. 1994, in Infrared Astronomy with Arrays, I. McLean (ed.), p. 503, Dordrecht: Kluwer

Massey, P., & Gronwall, C. 1990, ApJ, 358, 344

Massey, P., Strobel, K., Barnes, J. V., & Anderson, E. 1988, ApJ, 328, 315

Mather, J. C. et al. (the COBE team) 1994, ApJ, 420, 439

Matteucci, F. 1993, in Panchromatic View of Galaxies: Their Evolutionary Puzzle, ed. G. Hansler et al., Berlin: Springer Verlag, in press

Matteucci, F., & Padovani, P. 1993, ApJ, 419, 485

McCarthy, P. J. 1988, Thesis, University of California, Berkeley

McCarthy, P. J. 1993, ARAA, 31, 639

McCarthy, P. J., Dickinson, M., Fillipenko, A. V., Spinrad, H., & van Breugel, W. J. M. 1988, ApJ, 328, L29

McCarthy, P. J., Spinrad, H., Djorgovski, S., Strauss, M., van Breugel, W., & Liebert, J. 1987, ApJ, 319, L39

Meier, D. L. 1976, ApJ, 203, L103

Meier, D. L., & Terlevich, R. 1981, ApJ, 246, L109

Metcalfe, N., Shanks, T., Fong, R., & Roche, N. 1994, MNRAS, submitted

Møller, P., & Warren, S. J. 1993, A&A, 270, 43

Oke, J. B. 1974, ApJS, 27, 21

Oke, J. B., & Gunn, J. E. 1982, PASP, 94, 586

Oke, J. B., & Gunn, J. E. 1983, ApJ, 266, 713

Osmer, P. S. 1990, ApJ, 237, 666

Pagel, B. E. J. 1993, Phys Rep, 227, 251

Pahre, M., & Djorgovski, S. 1995, ApJ, submitted

Parkes, I. M., Collins, C. A., & Joseph, R. D. 1994, MNRAS, 266, 983

Partridge, R. B. & Peebles, P. J. E. 1967, ApJ, 147, 868

Peebles, P. J. E. 1989, in The Epoch of Galaxy Formation, C. Frenk et al. (eds.), p. 1, Dordrecht: Kluwer

Pritchet, C. J. 1994, PASP, 106

Pritchet, C. J. & Hartwick, F. D. A. 1987, ApJ, 320, 464

Pritchet, C. J. & Hartwick, F. D. A. 1990, ApJ, 355, L11

Rhee, G. F. R. N., Webb, J. K., & Katgert, P. 1989, A&A, 217, 1

Rowan-Robinson, M., Broadhurst T., Lawrence A., McMahon R. G., & Lonsdale C. J. 1991, Nature, 351, 719

Schmidt, M., Schneider, D. P., & Gunn, J. E. 1991, in Space Distribution of Quasars, D. Crampton (ed.), ASPCS, 21, 109

Schneider, D. P., Gunn, J. E., Turner, E. L., Lawrence, C. R., Hewitt, J. N., Schmidt, M., & Burke, B. F. 1986, AJ, 91, 991

Schneider, D. P., Gunn, J. E., Turner, E. L., Lawrence, C. R., Schmidt, M., & Burke, B. F. 1987, AJ, 94, 12

Schneider, D. P., Schmidt, M., & Gunn, J. E. 1989, AJ, 98, 6

Schneider, D. P., Schmidt, M., & Gunn, J. E. 1991, AJ, 102, 837

Schneider, D. P., Schmidt, M., & Gunn, J. E. 1994, AJ, 107, 880

Seaton, M. J. 1979, MNRAS, 187, 73P

Shields, G. A. 1990, ARAA, 28, 525

Shull, J. M. & Silk, J 1979, ApJ 234, 427

Silk, J. 1985, ApJ, 297, 1

Small, T. A., & Blandford, R. D. 1992, MNRAS, 259, 725

Smith, J. D., Thompson, D., & Djorgovski, S. 1993, in Sky Surveys: Protostars to Protogalaxies, ed. B.T. Soifer, ASPCS, 43, 185

Smoot, G. F., Bennett, C. L., et al. 1992, ApJ, 396, L1

Soifer, B. T., Neugebauer, G., Matthews, K., Lawrence, C. R., & Mazzarella, J. 1992, ApJ, 399, L55

Spinrad, H. 1987, in High Redshift and Primeval Galaxies, Bergeron, J., Kunth, D., Rocca–Volmerange, B., & Tran Thanh Van, J. (eds.), p. 59. Editions Frontières

Stasinska, G. 1982, A&AS 48, 299

Steidel, C. C., Sargent, W. L. W., & Dickinson, M. 1991, AJ, 101, 1187

Stone, R. P. S. 1974, ApJ, 193, 135

Stone, R. P. S. 1977, ApJ, 218, 767

Stover, R. J. 1988, in Instrumentation for Ground-Based Optical Astronomy, L. B. Robinson (ed.), New York: Springer Verlag, p. 443

Terlevich, E., Diaz, A. I., Terlevich, R., & Vargas, M. L. G. 1993, MNRAS, 260, 3

Terlevich, R. 1992, in The Stellar Populations of Galaxies, B. Barbuy & A. Renzini (eds.), IAU Symp #149, p. 271, Dordrecht: Kluwer

Terlevich, R. J., & Boyle, B. J. 1993, MNRAS, 262, 491

Thompson, D., & Djorgovski, S. 1991, ApJ, 371, L55

Thompson, D., Djorgovski, S., & Beckwith, S. V. W. 1994, AJ, 107, 1

Thompson, D., Djorgovski, S., & Trauger, J. 1992, in Cosmology and Large-Scale Structure in the Universe, ed. R. de Carvalho, ASPCS, 24, 147

Thompson, D., Djorgovski, S., & Trauger, J. 1995, AJ, in press (see chapter 2)

Thompson, D., Djorgovski, S., Trauger, J., & Beckwith, S. V. W. 1993, in Sky Surveys: Protostars to Protogalaxies, ed. B.T. Soifer, ASPCS, 43, 189

Turnshek, D. A. et al. 1991, ApJ, 382, 26

Tyson, J. A. 1988, AJ, 96, 1

Tyson, J. A. 1990, in Evolution of the Universe of Galaxies, Kron, R. G. (ed.), ASPCS 10, 292

Valls-Gabaud, D. 1993, ApJ, 419, 7

Wolfe, A., 1993, in Texas/PASCOS'92: Relativistic Astrophysics and Particle Cosmology, eds. C. Akerlof & M. Srednicki, Ann. N.Y. Acad. Sci., 688, 281

Wolfe, A. M. 1993a, ApJ, 402, 411

Wolfe, A. M. 1993b, Ann. New York Academy of Sciences, 688, 281

Wolfe, A. M., Turnshek, D. A., Lanzetta, K. M., & Oke, J. B. 1992, ApJ, 385, 151